Max-Planck-Institut
für Meteorologie

EXAMENSARBEIT Nr. 76

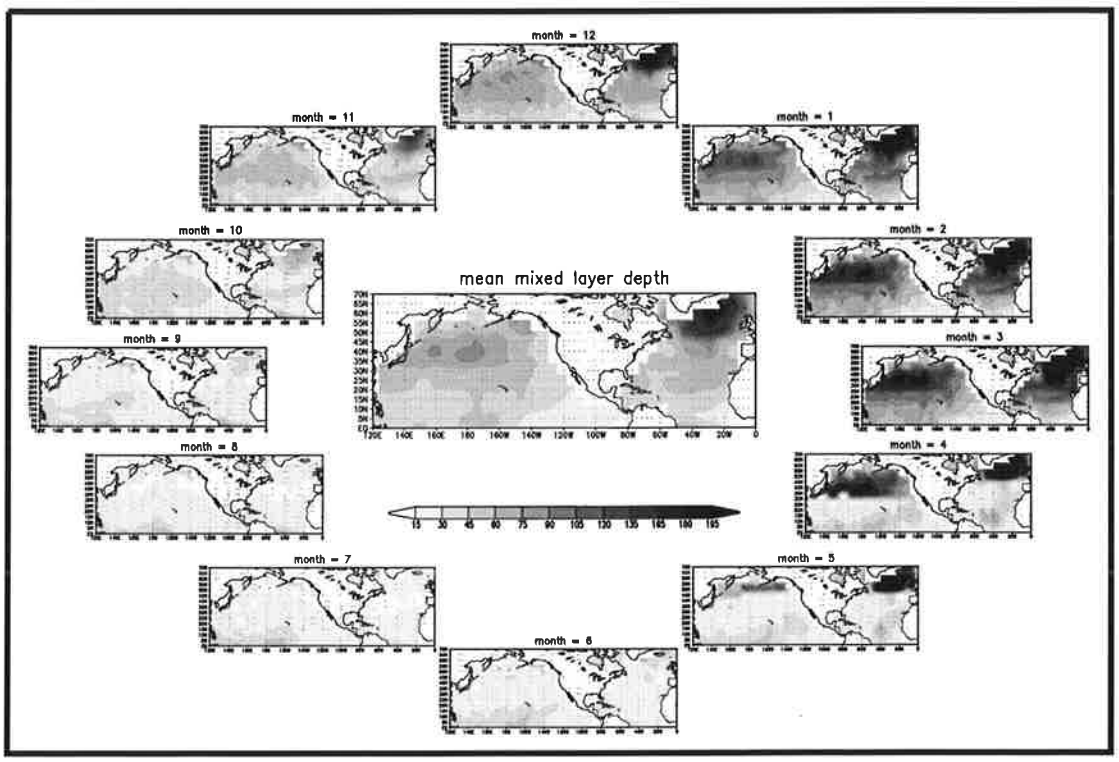

LARGE-SCALE SST VARIABILITY IN THE MIDLATITUDES AND IN THE TROPICAL ATLANTIC

by

Dietmar Dommenget

HAMBURG, July 2000

Dissertation zur Erlangung des Doktorgrades

Autor:

Dietmar Dommenget

Max-Planck-Institut
für Meteorologie

MAX-PLANCK-INSTITUT
FÜR METEOROLOGIE
BUNDESSTRASSE 55
D - 20146 HAMBURG
GERMANY

Tel.: +49-(0)40-4 11 73-0
Telefax: +49-(0)40-4 11 73-298
E-Mail: <name> @ dkrz.de

ISSN 0938-5177

Large-scale SST variability in the midlatitudes and in the tropical Atlantic

Dissertation

zur Erlangung des Doktorgrades

der Naturwissenschaften im Fachbereich

Geowissenschaften

der

Universität Hamburg

vorgelegt

von

Dietmar Dommenget

aus Berlin

Hamburg

2000

ISSN 0938-5177

Als Dissertation angenommen vom Fachbereich Geowissenschaften
der Universität Hamburg
auf Grund der Gutachten von Dr. Mojib Latif
und Prof. Dr. Klaus Hasselmann

Hamburg den 7. April 2000

Prof. Dr. U. Bismayer
Dekan
des Fachbereichs Geowissenschaften

Contents

List of Figures

Chapter 1

Introduction

How will the weather be over the weekend? Well this is an easy question, because the processes that determine the short time (a few days) weather fluctuations are relatively well understood. And how about the next summer or next winter in Germany or how is climate changing over the next few decades to centuries?

Understanding the causes of natural climate variability is one of the main goals of climate research. The increased CO_2 concentration in the atmosphere due to the human activities will enhance the greenhouse effect of the atmosphere which will therefore change the global climate in the future. In order to predict how the climate will change in the future, the knowledge of the natural climate variability is fundamental. In addition to being interested in anthropogenic climate change, society in general is interested in predictions of climate variability on the time scales of seasons to decades.

Climate variability exists on all time scales, ranging from time scales as short as seasons and ending on the time scales of the age of the earth. In this context the climate system is defined to consist of the entire atmosphere, the ocean, the cycrosphere, the solid earth, and the biosphere without human technology. The sources of climate variability can therefore be attributed to external forcing and internal variability. Climate variability, which is generated within the climate subsystems, is internal variability, whereas climate variability driven by external forcing, such as solar variability, volcanoes and human activities, is considered as externally forced climate variability.

In this thesis I shall focus on the internal climate variability from seasonal to decadal time scales. In this time window the interactions between the upper ocean and the atmosphere is one of the main sources of climate variability and it will therefore be the main subject of this thesis.

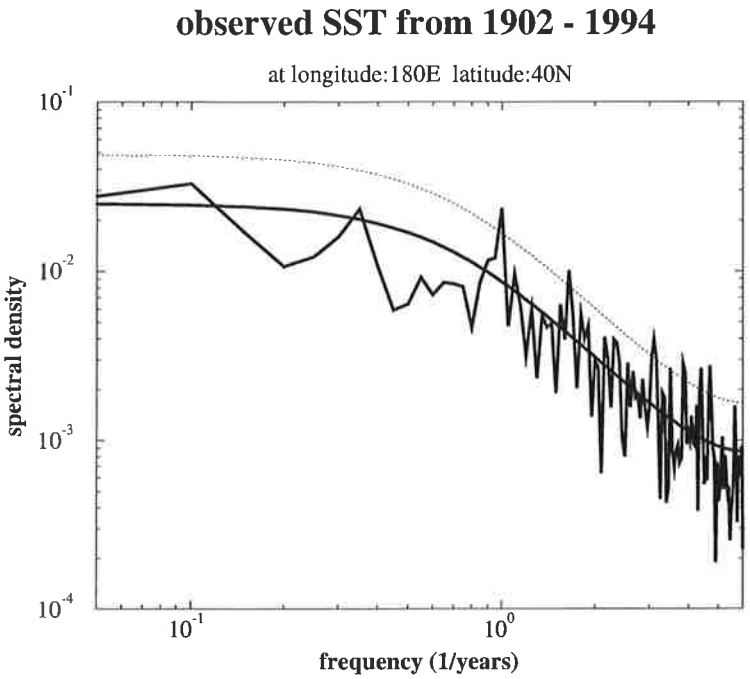

Figure 1.1: The spectral distribution of the monthly mean observed SST in the north Pacific. In comparison to the spectra of the SST the spectral distribution of a fitted AR-1 process (thick solid line) and the 95% confidence limited to the fitted AR-1 process (thin dashed line) are shown.

1.1 The Null hypothesis of internal climate variability

The stochastic climate model introduced by Hasselmann (1976) attempts to explain the natural climate variability by ocean-atmosphere interactions by dividing the climate system into a fast and a slow system. In this model the atmosphere is the fast system, where fluctuations can be regarded as random noise on the time scale of months and longer. The variability of the ocean, which is regarded as the slow component of the climate system, is explained by the integration of the atmospheric noise. In this picture the ocean is just a passive part of the climate system, which only amplifies the long term climate variability, due to its large heat capacity. Internal processes of the ocean are not considered.

The resulting stochastic model of the sea surface temperature (SST) variability is described by an auto-regressive process of the first order (AR(1)-process), which is the simplest statistical model that can be applied to a stationary process. The stochastic climate model introduced by Hasselmann is therefore often chosen as the Null hypothesis of SST variability. The spectral distribution of an AR(1)-process is defined by the standard deviation σ and the lag-1 correlation a of the SST time series:

$$C(\omega) = \frac{\sigma^2}{(1-a)^2 + \omega^2} \tag{1.1}$$

In Figure 1.1 the spectrum of the SST in the North Pacific and the fitted AR-1 process

according to equation 1.1 are shown. It can clearly be seen that the spectrum of the SST is basically following that of the AR-1 process. The most prominent feature of the SST spectrum is the increase of the spectral variance for longer time periods. This is often refereed as the 'redness of the SST spectrum.

If the internal climate variability, is just an AR-1 process, then the predictability of natural climate variability is very limited and seasonal or decadal weather forecasts will never achieve sufficient skill to be of use for economic applications. It is therefore important to investigate if the SST variability is really consistent with an AR-1 process.

1.2 The concept of this thesis

In this thesis I shall have a closer look at the Null hypothesis of SST variability. In most ocean regions the Null hypothesis is still considered as the best hypothesis. Many other hypothesis for the existence of ocean-atmosphere coupled modes exist. These are mostly associated with decadal time scales, but still unproven in the observations.

The El Niño phenomenon in the tropical Pacific is the only large-scale mode of SST variability which is found to be significantly different from an AR-1 process. It is also known that the El Niño phenomenon is strongly influencing the Indian Ocean and also, but not as strongly, the tropical Atlantic Ocean. In principle the equatorial Atlantic should have a similar type of El Niño like SST variability as the Pacific, but due to the smaller basin size it is much weaker.

This thesis will focus on those regions which are still considered to be consistent with the Null hypothesis and in which sufficient observations are available to analyze the large-scale characteristics of the SST variability. The midlatitudes of the Northern Hemisphere and the tropical Atlantic basically fulfill these requirements. The Southern Ocean, which in principle may also be consistent with the Null hypothesis, are not analyzed, as the observational data base is too sparse.

The limitations of the observational data in space, time and quality requires one to compare the observations with model simulations. The concept of my analysis is therefore based on a comparison of the large-scale features of the observed SST variability with a hierarchy of global coupled circulation models (CGCMs). The CGCMs simulations differ mainly in the complexity of the ocean models. The comparison of the different CGCM simulations offers the possibility of determining the processes which are important for certain features of the observed SST variability.

This work is organized as follows: In the following chapter I shall introduce some of the statistical methods used. In Chapter 3 the climate models that are used will be introduced and discussed. The analysis of midlatitude SST variability will be presented in Chapter 4, followed by the analysis of the tropical Atlantic in Chapter 5. For the analysis of the midlatitudes and the tropical Atlantic, simple ocean mixed layer models have been developed,

which are also useful to study the atmospheric response to SST anomalies in a coupled simulation. This new approach for so called 'AMIP-type' simulation will be introduced in Chapter 6. The work will be concluded with an outlook and a summary in Chapter 7.

Chapter 2

Statistical methods and observations

In the analysis of the interannual to decadal SST variability of the tropical Atlantic in Chapter 5 the interpretation of the pattern of empirical orthogonal functions (EOF) is a critical point in understanding the large-scale modes of variability. In past studies some researchers have interpreted the EOF-2 of the observed SST anomalies (see Figure 5.1) as a dominant mode of interaction between the trade wind regions of the Northern and Southern Hemispheres. However, the discussion of the EOF-pattern in Chapter 5 has shown that the VARIMAX rotation of the EOF-patterns provides another point of view, which indicates that there is no strong interaction between the two hemispheres. In order to understand the concept of EOF rotations better, I shall discuss the rotations of EOFs in the following section 2.1.

From Hasselmann's stochastic climate model it has to be assumed that the spectrum of the SST anomalies is following that of an AR(1)-process. In general, the AR(1)-process is the simplest stochastical model by which SST variability can be represented, assuming that our system is stationary. If the SST variability is in statistical agreement with the AR(1)-process, then all other mathematical models are negligible. From a physical point of view it must then be concluded that the internal dynamical processes of the ocean are not important for generating SST anomalies. It is therefore important for the analysis of ocean-atmosphere interaction to test whether the SST variability is in statistical agreement with the AR(1)-process. In section 2.2.1 a method is introduced, to test whether a spectrum is significantly different from a theoretical spectrum.

2.1 Rotation of EOFs

The EOF analysis is not only used to separate the modes of large-scale variability from the noise, but to get insight into the main physical mechanisms of SST variability. However, there are same objections to this approach, which has been discussed by North et al. (1982) and in an overview article by Richman (1986). The main argument regarding the interpretation

of the EOF patterns is that the EOF analysis in general produces a hierarchy of multi-poles, whereby the first EOF usually is a monopole, the second a dipole and so on, whereby multi-poles present "apparent" anti-correlations that in general does not exist in the SST record.

In order to illustrate the problem in interpreting the EOF patterns I present an artificial Monte Carlo (simulation based on random numbers) example, which is similar to the structure of the tropical Atlantic SST variability in Chapter 5. The artificial Monte Carlo example is a field of 10 by 20 points in which two independent (uncorrelated and spatially separated) circular patterns are present. Each point of the field is created by a random noise component that is independent for each point, and for the grid points in one of the two patterns an additional noise component is added, which is constant for each pattern but different for the different patterns. The standard deviation of the local noise has been chosen to be $\sigma_{local} = 1.0$ for the upper pattern $\sigma_{pattern1} = 2.0$ and for the lower pattern $\sigma_{pattern2} = 2.1$.

The two upper plots in Figure 2.1 show the first two EOFs of the Monte Carlo field. Although the two circular patterns of the Monte Carlo field are uncorrelated by construction, the EOF analysis presents dipoles in both EOF patterns, which may lead to the conclusion that the two patterns are related to each other. The EOF analysis does not indicate that the two patterns are indeed uncorrelated by construction.

North et al. (1982) have shown that the eigenvalues of the EOFs may be degenerated when the explained variances are not significantly different from each other. North et al. give an estimation for the statistical uncertainty of an EOF eigenvalue, which is given as:

$$\delta\lambda = \lambda\sqrt{2/N} \tag{2.1}$$

The statistical uncertainty $\delta\lambda$ of an EOF eigenvalue λ is therefore proportional to the eigenvalue itself and depends also on the number of degrees of freedom N. In the Monte Carlo example the number of degrees of freedom was chosen to be $N = 100$. The statistical uncertainty $\delta\lambda$ of the EOF-1 is therefore $\pm 4.8\%$ of the variance. North et al. consider that two EOF eigenvalues have to be considered as degenerated if the difference of two EOF eigenvalues is less than 1 or 2 $\delta\lambda$. If the EOF eigenvalues are degenerated all orthogonal rotations of the EOF pattern can be considered as the dominant EOF in the range of the statistical uncertainty.

In many EOF analysis the EOF eigenvalues are degenerated and all possible rotations can be considered. The degeneration of the EOF eigenvalues is also the reason for the tendency of the EOF analysis to come up with a hierarchy of multi-poles even if the multivariate data field does not have any anti-correlated regions. It is therefore useful to find an orthogonal presentation which can give a different point of view and which does not tend to produce artificial multi-poles. Such an alternative orthogonal presentation of the multivariate data field can be given by the VARIMAX criteria, which will be discussed in the following section.

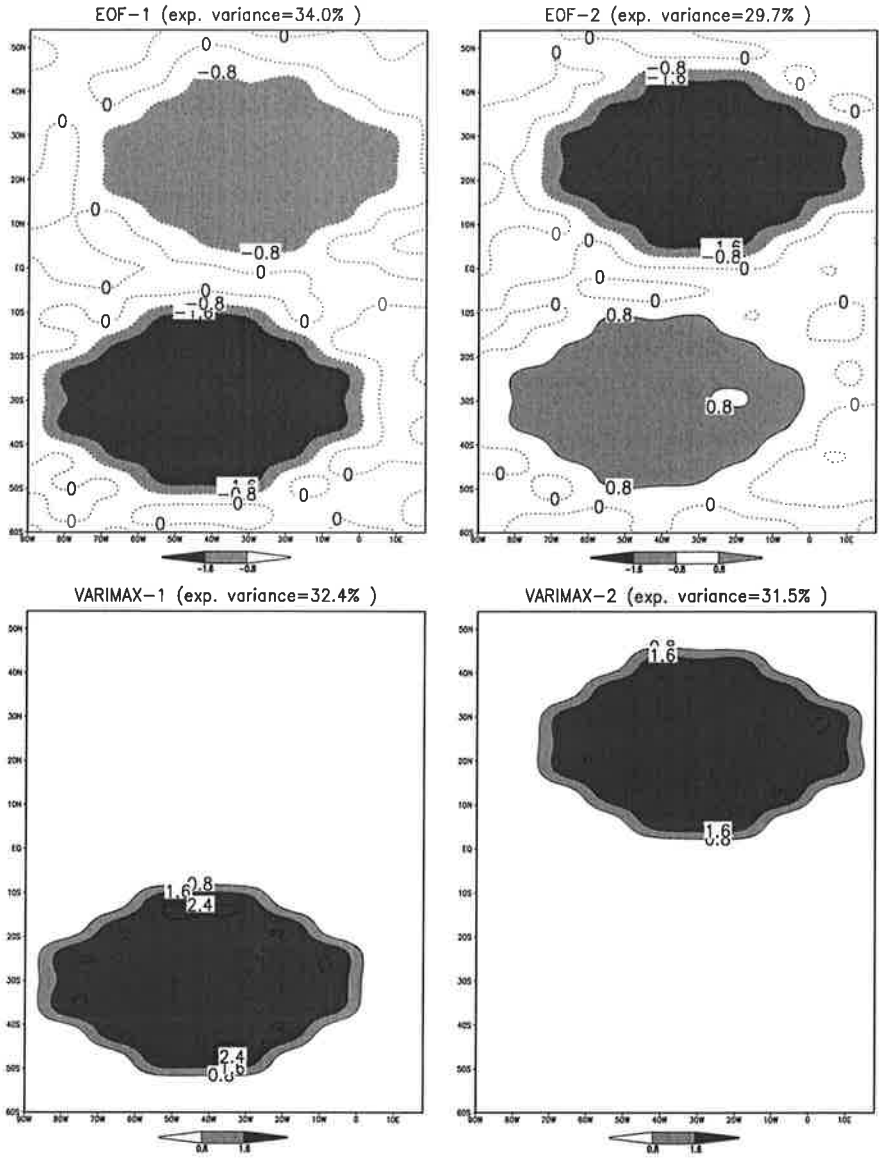

Figure 2.1: Artificial Monte Carlo example to demonstrate the effect of EOF rotations. The two upper plots show the EOF-1 and EOF-2. The lower plots show the two dominant VARIMAX pattern.

2.1.1 The VARIMAX criteria

A basis of a vector space can always be transformed into a different basis by an orthogonal rotation of the basis vectors. The two leading EOFs in the analysis presented above have comparable amounts of explained variances and have therefore to be considered as degenerated EOF eigenvalues. In addition to an ordinary EOF-analysis, a rotated EOF analysis can give a second set of orthogonal basis vectors, which may provide another interpretation. One useful criterion for this analysis is the VARIMAX criterion (Kaiser 1958, Kaiser 1959, and Richman 1986).

The VARIMAX method for rotating EOFs leads to the orthogonal rotation with the highest possible localization of the SST pattern. In other words, if an ordinary EOF-analysis

distributes the variability of one region into different EOF patterns, as into EOF-1 and EOF-2 of our example, the VARIMAX method finds the rotation in which the variability of that region is concentrated in one pattern as much as possible (see Figure 2.1). From a mathematical point of view the two representations of the SST variability are equivalent, but it has to be considered that, from a physical point of view, the different representations of the SST anomalies may lead to different explanations of the underlying physical mechanisms.

In the two lower plots in Figure 2.1 the two dominant VARIMAX patterns of the Monte Carlo field are shown. In the VARIMAX presentation of the Monte Carlo field the two patterns are clearly separated. It can therefore be concluded that the VARIMAX presentation is a better presentation of the multivariate Monte Carlo field than the ordinary EOF presentation. The VARIMAX presentation can always be used to present multivariate data fields, even if the first EOF is clearly separated from the second EOF or if the first EOF is a multi-pole.

In principle the VARIMAX method is always the better presentation of the multivariate data field, even if the EOF eigenvalues are well separated. If the EOF eigenvalues are well separated then the VARIMAX patterns are identical to the EOF patterns, but if the EOF eigenvalues are degenerated than the VARIMAX method creates more localized patterns which are generally more instructive.

2.1.2 Oblique rotations and cluster analysis

The EOF and the VARIMAX patterns are both orthogonal presentations of the multivariate SST record. Orthogonal presentations of the record have the advantage that they are spatially and temporally uncorrelated with each other and that they represent the total vector space of the SST record. The latter may definitively be a good characteristic, whereas the former can be a disadvantage for understanding the physical mechanisms which produces the large-scale SST variability. In principle it has to be considered that if more than one dominant pattern exists in the multivariate data record, it is very likely that the dominant pattern may be spatially well separated, but that such pattern usually interacting with each other and that they are therefore not orthogonal to each other.

In such a case an oblique presentation of the multivariate SST record can give a more insightful picture of the record. In cluster analysis or in oblique rotations of EOFs the multivariate data record is presented in patterns that are not orthogonal and that usually do not represent the total vector space of the data record. But in advantage to the orthogonal presentation the cluster analysis or oblique rotations of EOFs provide the possibility to introduce a subjective view of the data file, which can often be more instructive.

Again a Monte Carlo example can help to understand the nature of the problem. In the former Monte Carlo example the two circular patterns have been constructed as orthogonal patterns. We can now add a third pattern between the two original patterns which is

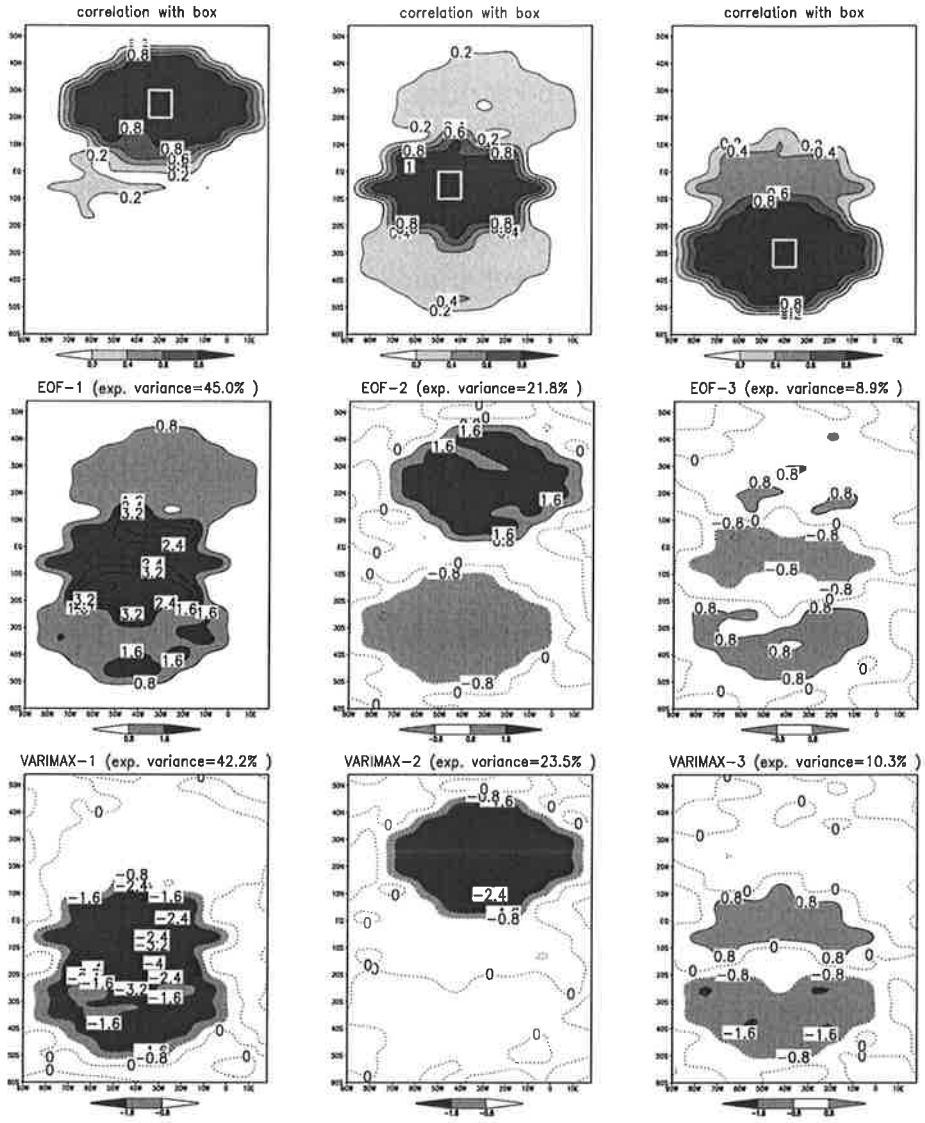

Figure 2.2: Artificial Monte Carlo example to demonstrate the effect of oblique patterns. The three upper plots show the correlation of the field with the averaged field in the rectangular boxes. The three middle plots show EOF-1, EOF-2 and EOF-3 of the field. The lower plots show the three dominant VARIMAX pattern of the field.

correlated with both circular patterns. By construction all three patterns are now not orthogonal to each other anymore.

In the upper row of Figure 2.2 the correlations between the box averaged Monte Carlo field and the Monte Carlo field itself are shown. The correlations clearly indicate that the field consists of three pattern, whereas the pattern in the middle is correlated with the upper and the lower pattern, but the upper and lower pattern are not significantly correlated.

The orthogonal presentation of the EOF analysis (shown in the middle row of Figure 2.2) or the VARMIAX method (shown in the lower row of Figure 2.2) cannot present the dominant pattern of the Monte Carlo field as clear as it is shown in the correlation fields. In both orthogonal presentations one or more patterns suggest that some of the regions of the

Monte Carlo field are anti-correlated, which is not the case.

This Monte Carlo example clearly demonstrates that orthogonal presentations of multivariate data fields are often not the most instructive presentation to understand the connections between dominant patterns. It is often necessary to use different methods to get a clear picture of the dominant modes of variability. In many analyses the best presentation may be achieved by a purely subjective choice of indices or it can be constructed by some kind of cluster analysis criteria or by an oblique rotation of an orthogonal presentation.

In more practically oriented weather forecast analysis the cluster analysis is often chosen to illustrate the dominant modes of variability in the so called 'weather regimes', which can only be defined by cluster analysis, because they are not orthogonal to each other.

2.2 The spectral distribution of SST anomalies

The spectral distribution of the SST variance is the most instructive quantity to understand the basic statistical processes that generate the SST variability. In many analyses the spectral distribution of the SST variance is compared with the spectral distributions of a fitted AR-1 process. By comparing the two distributions visually it is often claimed that the two distributions are different at least at some period.

The following section describes a method that quantifies the difference between the spectral distribution of the SST variance and a fitted theoretical spectral distribution. A similar test has been used by Reynolds (1978) to test the SST in the North Pacific against autoregressive processes.

2.2.1 The test criteria

The basic concept of the following test is described in the German textbook by Schlittgen and Streitberg (1991). They basically describe three different approaches, where the most practical for this work is based on the comparison of the spectral density distribution of the test quantity with the spectral density distribution of the fitted process. It can therefore be considered that the spectral coefficients of the spectra s_i have been determined from the time series of the SST anomalies and that the spectral coefficients of the hypothesis spectra t_i have also been calculated by using the standard deviation and the lag-1 correlation of the time series. I then define the test quantity Q_t as:

$$Q_t = \frac{1}{log(10.0)log(C_{conf})} * \sqrt{\sum_{i=2}^{N} \frac{(log(s_i) - log(t_i))^2}{N-1}} \tag{2.2}$$

Q_t = *test value*

s_i = *spectral coefficient of spectra*

t_i = *spectral coefficient of hypothesis spectra*

N = *number of channels*

C_{conf} = *confidence level of hypothesis spectra (i.e. 95%)*

Equation 2.2 quantifies that the spectral coefficients s_i are random fluctuations around the coefficients of the hypothesis spectra t_i. The test quantity can therefore be interpreted as the integrated error of the spectrum relative to the hypothesis spectrum. This approach is equivalent to the test Reynolds (1978) applied. In principle, the test quantity Q_t is not dependant on the length of the time series because Q_t has been normalized by $log(C_{conf})$, which is the statistical error of the spectral coefficient of the calculated spectrum. However, the time series has to be long enough to determine the spectral coefficients.

The distribution of Q_t, its dependency of the frequency range of the spectrum and the degree of dependence of Q_t to the slope of the hypothesis spectrum have not been calculated analytically, although this may be possible. However, in the textbook by Schlittgen and Streitberg (1991) it is assumed that the distribution of such a test quantity might be difficult to determine and they propose to compare the test quantity with a Monte Carlo distribution of the test quantity. I therefore compare the test results of the SST time series in Section 4.1.4 with a distribution of Q_t that has been based on 1000 time series of Monte Carlo realizations of monthly averaged AR(1)-processes.

2.2.2 Model time series

The output of the simulations is given by monthly mean values, which is the average over all time steps of the numerical integration. If the SST time series of the simulations are tested against a statistical model like the AR(1)-process, it has to be considered that the monthly mean values are the result of an averaging process which changes the spectral distribution of the SST variability.

In Figure 2.3, the spectrum of a Monte Carlo time series of an AR-1 process is shown. In addition, two different spectral distributions have been fitted to the time series based on the standard deviation and lag-1 autocorrelation of the time series. The dashed line is the spectrum of an AR(1)-process and the solid line is the spectrum of a monthly mean averaged AR(1)-process fitted to the time series. It can clearly be seen that the spectrum of the Monte Carlo time series is following the spectrum of the monthly mean averaged AR(1)-process (dashed line) and that the two fitted spectra are significantly different. Therefore the effect of the averaging process has to be taken into account when the spectral hypothesis is tested.

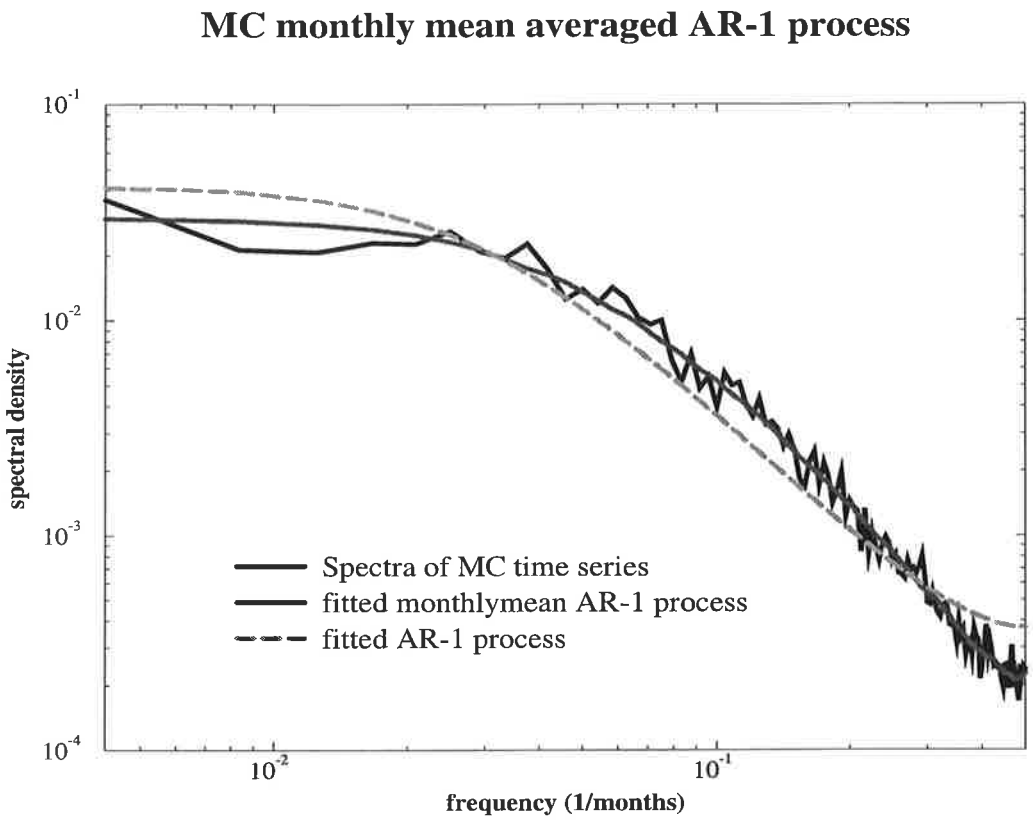

Figure 2.3: The spectral distribution of a monthly mean Monte Carlo AR-1 process compared to two different fitted spectral distributions. See text for details.

In the following chapters the spectra of the monthly mean SST time series will always be tested against a monthly mean averaged AR(1)-process and not against a fitted AR(1)-process.

2.3 Observational data

The observational SST data are based on the GISST-data set which provides gridded monthly mean SSTs for the period 1903 -1994 (Parker et al. 1995). The SST observations are based on in situ measurements from merchant vessels. The global field of the SST for all months was obtained by interpolating the local measurements in space and time. The density of the measurements is strongly variable in space and time, as most measurements are along the main trading routes. Therefore, the quality of the measurements are better in the Northern Hemisphere and is increasing with time.

For the analysis of the midlatitudes in Chapter 4 the data set was interpolated onto a 5.625^o x 5.625^o grid and for the analysis of the tropical Atlantic in Chapter 5 the data set was interpolated onto a 2.8125^o x 2.8125^o grid. Prior to all analyses the linear trend were removed.

2.3.1 Statistical characteristics of observational time series

In section 2.2, it has been shown that the averaging process, applied to produce the monthly mean, changes significantly the spectral distribution of the SST anomalies (see Fig. 2.3). Although, for the simulations, the process of producing the monthly means is the same for all time steps and grid points, it varies significantly in the observations. In the GISST data set, the SST value of a single month at a certain point is an average over an unknown number of measurements, and the time interval between the individual measurements are not known and are likely to be variable. In addition, the single measurements are in situ measurements unlike the values from the models, which represent the exact average of a grid box. This problem increases the uncertainty of the observational SST spectra and introduces complications in the comparison of the observed SST spectra with the simulated SST spectra. Therefore a statistical test as proposed in section 2.2.1 cannot be applied to the observations, or at least the test value Q_t must be significantly increased.

Chapter 3

Description of the models

3.1 Models used in Chapter 5

For the analysis of the tropical Atlantic in Chapter 5 the outputs of four different CGCMs has been discussed. The CGCMs were developed jointly at the Max-Planck-Institut für Meteorologie (MPI) and the Deutsches Klimarechenzentrum (DKRZ), and one model was developed at the Geophysical Fluid Dynamics Laboratory (GFDL). A list of the models is given in Table 3.1. The simulations differ in length, and the resolution of the models are also quite different. Thus, the analyzed CGCMs cover a large part of the parameter space. For more detailed descriptions of the CGCMs refer to the following publications: For the ECHAM3-LSG CGCM, see Maier-Reimer et al. (1993), Roeckner et al. (1992) and Voss (1998). The ECHAM4-HOPE2 CGCM is described in Frey et al. (1997). For the ECHAM4-OPYC CGCM see Bacher et al. (1998) and Roeckner et al. (1996). The CGCM of the GFDL is described in Manabe et al. (1991).

CGCM	time resolution	number of years	spatial resolution
ECHAM4 - HOPE2	annual mean, detrended	118	2.8125^o x 2.8125^o*)
ECHAM4 - OPYC	annual mean, detrended	240	2.8125^o x 2.8125^o*)
ECHAM3 - LSG	annual mean, detrended	700	5.625^o x 5.625^o
GFDL - MOM	annual mean, detrended	1000	7.5^o x 4.5^o
*)The ocean model has a meridional resolution of 0.5^o within the region 10^oN - 10^oS			

Table 3.1: List of CGCMs used in the analysis of the tropical Atlantic.

3.2 Models used in Chapter 4

A list of the simulations that have been discussed for the midlatitude SST variability in Chapter 4 can be found in the Table 3.2. The ECHAM Atmospheric Model has been used in all simulations. ECHAM is a atmosphere general circulation model described by Roeckner et al. (1992). ECHAM has been used in two different versions (ECHAM3 and ECHAM4) and in two different resolutions (T21, T42). In the following, the differences in the atmosphere model will not be discussed and we consider that the differences in the ECHAM versions are not relevant for this analysis.

coupled model	number of years	spatial resolution	short description of Ocean Model
ECHAM4 - HOPE2	118	2.8125^o x 2.8125^o*)	fully dynamical, levels
ECHAM4 - OPYC	240	2.8125^o x 2.8125^o*)	fully dynamical, isopycnal, variable Mixed Layer parameterization
ECHAM3 - LSG	700	5.625^o x 5.625^o	fully dynamical, fixed mixed layer 50meters, levels
ECHAM3 - MIX_{50}	500	5.625^o x 5.625^o	slab ocean, 50meter fixed mixed layer
ECHAM3 - MIX_{season}	300	5.625^o x 5.625^o	slab ocean, seasonal mixed layer
ECHAM3 - $MIX_{dynamic}$	300	5.625^o x 5.625^o	slab ocean, dynamical mixed layer
*) The ocean model has a meridional resolution of 0.5^o within the region 10^oN - 10^oS			

Table 3.2: List of simulations used for the study of the midlatitudes SST variability.

The main differences in the simulations are due to the different ocean models. Therefore, the simulations can be divided into two groups. In the first group we have three coupled models with fully dynamical ocean models and in the second group we have coupled model simulations with slab ocean models. The fully dynamical ocean models try to simulate all physical processes in the ocean. The different models, however, employ different approaches to reach this goal.

In the HOPE and the LSG models, the ocean quantities are organized on z-levels, whereby the spatial and temporal resolutions of the HOPE model are significantly higher. The LSG model has a fixed mixed layer parameterization which is simply realized by an increased mixing in the surface layer, which has a depth of 50 meters, and by integrating the surface

layer with a shorter time step of one day compared to the time step of lower levels of one month. In the HOPE model the mixed layer parameterization is kept more variable by introducing additional mixing at all levels for which the temperature differs from the temperature of the surface level by a prescribed threshold.

The OPYC model has a completely different structure. Here, the physical quantities are calculated on isopycnal levels. The OPYC model also includes a dynamical mixed layer model, which determines the depth and the temperature of the mixed layer. Therefore, the OPYC model is the only fully dynamical model in which the mixed layer depth is a dynamical quantity.

All three simulations exhibit El Niño-like behavior in the tropical Pacific. The El Niño-like variability simulated by the HOPE and OPYC models is much stronger than that in the ECHAM3-LSG model. However, the ECHAM3-LSG simulation has the advantage that the setup of the simulation is identical to the setup of the slab ocean simulations, whereby only the ocean model has been exchanged. For more detailed descriptions of the CGCMs the reader is refereed to the following publications: For the ECHAM3-LSG CGCM see Maier-Reimer et al. (1993), Roeckner et al. (1992) and Voss (1998). The ECHAM4-HOPE2 CGCM is described in Frey et al. (1997). For the ECHAM4-OPYC CGCM see Bacher et al. (1998) and Roeckner et al. (1996).

The general disadvantage of the fully dynamical ocean models is that it is difficult to determine which processes of the ocean models are relevant for certain structures of the variability. It is therefore necessary to compare the fully dynamical ocean models with ocean models that include fewer processes. From the differences between the fully dynamical ocean models and the simpler ocean models, one can determine the relevant processes for certain characteristics of the variability. Therefore, we have conducted three experiments with so called 'slab' ocean models. The three different slab ocean models will be described in the following section.

3.3 The slab ocean models

The basic idea of a slab ocean model is that the grid points of the ocean model are not interacting with each other, and that the SST variability for each point of the ocean is forced by the local interaction with the atmosphere. Such a model is a zero or one dimensional model, because it resolves only the vertical direction. Horizontal ocean dynamics such as advection by currents and waves are not simulated. The mean state of the ocean, which is strongly dependant on ocean currents, can therefore not be simulated correctly and must be introduced as a given climatology. However, a zero or one dimensional model is a good model to investigate different characteristics of a complex system, because the interactions in the model are kept very simple and different physical concepts can easily be introduced.

The Null hypothesis of SST variability in the midlatitudes, described by Hasselmann's

stochastic climate model (1976), assumes that the SST variability is well described by the integration of the atmospheric heat flux with the heat capacity of the ocean's mixed layer. All three slab ocean models simulate the SST variability by integrating the atmospheric heat flux with the heat capacity of the mixed layer, while the MIX_{50} slab ocean model exactly simulates the Null hypothesis of Hasselmann. In the MIX_{season} and $MIX_{dynamic}$ models we have considered a few characteristics which may be relevant for the SST variability in the midlatitudes but are not considered by the MIX_{50} model.

3.3.1 MIX_{50}

The MIX_{50} slab ocean model is the simplest of the three slab ocean models used in this study. The complete ocean model is described by equation [3.1] for ocean points without sea-ice. A simple sea-ice model is included in all slab ocean models, but we shall not discuss the regions with sea-ice extent. The equation [3.1] represents the realization of the Hasselmann stochastic climate model, in which the SST variability is only forced by the atmosphere.

$$\frac{d}{dT}SST = \frac{1}{(C_p \rho_{water} d_{mix})} * F_{atmos} + \Delta T_{clim} \tag{3.1}$$

C_p = *specific heat of sea water*

ρ_{water} = *density of seawater*

d_{mix} = *depth of mixed layer*

F_{atmos} = *net atmospheric heat flux*

ΔT_{clim} = *climatology temperature correction*

The only free parameter in this equation is the mixed layer depth d_{mix}, which was chosen to be 50 meters for all points. This value is roughly the global mean value for the mixed layer depth as was determined from the observations by Levitus from the observations (1982).

3.3.2 MIX_{season}

The MIX_{season} model is exactly the same model as the MIX_{50} model, but a seasonally dependant mixed layer depth d_{mix} is used. In the midlatitudes the depth of the mixed layer has a pronounced seasonal cycle. A theoretical study by Lemke (1984) has shown that a seasonal heat capacity of the ocean alters the spectrum of an AR(1)-process. According to equation [3.1] a change in the mixed layer depth must have an effect on the SST variability. The seasonal cycle of d_{mix} has been determined by equation [3.2] by using the 50 years mean values of the $MIX_{dynamic}$ model for the parameters of the right hand side of the equation.

$$d_{mix}(MIX_{season}) := \frac{H_q d_{mix}}{d_{mix} + 1.5H_p} \tag{3.2}$$

The seasonal cycle has been defined in this way, to create a the climatology of the mixed layer depth in the MIX_{season} model which is consistent with that of the $MIX_{dynamic}$ model. In equation 3.1, the change in SST is proportional to $1/d_{mix}$, while in equation 3.7, the change in SST is proportional to $H_q d_{mix}/d_{mix} + H_p$. In equation 3.2 a factor 1.5 for H_p has been introduced to reduce somewhat the mixed layer depth in the MIX_{season} model. This is done to account for the different structures of the equations 3.1 and 3.7. The mean mixed layer depth d_{mix} over all ocean points between 20^oN and 60^oN over the whole year accounts to 52 meters and for summer month to 26 meters and for the winter months to 99 meters (see also Fig. 3.3).

3.4 The $MIX_{dynamic}$ model

The ocean in the midlatitudes exhibit some characteristics that may influence the SST variability which are not captured by the Null hypothesis or the MIX_{50} slab ocean model. To further investigate the large-scale structures of the SST variability in midlatitudes, it can be assumed that the MIX_{50} ocean model can be improved in such a way that the model produces the main characteristic of the SST variability. The characteristics which may be important for the SST variability are:

1. The mixed layer interacts with the sub-mixed layer ocean, which in general has a much colder temperature than the mixed layer. This temperature difference may have a damping effect on the SST variability.

2. The depth of the mixed layer has a pronounced seasonal cycle and the depth of the mixed layer is a dynamical quantity which is determined by the state of the ocean and by the atmospheric forcing.

3. The sensitivity of the ocean to the atmospheric forcing is dependant on the strength of the wind. On stormy days, the ocean does not just integrate the atmospheric heat fluxes as on calm days, but it also mixes the upper ocean significantly so that sub-mixed layer water is entrained into the mixed layer.

These characteristics of the local ocean-atmosphere interaction in the midlatitudes can be included in the structure of a slab ocean model.

3.4.1 The dynamical ocean mixed layer model equations

In addition to the MIX_{50} and MIX_{season} models, a new equation to determine the value of the mixed layer depth d_{mix} at each time step of the ocean model is introduced. Karraca

and Mueller (1991) have used a Kraus and Turner type model (1967) to determine d_{mix} at different locations of the northern oceans by using the observed atmospheric heat fluxes and wind stresses. I implemented this model into the $MIX_{dynamic}$ ocean model to determine SST and d_{mix}.

$$R_0 = \int_0^{D_d} (T(h) - T_0)dh =: T_m H_q \tag{3.3}$$

$$R_1 = \int_0^{D_d} h(T(h) - T_0)dh =: R_0 H_p \tag{3.4}$$

$$F_q = \dot{R_0} = \frac{1}{(C_p \rho_{water})} F_{atmos} \tag{3.5}$$

$$F_p = \dot{R_1} = C_1 C_{wind} \vec{\tau^3} + C_2 H_p F_q \tag{3.6}$$

The diagram in Figure 3.1 illustrates the principle of the Kraus and Turner type ocean mixed layer model and introduces the new parameters. The integral R_0 in equation 3.3 determines the effective heat capacity of the ocean, while the integral R_1 in equation 3.4 determines the potential mechanical energy of the ocean due to the density distribution of the upper ocean. In contrast to equation 3.1, the heat capacity of the mixed layer and, additionally, part of the thermocline of the upper ocean are considered for the integration of the atmospheric heat fluxes. Based on the two integrals R_0 and R_1, the state of the ocean can be determined for each time step. Atmospheric mechanical energy input F_p and the atmospheric buoyancy flux F_q will lead to a change in the two integrals R_0 and R_1, as it is described by the equations 3.5 and 3.6. In the original Kraus and Turner type ocean mixed layer the atmospheric buoyancy flux F_q is calculated with salinity and temperature changes. However, in the model only the influence of the temperature changes are considered, which reduces the atmospheric buoyancy flux to the atmospheric heat flux times a constant and also simplifies the integrals R_0 and R_1 to the expression seen in equation 3.3 and 3.4.

$$\frac{d}{dT} SST = \frac{F_q(d_{mix} + H_p) - F_p}{d_{mix} H_q} + \frac{F_{ocean}}{(C_p \rho_{water} d_{mix})} + \Delta T_{clim} \tag{3.7}$$

$$F_{ocean} = C_{vo} * (T_c - SST) \tag{3.8}$$

$$\frac{d}{dT} d_{mix} = \frac{F_p - H_q F_q}{d_{mix}(SST - T_0 - \frac{SST - T_d}{\Theta})} + \Delta d_{clim} \tag{3.9}$$

$$\Theta = ln(\frac{SST - T_0}{T_d - T_0}) \tag{3.10}$$

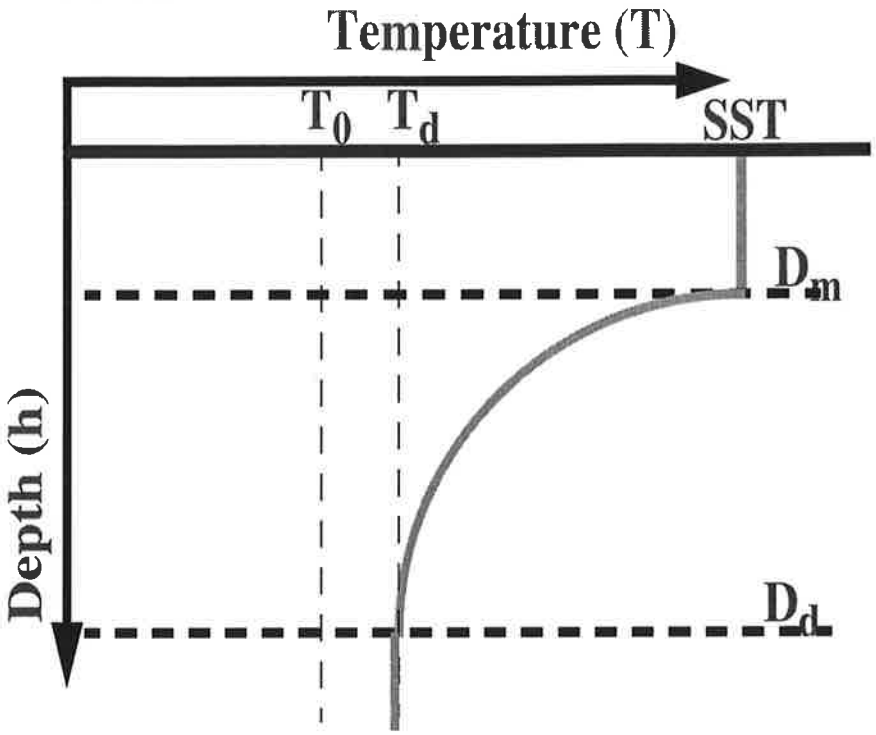

Figure 3.1: Schematic diagram illustrating the $MIX_{dynamic}$ mixed layer ocean model.

F_q	=	*surface buoyancy flux*
F_p	=	*mechanical energy input*
H_q	=	*effective mixed layer depth*
H_p	=	*reduced center of gravity*
ΔT_{clim}	=	*climatology temperature correction*
Δd_{clim}	=	*climatology mixed layer depth correction*
C_{vo}	=	*coupling parameter for the vertical heat exchange between the mixed layer and the sub-mixed layer ocean*
T_c	=	*constant reference temperature*

3.4.2 Boundary conditions and limitations of the $MIX_{dynamic}$ simulation.

Equations 3.7 and 3.9 determine the changes in SST and in mixed layer depth d_{mix}, respectively. For the integration of the equations 3.7 and 3.9 in the $MIX_{dynamic}$ simulation, a few boundary conditions and modifications of the Kraus Turner type mixed layer model have to be introduced.

Similar to Karraca and Mueller (1991), the conditions of the sub-mixed layer ocean has been kept as simple as possible. Therefore, the temperature profile between the SST, T_d

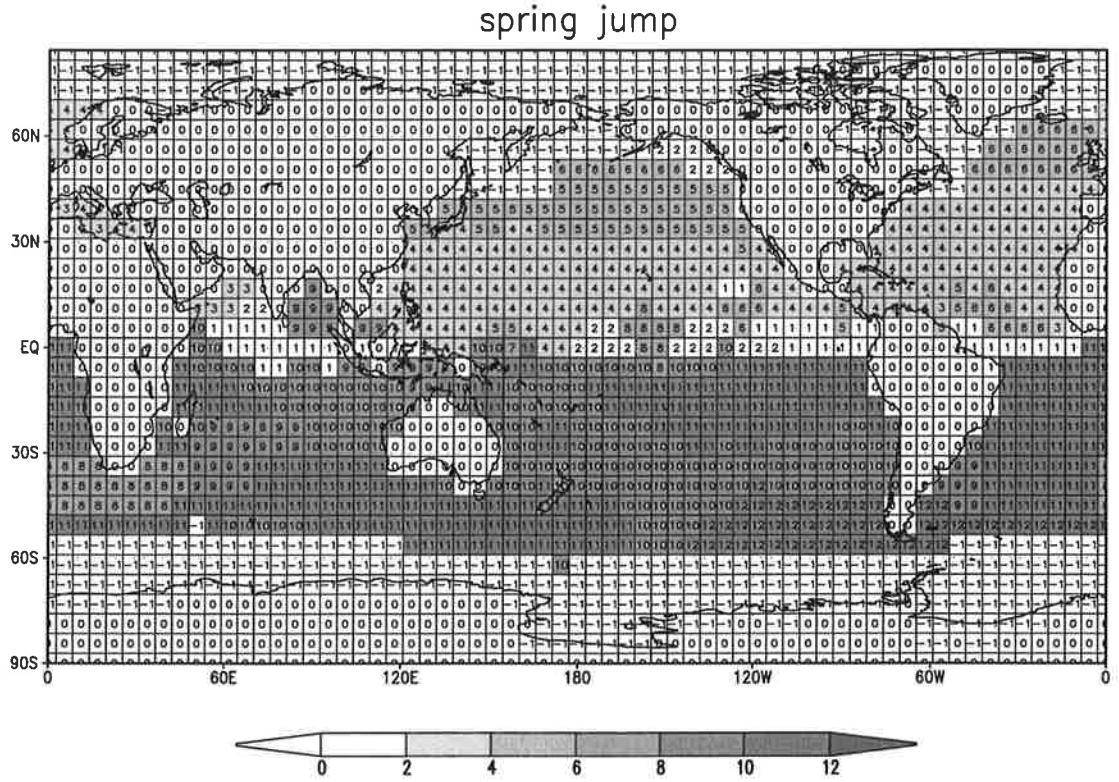

Figure 3.2: The climatology of the 'spring jump'. The values are the month in which the mixed layer depth is reset to a climatology value. Ocean points with -1 are not calculated with the dynamical mixed layer ocean model.

and T_0 has been defined as an exponential decrease. The temperature T_d was chosen to be constant and taken from the annual mean Levitus climatology and the depth $D_d = 400m$. Therefore the mixed layer depth is confined to range $10.0m < d_{mix} < 400m$. The temperature T_0 has been chosen to be $T_d - 0.05C^o$.

The surface buoyancy flux is only calculated by the atmospheric heat flux. Therefore the temperature T_d has to be smaller than the SST for all time steps. This is a principle problem of this model, which will lead to several problems in calculating the SST and the mixed layer depth and which has to be corrected by introducing some corrections to the dynamical equations . The temperature T_d has been corrected by setting $T_d = min(T_d(Levitus), SST(clima) - 2.0)$. This correction is basically effecting ocean points in the high latitudes of the oceans basin, where the winter SST gets colder than the sub-mixed layer ocean temperature.

In principle equation 3.9 should simulate the seasonal cycle of the mixed layer depth. However, the lack of salinity in the buoyancy calculation and the general problem of the Kraus Turner type model in simulating the fast detrainment of the mixed layer during the spring period, makes the seasonal cycle of the mixed layer depth unrealistic and the annual cycle of the mixed layer depth is in general not closed. This means that the mixed layer depth after one year of integration is deeper than at the start of the year. Therefore, a climatological mixed layer depth correction Δd_{clim} in equation 3.9 was introduced , which is

chosen to correct the mixed layer depth d_{mix} climatology to be equal to the Levitus mixed layer depth climatology. In Figure 3.3 the seasonal climatology of the mixed layer depth is shown.

In order to correct for long term trends in the mixed layer depth, which I consider to be a model artifact, the mixed layer depth is resetted at a fixed time step during the spring period to a climatological value. Equation 3.9 is in general not able to simulate the fast detrainment of the mixed layer as it is observed during the spring period in the midlatitudes. The 'spring jump' occurs at the first day of the month, in which the decrease of the Levitus mixed layer depth climatology is strongest. The climatology of the 'spring jump' is shown in Figure 3.2.

These boundary conditions and corrections are not sufficient to lead to a stable integration of the dynamical equations for points of the ocean that are frequently covered by sea ice or for regions of the higher latitudes which have a mixed layer that is mainly driven by the vertical salinity distribution. For all those points the $MIX_{dynamic}$ simulation has been reduced to the simple MIX_{50} model. These ocean grid points have the value -1 in Figure 3.2.

In addition to the Kraus Turner type model of the mixed layer, I also wanted to introduce a heat flux between the mixed layer and the sub-mixed layer ocean. I therefore introduced the ocean heat flux F_{ocean} in equation 3.7, which effectively damps the SST variability.

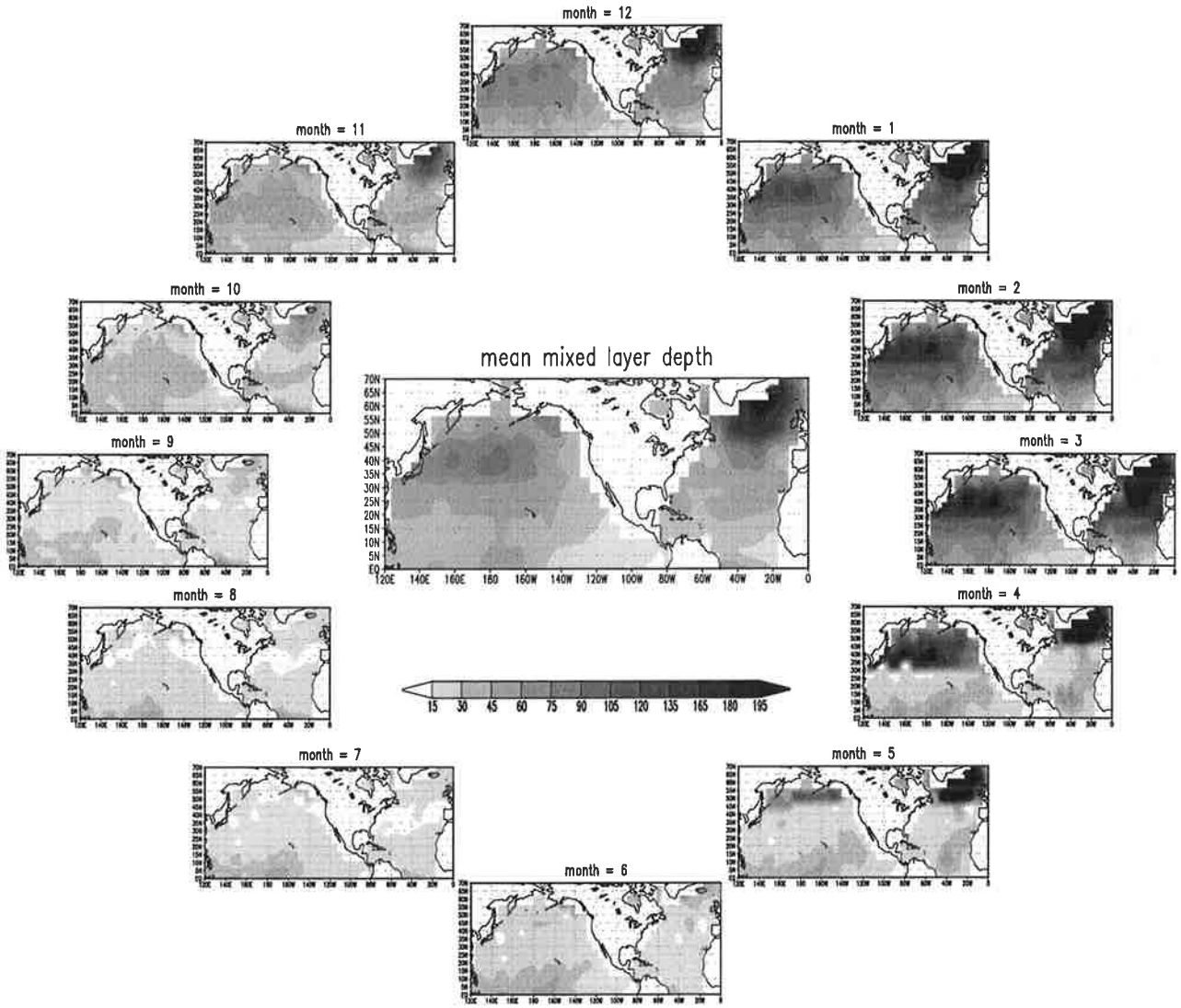

Figure 3.3: The climatology of the mixed layer depth as it is simulated in the dynamical mixed layer model $MIX_{dynamic}$.

Chapter 4

Midlatitude SST variability

The stochastic climate model introduced by Hasselmann (1976) attempts to explain the mechanism of natural climate variability, by dividing the climate system into a fast and a slow system. In this model the atmosphere is the fast system which is represented by random noise. The variability of the ocean, which is regarded as the slow component of the climate system, is explained by the integration of the atmospheric noise. In this picture the ocean is just a passive part of the climate system, which only amplifies the long-term variability, due to its large heat capacity, but dynamical processes in the ocean are not considered.

The resulting stochastic model of SST variability is described by an auto regressive process of the first order (AR(1)-process), which is the simplest statistical model that can be applied to a stationary process. The stochastic climate model introduced by Hasselmann is therefore often chosen as the Null hypothesis of SST variability.

Frankignoul and Hasselmann (1977) have shown that the observed interannual SST variability in the midlatitudes is consistent with this Null hypothesis. In a more recent study Hall and Manabe (1997) have shown that the SST variability at some locations in the midlatitudes cannot be adequately explained by an AR(1)-process. They argue that the SST variability in these locations is influenced by meso-scale eddies. A comprehensive overview on the interannual SST variability in midlatitudes is given in Frankignoul (1985).

In a recent work Sutton and Allen (1997) have found some indication that the SST variability in the northern Atlantic may be predictable on decadal time-scales, due to the advection of temperature anomalies within the Gulf stream extension. However, the origin of such variability cannot by determined by observations alone. Due to the limited length of observed SSTs it may be instructive to study decadal SST variability in coupled general circulation models (CGCMs). In these simulations many different coupled ocean-atmosphere modes have been found, which lead to increased SST variability on decadal time-scales (e.g., Latif and Barnett (1994); Manabe and Stouffer (1996); Gu and Philander (1997)). A comprehensive overview of this can be found in Latif (1998).

This chapter takes a closer look at the Null hypothesis of midlatitude SST variability, by comparing coupled models employing different ocean models. It will be tested whether

the large-scale features of the observed SST variability can be simulated by a simple global slab ocean-atmosphere coupled model, which can be regarded as a numerical realization of the Null hypothesis (AR(1)-process) of Hasselmann's simplest stochastic climate model. This question will be addressed by comparing the results obtained from the simple slab ocean model with the observations and with a hierarchy of different ocean models coupled basically the same atmosphere model. Such a comparison may reveal, the internal processes in the ocean, which are important for SST variability on seasonal to decadal time-scales.

This chapter is organized as follows: In the first section a comparison of the SST variability in the different models and in the observations will be presented. This comparison is focused on the standard deviation and the spectral distribution of SST variability. The results of the model comparison lead to the discussion of the sensitivity of SST variability to different physical processes in section 4.2. I shall then present a study of the seasonal predictability of midlatitude SST anomalies in the $MIX_{dynamic}$ model in section 4.3. The chapter will be concluded with a summary and discussion. The work presented in this chapter will be published in the Journal of Climate by Dommenget and Latif (submitted).

4.1 Model comparison

A description and list of the models discussed in this chapter is given in Chapter 3. The comparison of the different simulations with each other and with the observations will be focused on the Null hypothesis of SST variability. The comparison should show whether the large-scale features of SST variability can be explained by the Null hypothesis or if other processes are important. The large-scale features of SST variability are characterized by the following three quantities:

1. The standard deviation of SST anomalies

2. The redness of SST spectra

3. The spectral distribution of SST anomalies

The standard deviation of SST anomalies is the most important characteristic for the comparison, since it is a relatively robust quantity and not significantly affected by the interpolation of the observations in space and time. The other two characteristics cannot be compared with the observations in all details, because the calculation of the redness and the spectral distribution are affected by the interpolation and averaging of the SST data, as it is done to produce global observed SST fields. The different statistical characteristics of the observed data relative to the simulated data are discussed in section 2.3.1.

4.1.1 The standard deviation of SST anomalies

Figure 4.1 shows the standard deviations of the monthly mean SST anomalies for the different simulations and for the observed SST obtained from the GISST data set from 1903 to 1994 (Parker et al. 1995). Figure 4.1 shows the zonally averaged standard deviations for all the models and the observations. Only ocean points that do not frequently exhibit the coverage of sea ice have been taken into account.

The main spatial structure of the observed SST standard deviation is an increase of the variability from the lower latitudes up to about 40^oN. The absolute maximum of variability is reached here and the standard deviation decreases towards higher latitudes. The maximum of the SST standard deviations in the Pacific as well as in the Atlantic seem to be tied to the regions were the storm tracks are active. The simulations with fully dynamical ocean models and the $MIX_{dynamic}$ simulation are very similar to the observations. Only the two simulations MIX_{50} and MIX_{season} are quite different from the observations, with no absolute maximum at 40^oN, and a monotonic increase of the standard deviation of SST with latitude. Overall, the variability of these two models is significantly larger than in all other data sets, while the mismatch becomes largest polward of 40^oN.

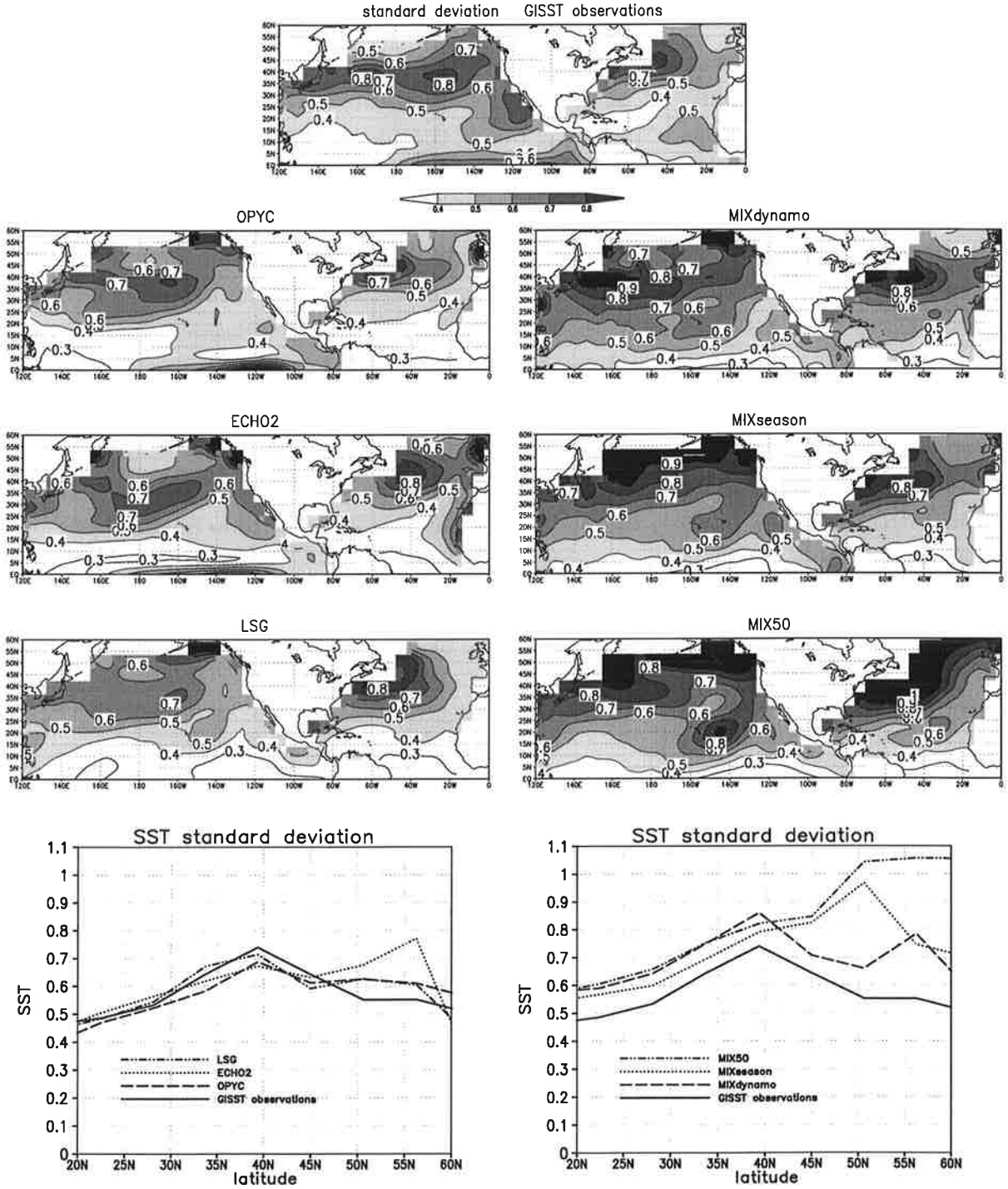

Figure 4.1: The upper plots show the standard deviations of the monthly mean SST anomalies for the different simulations and the observations. In the two lower plots the zonally averaged standard deviations of the monthly mean SST anomalies of the fully dynamical ocean models (left) and of the slab oceans (right). The GISST observations are shown for comparison.

4.1.2 The redness of SST anomalies

The standard deviations of SST anomalies do not alone describe the large-scale character of SST variability. An important feature of SST variability is the increase of the variance in the power spectra with period, which is the so called 'redness' of the spectra. If one considers that the spectra of SST anomalies are basically following an AR(1)-process, than the redness can be estimated by the lag-1 autocorrelation. The spectral density function $C(\omega)$ of an AR(1)-process is determined by equation 1.1. Here the increase of the variance of an AR(1)-process with the period is only a function of the lag-1 autocorrelation a in equation 1.1. The 'redness' Q_{red} can therefore be defined as:

$$Q_{red} = \frac{1}{(1-a)^2} \tag{4.1}$$

Q_{red} = *redness of SST*

a = *lag-1 correlation based on monthly mean time series*

In Figure 4.2 the redness Q_{red} is shown for all models and the observations. It is found that the western part of the oceans have in general a smaller redness than the eastern part of the ocean. This feature is also well captured in the MIX_{50} simulation, which has by construction a 50 meter mixed layer depth for all ocean points and therefore no spatial structures in the ocean. It therefore has to be concluded that the spatial structures of the redness arise from the spatial differences in the atmospheric heat flux, which is relatively large near the western boundary and relatively small at the eastern boundary. The differences in the atmospheric heat flux may mainly stem from the differences in the mean state of the SST, which are a result of the large-scale ocean circulations.

The comparison of the observations to the simulations obviously shows that the redness of the observed SST variability is significantly smaller than in the simulations. In order to understand the differences in the redness, the spectra for all points of all data sets have been calculated to determine the decadal SST and higher frequency variances, which I shall call "the low-frequency variability" and "high-frequency" variances, respectively. The low-frequency variability has been defined as the spectral variance of the SST at about 20 years periods and the high-frequency is defined by the spectral variance of the monthly periods. In Figure 4.2 the zonally averaged low-frequency variability, redness and high-frequency variance are shown.

The comparison of the different simulations with the observations shows that the largest differences in the SST variance are at the high-frequency time-scale, while the differences in the low-frequency SST variance are much weaker. It can therefore be concluded that the smaller redness of the observed SST variability compared to the simulations is mainly due to the fact that the high-frequency variability in the observations is significantly larger than in

all simulations. One possible reason for the significantly larger high-frequency variability in the observations is discussed in section 2.3.1. In this section, the differences in the statistical characteristics between the observations and the simulations are considered.

In addition to the statistical problems discussed in section 2.3.1, the lag-1 autocorrelation of the observed SST variability during 1903 - 1950 is significantly smaller than that during 1950 - 1994. I assume that this difference is a result of the lower density of SST measurements during this period. I therefore based my analysis of the lag-1 autocorrelation of the observations on the time period 1950 - 1994. However, to calculate the spectral density at decadal time-scales the whole time range from 1903 - 1994 was used. Although the larger high-frequency variability in the observations relative to all simulations is partly due to statistical reasons, I discuss the differences between the simulations and the observations while keeping in mind these problems.

The redness simulated by the fully dynamical ocean models, the $MIX_{dynamic}$ model and that of the observations are of the same order. However, one has to keep in mind that the redness of the observed SST anomalies may be reduced by the different statistical characteristics noted above. The rednesses of the MIX_{50} and MIX_{season} simulations are significantly larger than in the observations and all other simulations, whereby the larger rednesses of the MIX_{50} and MIX_{season} simulation can mainly be explained by the much smaller SST variances on the high-frequency time-scale, shown in the right plot of Figure 4.2. The differences in the low-frequency or decadal range are, on the other hand, much smaller.

The more realistic redness of the $MIX_{dynamic}$ simulation compared to the MIX_{50} and MIX_{season} simulations is mainly due to the introduction of the ocean heat flux F_{ocean} in equation 3.7, which damps the SST variability. It can therefore be assumed that the SST variability is significantly damped on seasonal to interannual time-scales by the heat exchange of the mixed layer with the sub-mixed layer ocean.

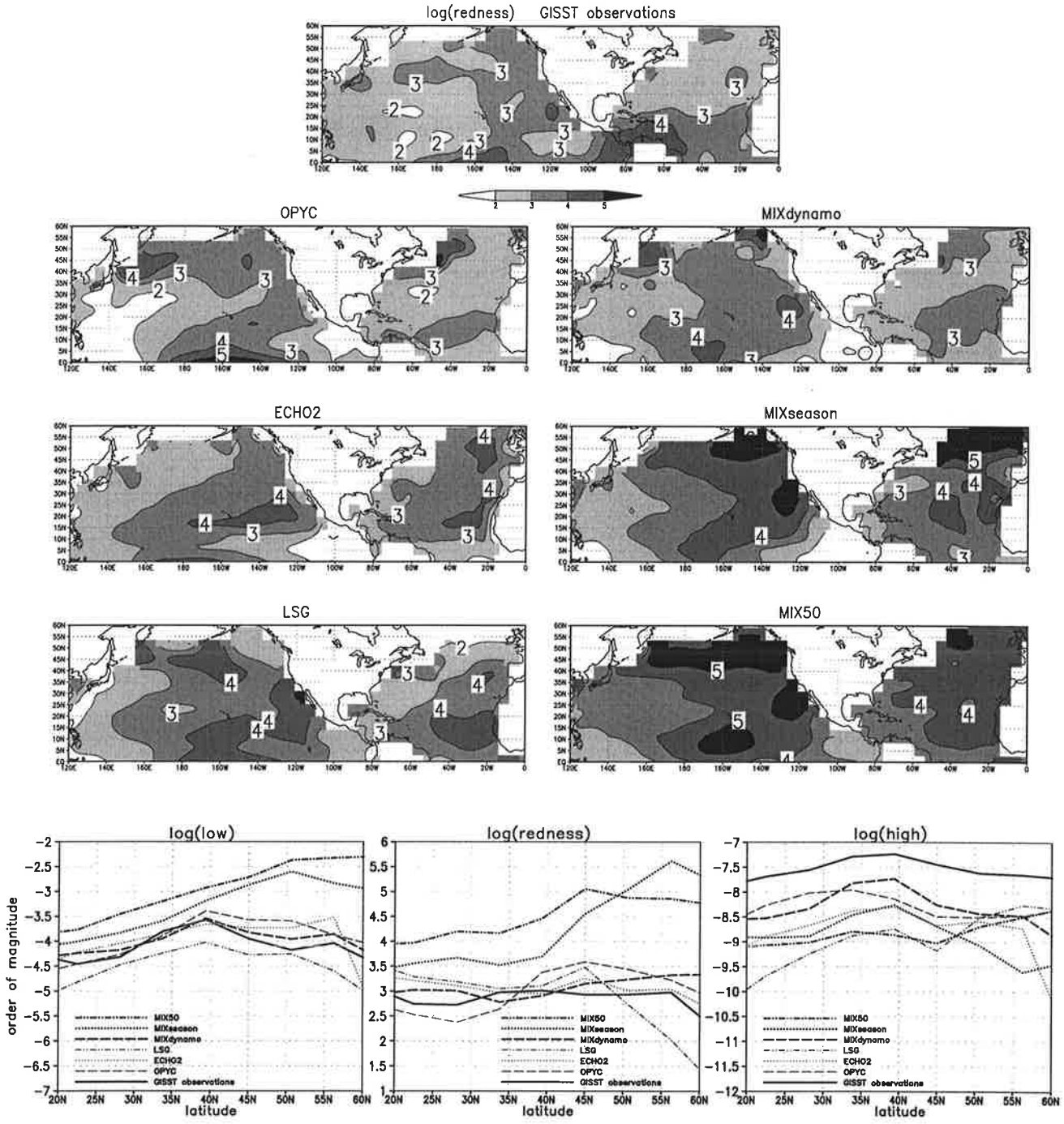

Figure 4.2: The upper plots show the 'redness' of the monthly mean SST anomalies for the different simulations and the observations. In the lower row the left plot shows the zonally averaged low-frequency (1/20yrs) variance of the SST anomalies and the right plots shows the high-frequency variance (1/2months) of the different models and the observations. The middle plot shows the zonally averaged 'redness' of the monthly SST anomalies. See test for details.

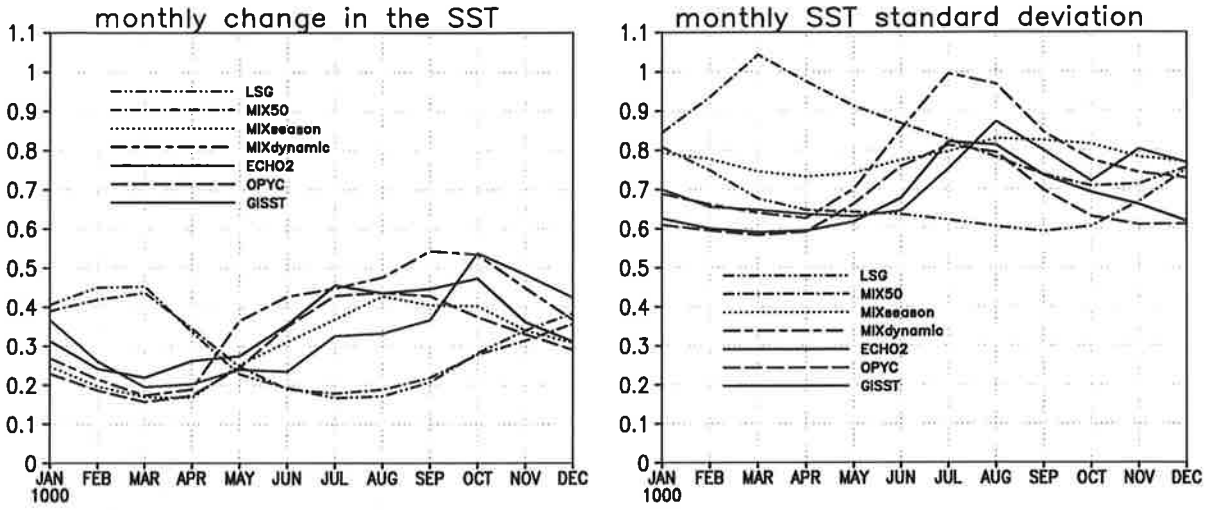

Figure 4.3: The mean $\frac{d}{dt}SST$ for each month (left plot) and the standard deviation of the SST anomalies for each month (right plot) for all simulations and the observations.

4.1.3 The seasonally varying persistence of the SST anomalies

In summer, the mixed layer depth in midlatitudes amounts to about 20 meters, while in winter the mixed layer depth is greater than 150 meters. It has to be considered that the varying mixed layer depths will lead to different integrating processes in the different seasons. A larger mixed layer depth d_{mix} will lead to larger SST persistence. Therefore, the lag-1 autocorrelations of the SST anomalies or the persistence of the SST should be smaller in summer than in winter.

In Figure 4.3, the mean $\frac{d}{dt}SST$ for each month and the standard deviations of the SST anomalies for each month are shown for all simulations and the observations. It can clearly be seen that the observations, the $MIX_{dynamic}$, MIX_{season}, ECHO2 and the OPYC simulations all have in common that the change in SST is relatively small in winter and strongest in the late summer. The seasonal behavior of the mean $\frac{d}{dt}SST$ is also reflected in the standard deviations of the SST which is strongest in late summer. In contrast to this the MIX_{50} and LSG simulations show the opposite behavior.

The $MIX_{dynamic}$, MIX_{season}, ECHO2 and the OPYC models employ a parameterization of the mixed layer depth, which includes the seasonal cycle of the mixed layer depth, while the MIX_{50} and the LSG simulations do not simulate the seasonal cycle of the mixed layer depth. From this comparison it has to be concluded that the seasonality of the mixed layer depth is an important factor for the simulation of midlatitude SST variability. Models that do not include the seasonal cycle of the mixed layer depth will simulate the SST variability with the wrong seasonal characteristics.

The seasonal difference in the persistence of the SST anomalies between winter and summer indicates that the processes that produce the winter SST variability are significantly different from those which produce the summer SST anomalies and should therefore by analyzed separately. Most investigations take this into account and focus their study on the summer or the winter separately. It is therefore important that the model simulations, on which these investigations are based, include the seasonal cycle of the mixed layer depth.

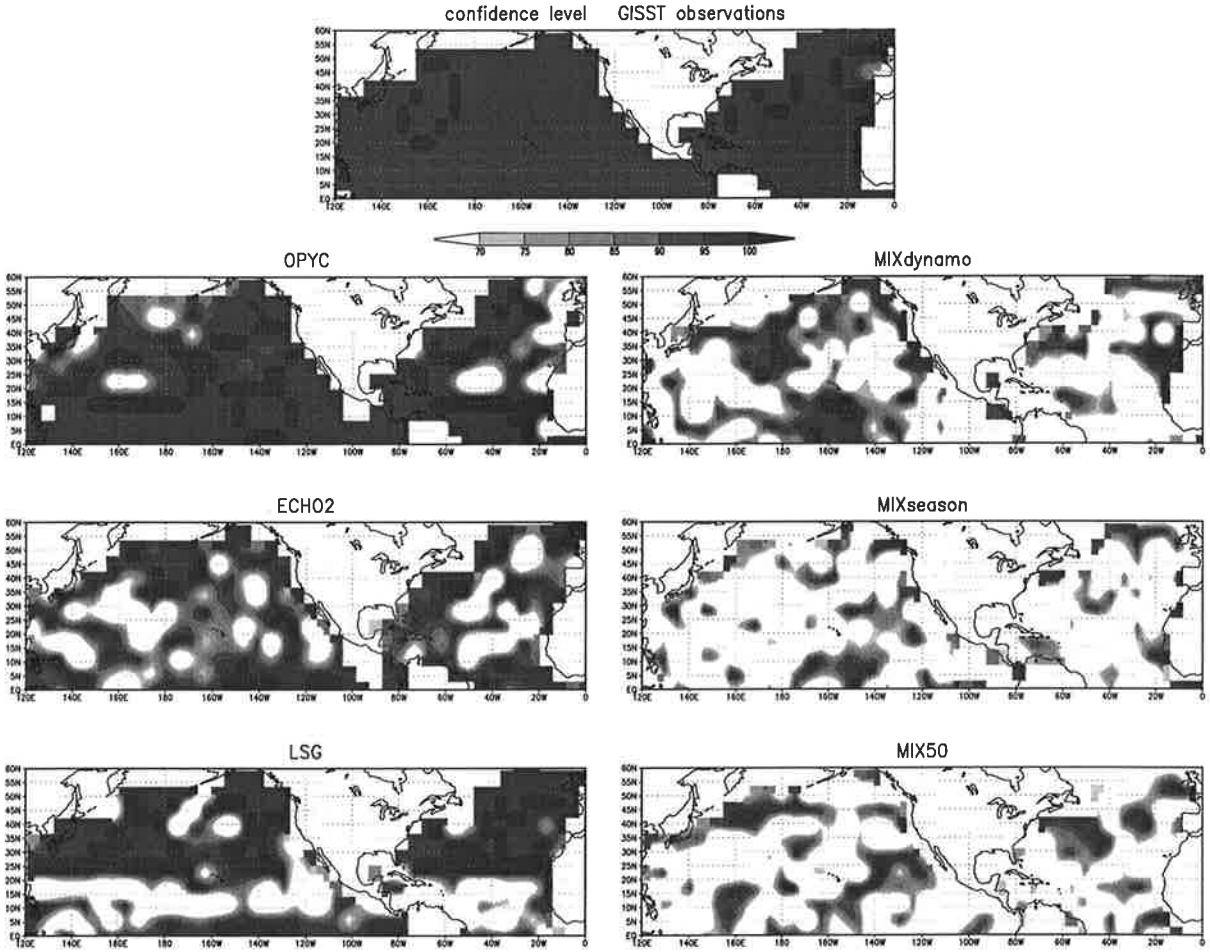

Figure 4.4: The confidence level based on a Monte Carlo distribution of the test value Q_t for the different simulations and the observations.

4.1.4 The test for an AR-1 process

Based on the spectral test described in section 2.2.1 one can define a confidence level for the hypothesis that the SST spectra are not in statistical agreement with a monthly averaged AR(1)-process. The confidence levels for the different simulations and the observations are shown in Figure 4.4. The confidence level of the observations is only shown for the sake of completeness of the analysis, while one has to keep in mind that the confidence level based on the test value Q_t is not the real confidence level for the observed data sets ,due to the different statistical characteristics of the observations as discussed in section 2.3.1. It has to be expected that the real confidence level will be smaller.

The confidence levels of the MIX_{50} and the MIX_{season} simulations are for the most part less than 65%, which indicates that the SST variabilities are basically consistent with

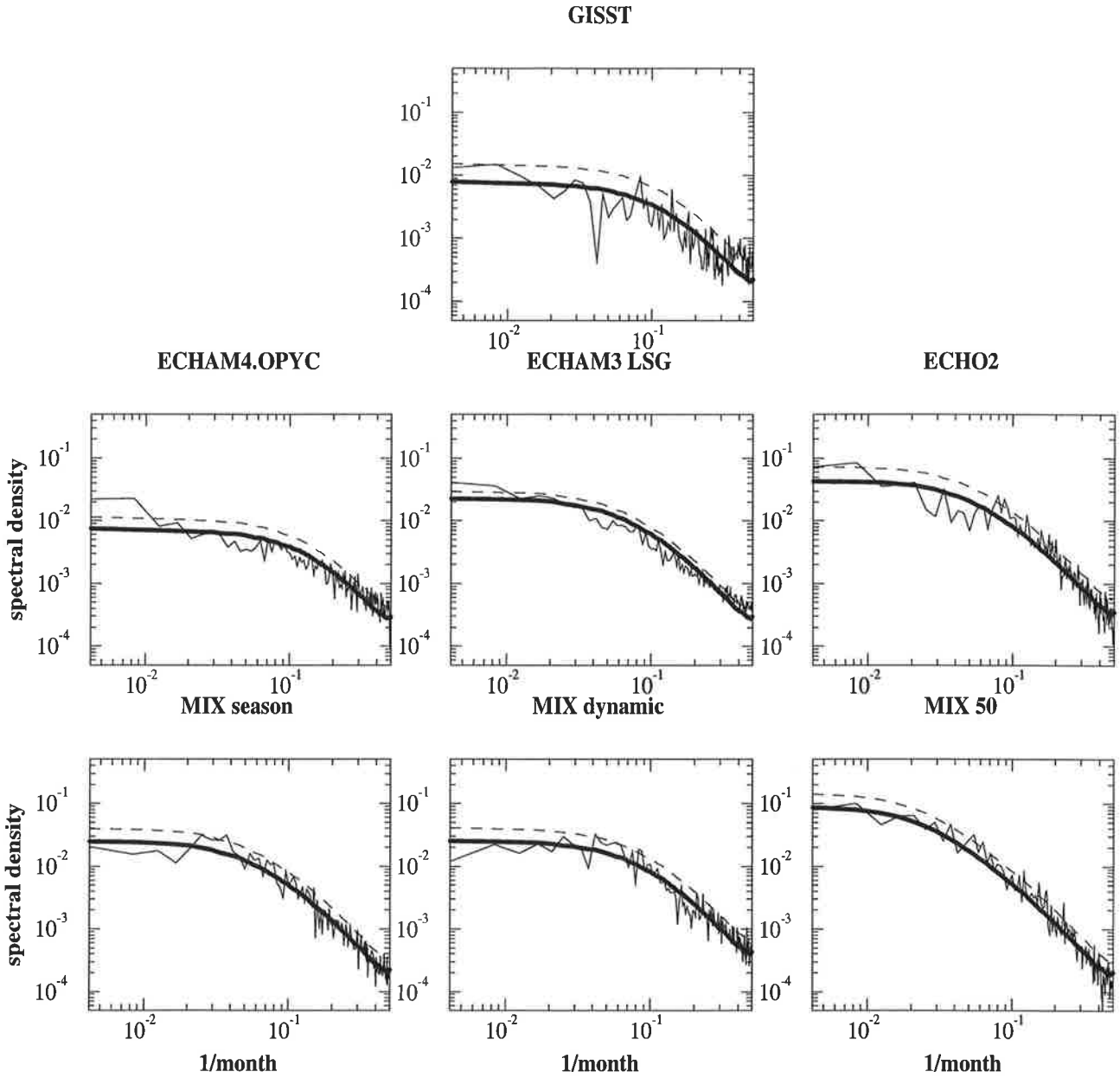

Figure 4.5: Spectra of the SST anomalies (at the location: 35°N, 40°W) compared to the fitted spectral distributions of a monthly averaged AR(1)-process for the different simulations and the observations.

an AR(1)-process. This supports the idea behind Hasselmann's stochastic climate model and is in clear contrast to the simulations with the fully dynamical ocean models, which all have much higher confidence levels ($> 95\%$). This indicates that the ocean dynamics, which are only included in the fully dynamical ocean models, clearly alter the spectra of the SST anomalies to a spectral distribution that is not consistent with an AR(1)-process.

In order to see which feature of the SST spectra leads to the significant difference from the AR(1)-process, the spectra of the SST anomalies at a point in the North Atlantic (lon:45°W, lat:35°N) for the different simulations and the observations are shown in Figure 4.5. The difference between the AR(1)-process and the spectra of the SST anomalies in the fully

dynamical simulations is characterized by a slower increase of the SST variance from shorter to longer periods, which leads to increased variance of the SST on the seasonal and the decadal time scale relative to the fitted AR(1)-process. The significant difference between the AR(1)-process and the spectra of the SST is therefore not due to an increase of the SST variance at a certain period, as it is found in the tropical Pacific SST due to the El Nino phenomenon.

The spectrum of the $MIX_{dynamic}$ simulation does show a significant difference relative to the fitted AR(1)-process as well as the fully dynamical ocean models, but the basic structure of the spectrum is significantly different from those of the simulations with fully dynamical ocean models.

The most striking feature of the SST spectrum of the $MIX_{dynamic}$ simulation compared to the observations and the fully dynamical simulations is the missing increase of the SST variance from the interannual time scale to the decadal time scale. Although the characteristics of the SST variability in the $MIX_{dynamic}$ simulation are in good agreement with the observations and the simulations which include fully dynamical ocean models for the seasonal and interannual SST variability, the $MIX_{dynamic}$ simulation fails to simulate the increase of the SST variance from interannual to decadal time scales.

In the $MIX_{dynamic}$ simulation the ocean heat flux F_{ocean} term simulates all influences of the sub-mixed layer ocean to the SST. In the construction of the ocean flux term F_{ocean}, these influences can only damp the SST variability. The comparison of the $MIX_{dynamic}$ simulation with the two other slab ocean simulations MIX_{50} and MIX_{season} shows, that the damping effect of the F_{ocean} term seems to be important on the time scales from seasons to decades.

However, the comparison with the simulations with fully dynamical ocean models indicates that the influences of the sub-mixed layer ocean to the SST variability on decadal time scales cannot be simulated by an ocean heat flux F_{ocean} term, which is just damping the SST variability. In section 4.2.4 a possible explanation for the observed increase of the SST variance from the interannual to the decadal time scale is given, which can easily be introduced in the $MIX_{dynamic}$ model.

The results of this comparison indicate that the source of decadal time scale SST variability in midlatitudes is not just the 'redness' of the spectra due to the integration of atmospheric noise as found in the MIX_{50} and MIX_{season} simulations. Rather, the decadal time scale SST variability in the simulations with fully dynamical ocean models is caused by the interaction between the mixed layer and the sub-mixed layer ocean.

4.2 Sensitivity of the SST variability in midlatitudes to different physical processes

The dynamic mixed layer ocean model $MIX_{dynamic}$ simulates the large-scale features of the midlatitude SST variability as well as the fully dynamical ocean models as shown in the comparison of the different models with each other and with the observations. I now study the sensitivity of the SST variability in midlatitudes to different physical processes by comparing the $MIX_{dynamic}$ simulation with different sensitivity experiments, in which some of the processes that are simulated in the $MIX_{dynamic}$ simulation have been excluded. The comparison with these sensitivity experiments will then show which processes are important for the large-scale characteristics of SST variability in the midlatitudes.

name	number of years	short description of the slab ocean model
MIX_{50}	300	slab ocean, 50meter fixed mixed layer depth
MIX_{season}	300	slab ocean, with seasonal mixed layer depth
$MIX_{noentrain}$	10	slab ocean, using equation 3.1 for the SST and equation 3.9 for d_{mix}
MIX_{KT}	10	like $MIX_{dynamic}$ but setting $F_{ocean} = 0.0$ in equation 3.7
$MIX_{dynamic}$	300	slab ocean, with dynamic ocean mixed layer

Table 4.1: List of slab ocean models used in this study.

In Table 4.1, all different slab ocean models are listed for an overview of the different sensitivity experiments that will be discussed in the following sections. The atmospheric model ECHAM3 with a T21 resolution has been used in all of these simulations.

While the simplest possible model for the SST variability in the midlatitudes is represented by the MIX_{50} simulation, I shall present the characteristics of the SST variability in midlatitudes as a comparison of the $MIX_{dynamic}$ simulation relative to the MIX_{50} simulation. Therefore the physical processes can be listed by the time scale on which the $MIX_{dynamic}$ simulation alters the spectrum of the SST variability relative to the MIX_{50} simulation, which is shown in Table 4.2.

The effect of the seasonal cycle of the mixed layer depth has already been discussed in section 4.1.3. In the following sections, I shall discuss the other physical processes.

physical process	time scale
Wind amplified mixing of the ocean	increased daily variability
Entrainment of sub-mixed layer water	increased monthly variability
Variability of the mixed layer depth	increased seasonal to interannual variability
Seasonal mixed layer depth	increased monthly variability in summer decreased monthly variability in winter
Damping by ocean heat flux	decreasing seasonal to decadal variability
Re-emergence of temperature anomalies	increasing interannual to decadal variability

Table 4.2: List of the physical processes that are included in the $MIX_{dynamic}$ simulation and are not included in the MIX_{50} simulation. In the right column the time scale, on which the physical process is effecting the SST variability of the $MIX_{dynamic}$ simulation, is listed.

4.2.1 Wind amplified mixing of the ocean

In the dynamic mixed layer ocean model $MIX_{dynamic}$ the SST is calculated following equation 3.7. In this equation, the change of SST is a function of the mechanical energy input F_p, which is a function of the wind stress $\vec{\tau}$. Therefore, the change of SST in this model is a direct function of the wind stress $\vec{\tau}$, unlike in the MIX_{50} model in which the change of the SST is only a function of the atmospheric heat flux.

In equation 3.6, a strong wind stress $\vec{\tau}$ will increase the mechanical energy input F_p, which will lead to a negative SST change in equation 3.7. A positive mechanical energy input F_p will increase the mixed layer depth and sub-mixed layer water will be entrained into the mixed layer. While the sub-mixed layer ocean in this model is always colder than the SST, the entrainment of sub-mixed layer water has to result in a cooling of the SST.

To analyze the effect of the wind stress on the SST variability the daily SST time series in the $MIX_{dynamic}$ is compared with that of the MIX_{season} simulation. Both models are integrated with a time step of one day, which therefore represents the shortest time scale.

In the $MIX_{dynamic}$ simulation, the SST exhibits some characteristic decreases at the beginning and at the end of the summer (days 100 - 240), which is shown in Figure 4.6. These SST changes coincide with strong wind stresses and do not appear in the MIX_{season} model.

This can be quantified by composite histograms of windy days that are also shown in Figure 4.6. For both simulations, two different histograms are shown. The darker line shows the histogram of $\frac{d}{dt}SST$ for all summer and all winter days separately (normal composite). The lighter graph shows the histogram of $\frac{d}{dt}SST$ only for time steps in which the $\vec{\tau}^2 > 0.2$ (windy composite).

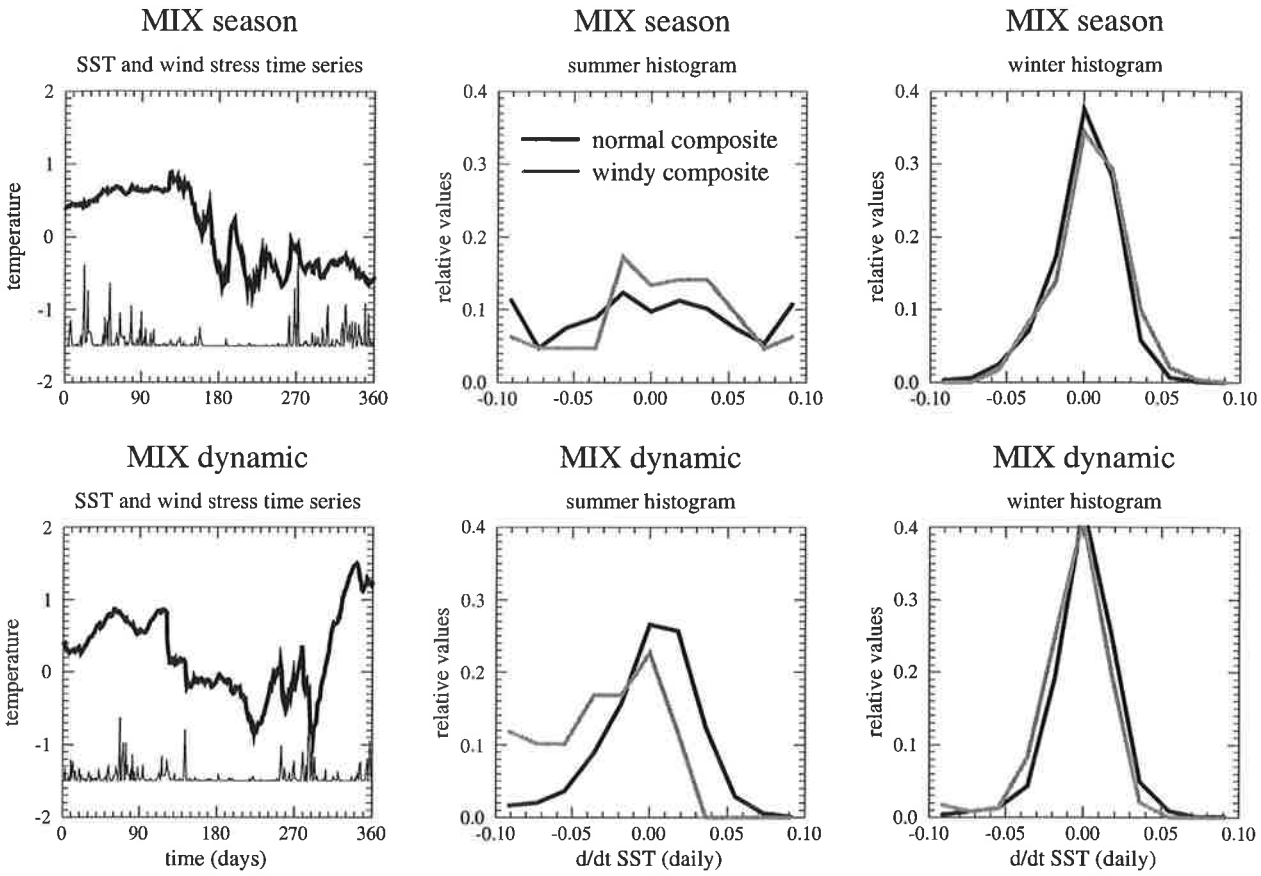

Figure 4.6: The left plots show a one year long time series of the SST anomalies (thick lines) and the wind stress $\vec{\tau}^2$ (thin lines) of the MIX_{season} and $MIX_{dynamic}$ simulations. The right and the middle plots show different histograms of the daily $\frac{d}{dt}SST$ for the two simulations. See text for details.

In the $MIX_{dynamic}$ simulation, a comparison of the two summer histograms shows that the histogram of the windy composite is significantly shifted to negative $\frac{d}{dt}SST$, while the normal composite is basically normally distributed. The same shift can be seen in the winter histograms, but it is not as strong as in the summer histograms.

In the MIX_{season} simulation, the windy and the normal composite histograms are not significantly different nether in summer nor in winter. However, neither of the two summer histograms of the MIX_{season} simulation is normally distributed. It can be concluded that in the $MIX_{dynamic}$ simulation the SST changes during summer are significantly influenced by strong wind stress. These will lead to strong cooling of the SST mainly during spring and fall. The cooling of the SST normally lasts only one or two time steps, which will lead to increased power of the SST spectrum at the shortest simulated time periods.

In the $MIX_{dynamic}$ simulation, the sub-mixed layer ocean is always colder than the SST. In the real world, the temperatures of the sub-mixed layer ocean are often warmer than the SST during the winter period in higher latitudes and at some locations in the midlatitudes.

At these locations, strong wind stresses will lead to warming during the winter period.

In the dynamical mixed layer model of the $MIX_{dynamic}$ simulation, it is assumed that the temperature of the sub-mixed layer ocean is always colder than the SST. The effect of warmer sub-mixed layer temperatures can be included in the $MIX_{dynamic}$ simulation by introducing salinity into the buoyancy equations. This has not been done in this simulation to keep the model as simple as possible in the first realization, but can easily be introduced.

The comparison has shown that the $MIX_{dynamic}$ simulation is more sensitive to wind induced SST change than the MIX_{50} simulation. This is the main reason why the $MIX_{dynamic}$ simulation is able to reproduce the observed enhanced standard deviation of the SST anomalies in the region of the storm tracks (see Figure 4.1), and this may also be the reason why the MIX_{50} and MIX_{season} simulations fail to reproduce this feature of the SST variability in the midlatitudes.

4.2.2 Entrainment of sub-mixed layer water

In the $MIX_{dynamic}$ simulation, the deepening of the mixed layer leads to entrainment of sub-mixed layer water into the mixed layer. As shown in the preceding section, the entrainment usually occurs during short-lived strong wind stress events.

The effect that the entrainment of sub-mixed layer water into the mixed layer has on the SST variability can be quantified by comparing two different slab ocean simulations. Therefore, I have performed the simulations MIX_{kt} and $MIX_{noentrain}$. The MIX_{kt} simulation is similar to the $MIX_{dynamic}$ simulation, but the ocean heat flux F_{ocean} has been set to zero. The experiment $MIX_{noentrain}$ is the same as the MIX_{kt} simulation, but the equation 3.7 for the SST change has been replaced by the equation 3.1 of the MIX_{season} and MIX_{50} simulations. A change in the mixed layer depth d_{mix} due to surface buoyancy flux or mechanical energy input is still simulated in the experiment $MIX_{noentrain}$, but it will not lead to a change in the SST due to entrainment of colder sub-mixed layer water, as discussed in the previous section. It can therefore be assumed that the high-frequency SST variability in the $MIX_{noentrain}$ simulation will be reduced relative to the MIX_{kt} simulation.

The Fourier spectra of the monthly mean SST anomalies for the different simulations have been calculated for Figure 4.7. All spectra are based on 10 years long time series. On the left hand side, the average of the spectral coefficients from 24 month to 8 month periods is shown, which I shall refer to as the low-frequency SST variability, and on the right hand side, the average of the spectral coefficients from $2\frac{2}{3}$ month to 2 month periods is shown, which I shall refer to as the high-frequency SST variability.

The comparison of the low-frequency variances indicates that the variance of the $MIX_{noentrain}$ simulation is significantly larger than in the MIX_{kt} simulation in the northern Pacific. However, the time series of the $MIX_{noentrain}$ simulation, which is only 10 years long, may be too short. It is possible that the entrainment of sub-mixed layer water can damp

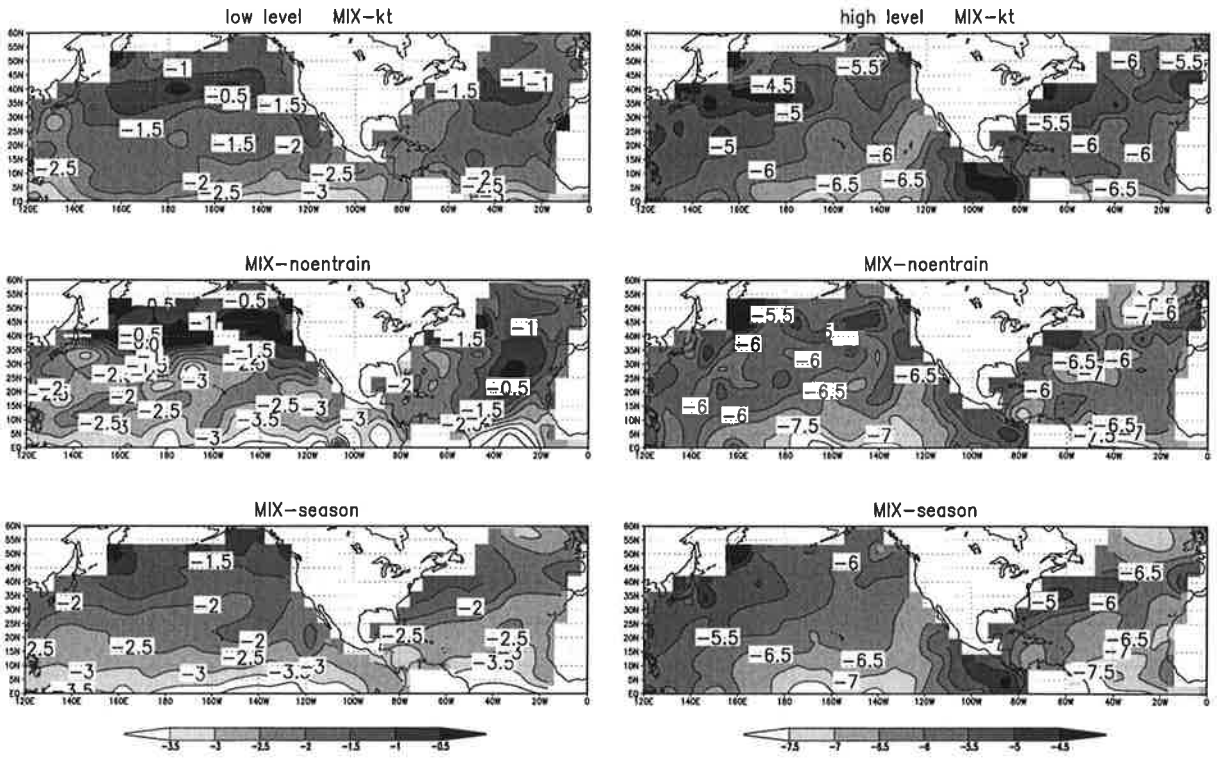

Figure 4.7: The plots show the low-frequency (left) and the high-frequency (right) variance of the SST anomalies of three different slab ocean simulations. The values are in relative orders of magnitudes. See text for details.

the SST variability in the Pacific north of 40^oN, which may explain the smaller values for the low-frequency SST variance in the MIX_{kt} simulation.

The comparison of the high-frequency variance in Figure 4.7 shows that the variance of the MIX_{kt} simulation is significantly larger than in the $MIX_{noentrain}$ simulation, especially around 40^oN. From this comparison, it can be concluded that the entrainment of colder sub-mixed layer water into the mixed layer leads to increased SST variability on time scales of weeks to months.

4.2.3 Variability of the mixed layer depth

The basic idea of slab ocean models is that the atmospheric heat flux is fully absorbed by the mixed layer. This is captured by the equations 3.1 and 3.7, in which the $\frac{d}{dt}SST$ is proportional to the atmospheric heat fluxes F_{atmos} times the inverse of the heat capacity of the mixed layer, which, in turn is proportional to the depth of the mixed layer d_{mix}.

An anomalously deep mixed layer will therefore increase the heat capacity of the mixed layer, which, for instance, will lead to negative SST anomalies when the normal atmospheric heat flux warms the ocean or it will lead to positive SST anomalies when the normal at-

mospheric heat flux cools the ocean. The SST in the dynamic mixed layer ocean model, in which the mixed layer depth is variable, will therefore be anti-correlated to the mixed layer depth anomalies at all time scales.

While the entrainment of colder water from the sub-mixed layer ocean is leading to increased SST variability only at the shorter time scales as shown in the two previous sections, the correlation between the SST and the mixed layer depth due to the basic structure of equation 3.7 will lead to an increase of the SST variability over the entire frequency range.

This can be quantified by comparing the spectra of the SST anomalies of the MIX_{kt} with the spectra of the MIX_{season} and $MIX_{noentrain}$ simulations, which are shown in Figure 4.7. The MIX_{season} and $MIX_{noentrain}$ are identical simulations, with the only difference that the mixed layer depth d_{mix} is variable in the $MIX_{noentrain}$ simulation, while it is constant in the MIX_{season} simulation.

The low-frequency variance of the SST in the $MIX_{noentrain}$ simulation is significantly larger than in the MIX_{season} simulation, while the high-frequency variance of the SST attains similar levels in both simulations. This demonstrates that the variability of the mixed layer depth is increasing the interannual SST variability, while the entrainment of sub-mixed layer water into the mixed layer due to atmospheric wind stress variability is only effecting the short time scales of days to months, as it has been shown in the previous section.

4.2.4 Damping by ocean heat flux

An oceanic heat flux F_{ocean}, proportional to the SST anomalies has been introduced in the $MIX_{dynamic}$ simulation (see equation 3.7). In Hasselmann's Null hypothesis of midlatitude SST variability, it is assumed that the SST variability is only effected by the atmospheric heat fluxes and that, therefore, the mixed layer of the ocean is not exchanging heat with the sub-mixed layer ocean. In general, the temperature profile of the upper ocean in the midlatitudes exhibits a roughly exponential decrease of the temperature beneath the mixed layer, similar to its portrayal in the schematic diagram of Figure 3.1. The exponential decrease of the temperature indicates that the mixed layer and the sub-mixed layer ocean are exchanging heat. It is therefore important to consider an oceanic heat flux between the mixed layer and the sub-mixed layer ocean.

In the $MIX_{dynamic}$ simulation, the oceanic heat flux F_{ocean} is a pure damping, and will be most effective in the regions with the largest SST variability. In Figure 4.1, it can be seen that the SST variability of the MIX_{50} or MIX_{season} simulations is increasing with latitude and that the standard deviations in the mid and higher latitudes are significantly larger than those observed. The effect of the oceanic heat flux F_{ocean} in the $MIX_{dynamic}$ simulation is especially important in those regions, because it is damping the SST variability to more realistic values.

The strength of the oceanic heat flux parameter C_{vo} in equation 3.8 was chosen to be

$4W/(m^2K)$, which is consistent with values found in the literature for the vertical heat flux in the upper ocean. However, the SST anomalies in the midlatitudes of the $MIX_{dynamic}$ simulation are still too strong, as seen in Figure 4.1. A higher value for C_{vo} can reduce the SST variability in the $MIX_{dynamic}$ simulation further. A comparison of the $MIX_{dynamic}$ simulation with the MIX_{kt} simulation indicates that a value of $C_{vo} = 8.0W/(m^2K)$ would yield a more realistic SST variability in the $MIX_{dynamic}$ simulation.

The construction of the ocean heat flux F_{ocean} in the $MIX_{dynamic}$ simulation will not only effect the standard deviation of the SST variability, but it will also change the spectral distribution of the SST. Due to the fact that F_{ocean} is proportional to the strength of the SST anomaly and that the spectral variance is increasing with the period, the spectral variance of long term variability will be damped more efficiently than short term variability. In Figure 4.5, the spectrum of the SST variability of the $MIX_{dynamic}$ simulation is slightly decreasing from the interannual to the decadal time scale. In contrast to this behavior, the fully dynamical ocean model simulations show a significant increase of the SST variability from the interannual to the decadal time scale. This indicates that the construction of the ocean heat flux F_{ocean} is missing an important process, which is producing the increase to decadal time scale SST variability. Although the general damping effect of the ocean heat flux F_{ocean} seems to be realistic for seasonal to decadal time scales, it has to be considered that, in the fully dynamical ocean model simulations, the sub-mixed layer ocean must have some amplifying effect on the SST variability on decadal time scales, which is not simulated by the construction of the ocean heat flux F_{ocean} in the $MIX_{dynamic}$ simulation.

In a more realistic simulation one can consider that the sub-mixed layer ocean has internal variability on longer time scales and that therefore the heat flux F_{ocean} is not just depending on the SST anomalies but also on the temperature anomalies of the sub-mixed layer ocean. In order to investigate how a variable sub-mixed layer ocean can change the spectrum of the SST due to the effect of the heat flux F_{ocean} a simple Monte Carlo study of the slightly changed equation 3.1 can be instructive.

For a simple study of the effect of the ocean heat flux F_{ocean}, the following equation can be used:

$$\frac{d}{dT}SST = \frac{1}{(C_p \rho_{water} d_{mix})} * (F_{atmos} + F_{ocean}) \tag{4.2}$$

It is similar to equation 3.1 but the heat flux F_{ocean} has been introduced. For a simple Monte Carlo study it can be assumed that the atmosphere can be simplified to:

$$F_{atmos} = C_{damp} * (T_{atmos} - SST) \tag{4.3}$$

First, it can be assumed that $F_{ocean} = 0.0$ and that T_{atmos} is some random weather noise. The equation 4.2 is than a realization of an AR-1 process. In the left plot of Figure 4.8 the spectrum of a Monte Carlo realization is shown (thick solid line). In the $MIX_{dynamic}$

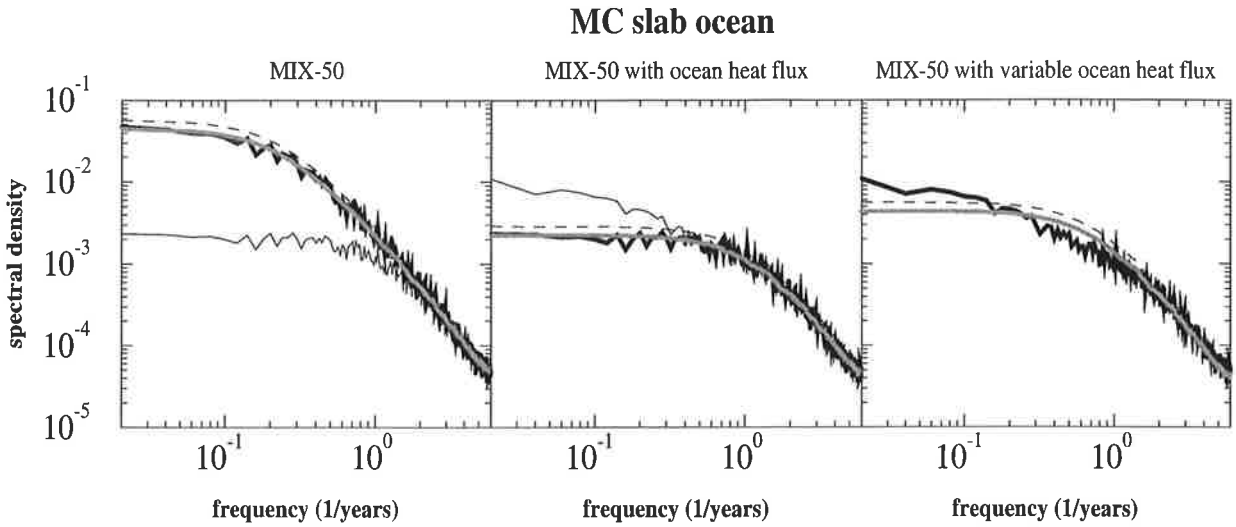

Figure 4.8: Monte Carlo spectra of different mixed layer equations. See text for details.

simulation the heat flux to the sub-mixed layer ocean F_{ocean} has been introduced as:

$$F_{ocean} = C_{damp} * (T_{ocean} - SST) \tag{4.4}$$

Here T_{ocean} was chosen to be constant. The left and the middle plots of Figure 4.8 show the spectrum of a Monte Carlo realization of equation 4.2, in which the T_{ocean} is constant. In comparison to the Monte Carlo realization with $F_{ocean} = 0.0$ it can clearly be seen that the spectrum is strongly damped on longer time scales, but it can also be seen that the spectrum is still an AR-1 process.

In a third realization of equation 4.2 the temperature of the sub-mixed layer ocean T_{ocean} was chosen to have some red noise fluctuations with a lifetime of the temperature anomalies of about one year. In the middle (thin line) and the right (thick line) plot of Figure 4.8 the spectrum of this realization is shown. Compared to the realization with the fixed T_{ocean} the spectrum of the SST is now significantly increasing from the interannual time scale to the decadal time scale, similar to what is seen in the observations and the fully dynamical ocean simulations (see Figure 4.1). The comparison with a fitted AR-1 process (shown in the right plot) shows that the spectrum has now a significantly different shape, with a flatter but longer increase of the variance from shorter to longer time scales. Thus, that the heat flux between the mixed layer and a variable sub-mixed layer ocean may be the source of the increase of the SST variance from interannual to decadal time scales.

In the simple ocean model of the $MIX_{dynamic}$ simulation, the ocean heat flux F_{ocean} simulates all influences of the sub-mixed layer ocean on the mixed layer. In following section I will discuss an additional improvement of the $MIX_{dynamic}$ simulation, which may also be important for simulating decadal time scale SST variability in a more realistic way.

4.2.5 Re-emergence of temperature anomalies

In the construction of the slab ocean models it is assumed that the mixed layer is forced only by the atmosphere and that the sub-mixed layer ocean is not directly effected by the atmosphere. The mixed layer of the ocean is exhibiting a distinct seasonal variation in the midlatitudes. The minimum mixed layer depth of about 20 meters is reached during summer and the maximum of about 200 meters is reached during winter. In the early winter or late fall, the mixed layer depth is increasing for the summer minimum to winter maximum values and is thereby entraining the water of the layers underneath the summer mixed layer. While the depth of the new winter mixed layer is several times larger than that of the summer, most of the water is from the layers underneath the summer mixed layer.

The temperature anomalies of the new winter mixed layer should, therefore, be stronger correlated with the temperature anomalies of the sub-mixed layer ocean than with the SST, which is supported by the findings of Namias and Born (1970, 1974). They found that SST anomalies in midlatitudes recur from one winter to the next, without being persistent during the summer. They speculated that the temperature signal is stored in the sub-mixed layer ocean during the summer month, when the mixed layer is shallow.

In the $MIX_{dynamic}$ simulation, the temperature of the sub-mixed layer ocean is parameterized by an exponential decrease from the SST to the constant deep ocean temperature T_d (see Figure 3.1). Therefore, temperature anomalies of the sub-mixed layer ocean are only a function of the SST anomalies. The entrainment of sub-mixed layer ocean water during the fall period in the $MIX_{dynamic}$ simulation does therefore not generate new SST anomalies due to the re-emergence of temperature anomalies from the sub-mixed layer ocean, but it just damps the existing SST anomalies. This seems to be unrealistic and it has to be assumed that the sub-mixed layer ocean is mainly independent from the actual atmospheric forcing and SST.

In order to make the behavior of the temperature anomalies of the sub-mixed layer ocean more realistic and in order to investigate the characteristics of the decadal time scale SST variability, which is not sufficiently strong in the $MIX_{dynamic}$ simulation as it has been shown in section 4.2.4, an improvement of the $MIX_{dynamic}$ simulation can be proposed.

In the winter time, the mixed layer in the midlatitudes reaches a depth of roughly 200 meters. During this time the temperature anomaly at 200 meter depth is, by construction, equal to the SST anomaly. In spring, the detrainment of the mixed layer depth in the $MIX_{dynamic}$ simulation resets the mixed layer depth to the flat spring mixed layer depth. At the time step at which this spring jump occurs, the temperature anomaly in 200 meters depth gets lost and is replaced by the parameterized exponential decrease of the SST anomaly. The $MIX_{dynamic}$ simulation can be improved by keeping the temperature anomaly of the sub-mixed layer ocean at the value which was present at the last time step before the spring jump occurs and conserving the temperature anomaly over the summer until the next fall, when the entrainment of the sub-mixed layer water increases the mixed layer depth again.

During the entrainment of the sub-mixed layer water temperature anomalies re-emerge that have been formed during last winter.

In this modification of the $MIX_{dynamic}$ model, the temperature anomalies in the sub-mixed layer ocean are only changing during the winter time when the SST change is more persistent and they will not be changed during the summer time when the SST variability is less persistent. This will lead to an increase of decadal time scale SST variability. Alexander et al. (1996) have analyzed an one-dimensional dynamical mixed layer ocean model, which includes the re-emergence of temperature anomalies coupled to a stochastic atmosphere model. In their model simulation the spectrum of the SST anomalies is increasing from the interannual to the decadal time scales, which may be caused by the re-emergence of temperature anomalies as they conclude.

As the comparison of the decadal SST variability of the $MIX_{dynamic}$ simulation with the fully dynamic ocean model simulations has shown, an increase of the decadal time scale SST variability will make the SST variability of the $MIX_{dynamic}$ simulation more realistic. Although the proposed construction of the temperature anomalies in the sub-mixed layer ocean may be artificial to some extent, the integration of this model can indicate whether the amount and structure of decadal SST variability can really be explained by such a one-dimensional slab ocean or whether the decadal SST variability is, caused by processes different from local air-sea interaction.

4.3 Seasonal predictability of midlatitude SST anomalies

The comparison of the different simulations with the observations has shown that the $MIX_{dynamic}$ simulation is a realistic model that simulates the seasonal to interannual SST variability in its large-scale features as well as any other simulations that employ a fully dynamical ocean model. In some aspects it may be even better.

The characteristic feature of the $MIX_{dynamic}$ simulation, which leads to a more realistic simulation of the midlatitude SST variability compared to the simple mixed layer models MIX_{season} and MIX_{50}, is the dynamical mixed layer depth. The fact that the variability of the mixed layer depth is important for the generation of SST anomalies implies that the knowledge of the current mixed layer depth may be important for the development of SST anomalies and can therefore lead to improved predictability in the midlatitudes.

In principle the predictability of the midlatitudes SST anomalies in the $MIX_{dynamic}$ model can be studied by using ensemble integrations of the $MIX_{dynamic}$ model. In such ensemble integrations, each simulation will be started with the same SST anomalies and mixed later depth anomalies, but the atmospheric state will be changed. The variance of the SST anomalies of the ensemble members relative to the mean SST anomalies of all ensemble

members is a good measure for the predictability of the SST anomalies.

However, such ensemble integrations are computationally expensive, and they have the disadvantage that the results of these numerical simulations do not give any physical understanding of how the development of SST anomalies depend on the initial conditions.

It is therefore helpful to investigate the predictability of the midlatitudes SST anomalies with simple statistical forecast models. With these models one can easily check different forecast methodologies that, for example, use the SST and the mixed layer depth anomalies or only one of them as a predictor. The disadvantage of statistical forecast models is that one has to specify a simple relationship between the initial state and its further development. However, the simple statistical forecast models can give a crude indication of the predictive skill for the coupled system.

4.3.1 Simple statistical forecast models

In the simplest forecast model, based only on the SST anomalies, one can assume that the SST anomalies are persistent, which leads to the following statistical forecast model:

$$\text{Model } F_{SST_0} : SST(t) = SST(T_0) \tag{4.5}$$

If we assume that the SST anomalies are produced by an AR-1 process, then the SST anomalies are damped according to the lag-1 autocorrelation, which leads to a more realistic forecast model:

$$\text{Model } F_{SST_1} : SST(t) = C^t_{lag-1} * SST(T_0) \tag{4.6}$$

However, the optimal linear forecast model using the SST or the mixed layer depth d_{mix} is obtained by determining empirical relation coefficients $C_{T(t)}$ for each time lag:

$$\text{Model } F_{SST_2} : SST(t) = C_{T(t)} * SST(T_0) \tag{4.7}$$

The same structure as in equation 4.7 can be used for a forecast model using the mixed layer depth to forecast the SST:

$$\text{Model } F_d : SST(t) = C_{d(t)} * d_{mix}(T_0) \tag{4.8}$$

A statistical forecast model using the SST and the mixed layer depth d_{mix} is much more complicated, because no linear interactions of the SST and the mixed layer depth d_{mix} can be retained. However for a first crude estimate of the forecast skill a simple linear approach should be sufficient:

$$\text{Model } F_{d,SST} : SST(t) = C_{d(t)} * d_{mix}(T_0) + C_{T(t)} * SST(T_0) \tag{4.9}$$

The empirical coefficients $C_{T(t)}$ and $C_{d(t)}$ in equations 4.7 and 4.8 are in principle determined by the lag correlations between the SST or d_{mix} of the forecast month and those of the predicted month and the standard deviation of the quantities. However, all parameters for the different forecast models have been calculated by a black box fit routine, which minimizes the squared error of the forecast model over the 300 years of the $MIX_{dynamic}$ simulation for each model grid point.

4.3.2 The skill of the simple statistical forecast models

In order to determine the skill of a forecast model, one usually compares the variance of the SST with the variance of the forecast, which leads to the following equation:

$$Q_{skill} := 1 - \frac{\sigma^2_{forecast}}{\sigma^2_{SST}} \tag{4.10}$$

Where σ^2_{SST} is the variance of the SST for the predicted month and $\sigma^2_{forecast}$ is defined as:

$$\sigma^2_{forecast} := \sum^{allforecasts} (SST(t) - F(t, SST(t_0), d_{mix}(t_0)))^2 \tag{4.11}$$

$\sigma^2_{forecast}$ is therefore the variance of the SST relative to the statistical forecast model $F(t, SST(t_0), d_{mix}(t_0))$. The skill Q_{skill} is close to 1.0 if the statistical forecast model $F(t, SST(t_0), d_{mix}(t_0))$ is close to the observed (simulated) SST and it is near to or less than zero if the statistical forecast model $F(t, SST(t_0), d_{mix}(t_0))$ is relatively far away from the observed (simulated) SST.

The skill Q_{skill} of the statistical forecast models in the $MIX_{dynamic}$ simulation can be determined by equation 4.10 and equation 4.11 using the 300 years of the $MIX_{dynamic}$ simulation. The skill Q_{skill} has been calculated for forecasts starting in the months May, September, December and March as T_0 and predicting the next four months. The parameters for the forecast models have also been determined by the 300 years of the $MIX_{dynamic}$ simulation.

In order to compare the different statistical forecast models the skill Q_{skill} for the four different starting months at a model grid point in the Pacific is shown for all forecast models in Figure 4.9. This grid point was chosen because it nicely shows the seasonal differences in the forecast skill of the different forecast models. The spatial structure of the forecast skill Q_{skill} for the forecast models F_{SST_2}, F_d and $F_{d,SST}$ predicting three month in advance are shown in the Figures 4.13 (for the staring month March), 4.14 (May), 4.15 (September) and 4.16 (December).

The comparison of the forecast models using SST only (F_{SST_0}, F_{SST_1} and F_{SST_2}) shows that the different forecast models have similar skill, which indicates that the forecast skill of the SST is mainly due to the persistence of the SST. However, the skill of the forecast models is very different for different starting months. The skill of the forecast models is

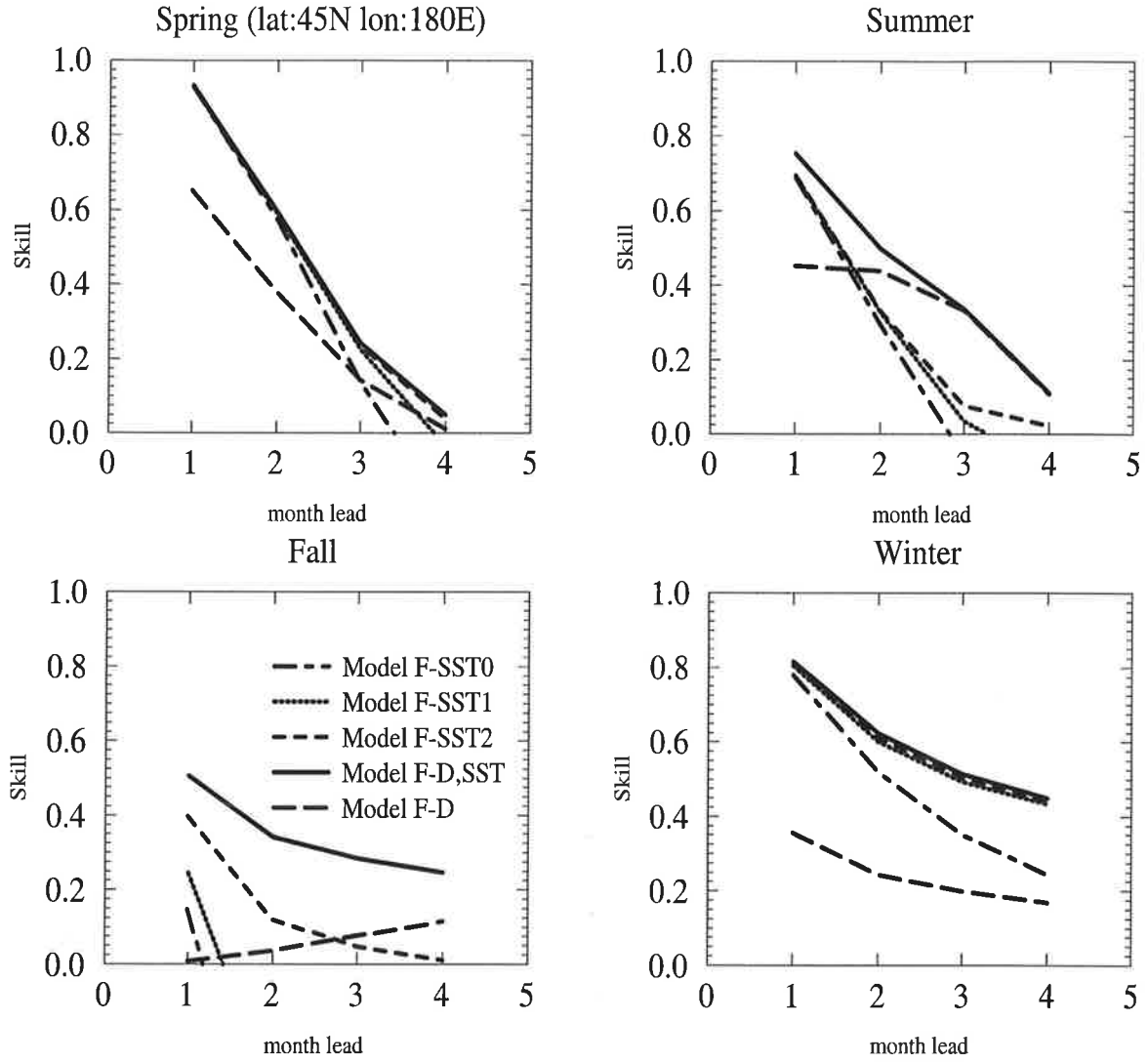

Figure 4.9: The skill Q_{skill} of the different statistical forecast models for four different starting months at a model grid point in the Pacific($lat. = 45^oN, lon. = 180^oE$). For details see text.

largest in the winter period and in the beginning of the spring. The skill is still high for three to four months forecasts in winter but, it drops very fast at the end of the spring period. The forecast skill in summer is relatively low and is not significantly different from zero for three and four months forecasts. For the fall period there is almost no forecast skill using the SST.

Before we can discuss the differences of the forecast models, it has to be shown that the increased forecast skill of the forecast models based on empirical parameters like the F_{SST2} and $F_{d,SST}$ models is not due to an artificial forecast skill. This is because the parameters for the statistical forecast models have been determined from the same 300 years of the $MIX_{dynamic}$ simulation for which the skill (in the following called Q_{skill}-300) has been determined. In order to determine how much of the improved forecast skill of the model $F_{d,SST}$ is artificial, the parameters for the model $F_{d,SST}$ have been calculated for only 250 years of the

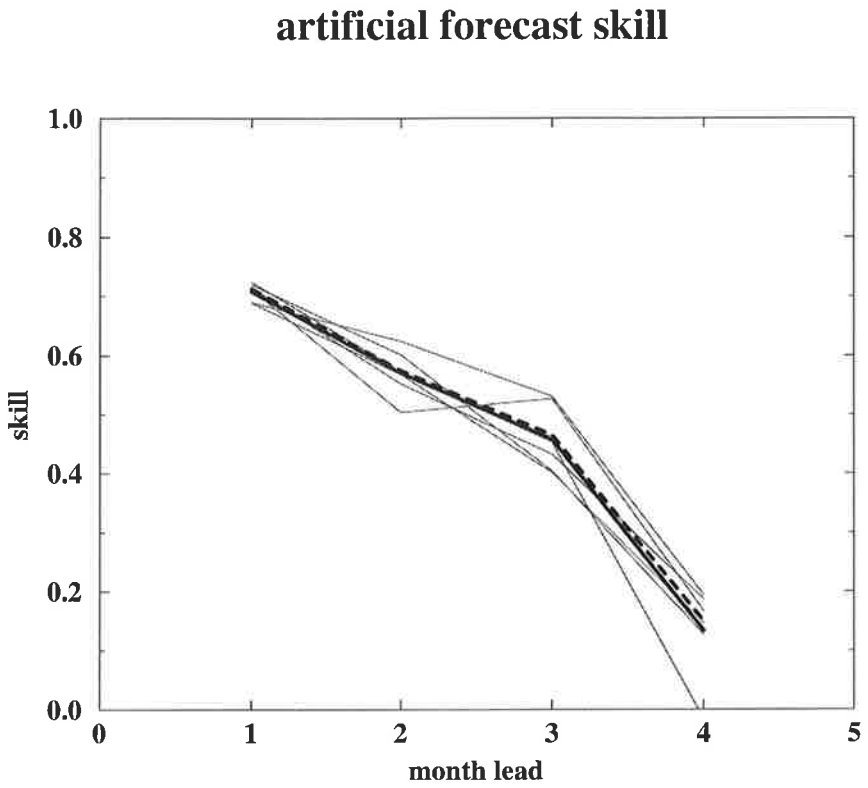

Figure 4.10: Artificial skill Q_{skill} of the forecast model $F_{d,SST}$ in summer. The starting month are March (spring), May (summer), September (fall) and December (winter). For details see text.

$MIX_{dynamic}$ simulation and the skill Q_{skill} has been calculated for the remaining 50 years of the $MIX_{dynamic}$ simulation (in the following called Q_{skill}-50). This has been done for six different 50 years time intervals of the $MIX_{dynamic}$ simulation and the results are shown in Figure 4.10. The six different estimates of the skill are now free of artificial forecast skill, because the parameters and the skill for the model $F_{d,SST}$ have now been calculated for independent time intervals.

The mean of the six different estimates of the skill Q_{skill}-50 is just a little bit smaller than the skill Q_{skill}-300, which indicates that the increased skill of the model $F_{d,SST}$ relative to the forecast models using SST only is not due to artificial skill.

By construction the forecast model $F_{d,SST}$ has more free parameters than the model F_{SST_2} and must therefore have a larger skill than the model F_{SST_2}. However, the small difference between the mean of the skill Q_{skill}-50 and the skill Q_{skill}-300 indicates that the increased skill of the model $F_{d,SST}$ due to the additional parameters for the mixed layer depth, is mainly not artificial. We can therefore assume that the skill of the different forecast models shown in Figure 4.9 are significantly different, if the difference is larger than the thickness of the lines.

The forecast skill of the combined forecast with SST and mixed layer depth increases

only in the summer and fall periods. The forecast skill in fall is almost entirely due to the mixed layer depth anomalies, while the forecast skill in summer is due to both the SST and the mixed layer depth anomalies. In order to understand the different characteristics of the forecast skills one has to take a closer look at equation 3.7.

The influence of d_{mix} anomalies on the SST change can be studied by examining the derivative of equation 3.7 with respect to d_{mix}. For the calculation of the derivative of equation 3.7 it can be assumed that the quantities F_p, F_q, h_p and h_q are not depending on d_{mix}, which is true for F_q, while it is only a crude assumption for the other quantities. This leads to the following equation:

$$\partial \frac{d}{dT} SST = \frac{F_p - F_q H_p}{d_{mix}^2 h_q} \partial d_{mix} \tag{4.12}$$

In Figure 4.11 the climatological mean values of the terms F_p, $F_q H_p$, $d_{mix}^2 h_q$, ∂d_{mix}(standard deviation of d_{mix}) and the right hand side of equation 4.12 are shown. In comparison to the right hand side of equation 4.12 the standard deviation and the mean change of SST per month are shown.

The forecast skill of the SST is mostly due to the persistence of the SST anomalies. The skill of the forecast model with SST only should therefore be largest if the relative change in the SST is small. Therefore, the seasonal differences of the forecast model using SST only can be understood by comparing the standard deviation of the monthly SST and the mean change of SST per month. In the winter and early spring the change in SST is small compared to the standard deviation, which leads to relatively high forecast skill in these times of the year. In summer and particularly in fall the change in SST is relatively large, which leads to the low forecast skill of the forecast model using SST only.

The seasonal differences of the forecast models using the mixed layer depth d_{mix} are represented by the right hand side of equation 4.12. During the winter and spring the influence of the mixed layer depth on changes in SST is relatively weak compared to the mean change of SST per month, while it is relatively large during the summer and fall. In order to understand the different behavior for the different seasons one has to take a closer look at the terms of the right hand side of equation 4.12. Although the surface buoyancy flux F_q, the mechanical energy input F_p and the standard deviation of the mixed layer depth d_{mix} are large in winter, the effect for the change in the SST is compensated by the large mixed layer depth during the winter and early spring. In summer and fall the small mixed layer depth makes the SST more sensitive to the surface buoyancy flux F_q, mechanical energy input F_p and more sensitive to mixed layer depth anomalies. In summer the effect of the surface buoyancy flux F_q is dominating the change of SST, while in fall the mechanical energy input F_p is most important.

Although the crude estimate of the influence of the mixed layer depth on changes in SST with equation 4.11 gives a good account of the main characteristics, the temperature profile underneath the mixed layer has not been considered.

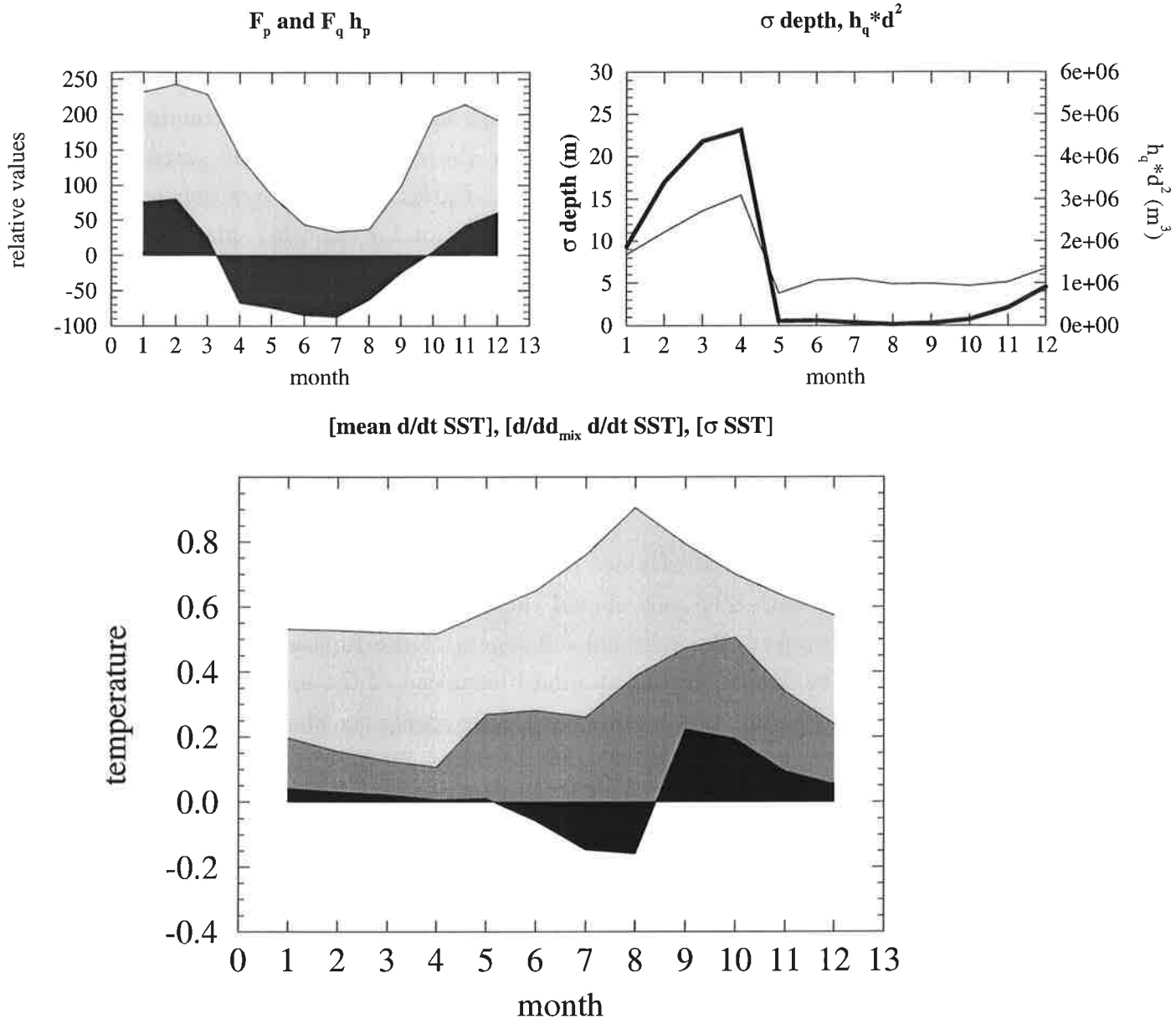

Figure 4.11: The climatological mean values of the terms F_p (light shaded) and $F_q H_p$ (dark shaded) in the upper left plot, $d_{mix}^2 h_q$ (thick line) and ∂d_{mix}(standard deviation of d_{mix}) in the upper right plot and the right hand side of equation 4.12 in the lower plot. In comparison to the right hand side of equation 4.12 the standard deviation and the mean change of the SST per month are shown. For details see text.

The schematic diagram in Figure 4.12 illustrates the relation between the effective heat capacity of the ocean for the dynamical equations 3.7 and 3.9 and the change in SST or in the mixed layer depth. The shaded area indicates the effective heat capacity of the ocean. A small change in the SST or in d_{mix} will in general move the point defined by the SST and d_{mix} along the dashed line.

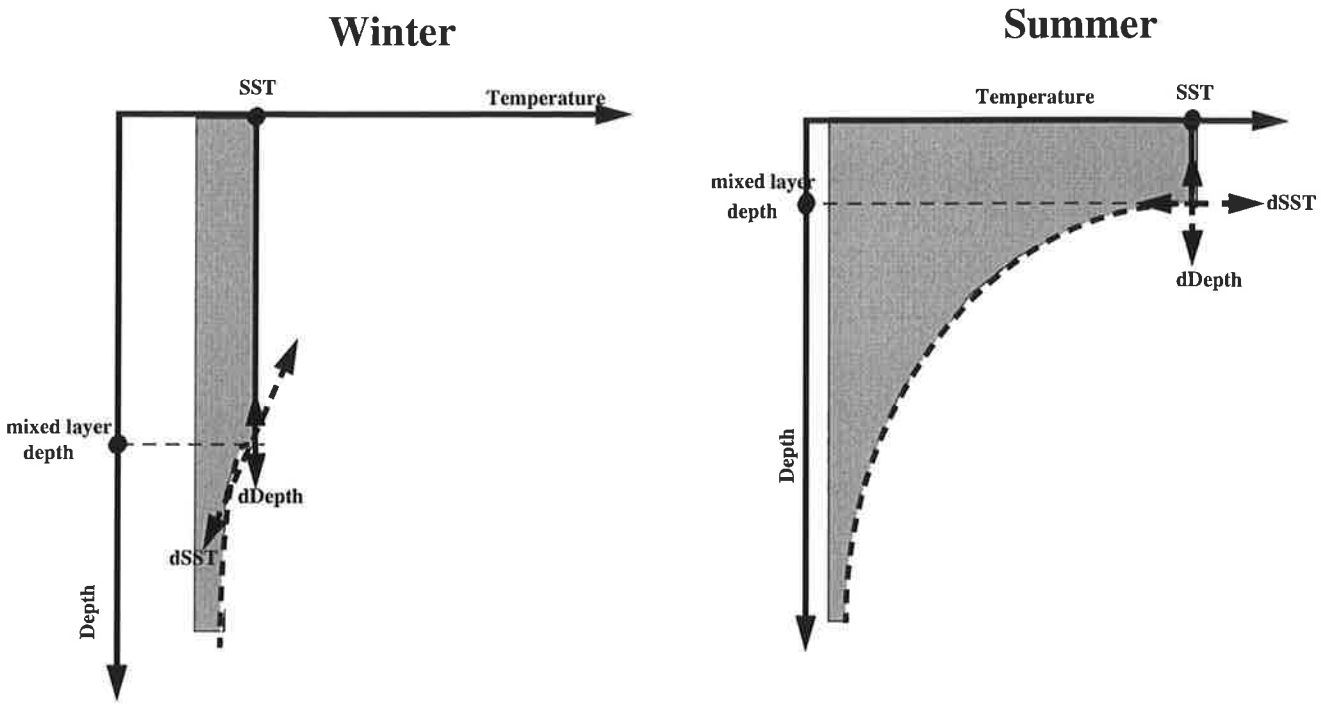

Figure 4.12: Sketch to illustrate the relation between the change in SST and mixed layer depth in winter and summer.

In winter the temperature gradient beneath the mixed layer is relatively small. A change in the mixed layer will then have no strong influence on the SST or the effective heat capacity of the $MIX_{dynamic}$ model, which explains why the mixed layer depth anomalies are not important for the SST development in winter. On the other hand a change in SST will change the mixed layer depth significantly, which leads to the fact that the SST and mixed layer depth anomalies are highly correlated in winter.

In summer the temperature difference between the mixed layer and the sub-mixed layer is very large, and a change in the mixed layer depth will have a strong effect on the heat capacity in the $MIX_{dynamic}model$, whereas a change in the SST has almost no influence on the mixed layer depth. This explains why the mixed layer depth anomalies are important in summer.

The skill of the different forecast models is not only varying with the season, but it also has significant spatial structure. The local differences in the forecast skill are shown in the Figures 4.13 (for the staring month March), 4.14 (May), 4.15 (September) and 4.16 (December). The Figures show the forecast skill of the models F_{SST_2}, $F_{d,SST}$ and F_d for predictions made three month in advance. A temporal interval of three months was chosen, because it nicely shows the differences in the forecast models.

In spring and winter the skill of the forecast models F_{SST_2} and $F_{d,SST}$ are similar, while the skill of the F_d model is not significantly different from zero, with the exception of the higher latitudes of the North Atlantic, where the F_d model shows some skill. In fall, the

$F_{d,SST}$ model is much better than the F_{SST_2} model over almost the entire domain. While the F_{SST_2} model has almost no forecast skill in the midlatitudes, the F_d model shows some skill in the midlatitudes.

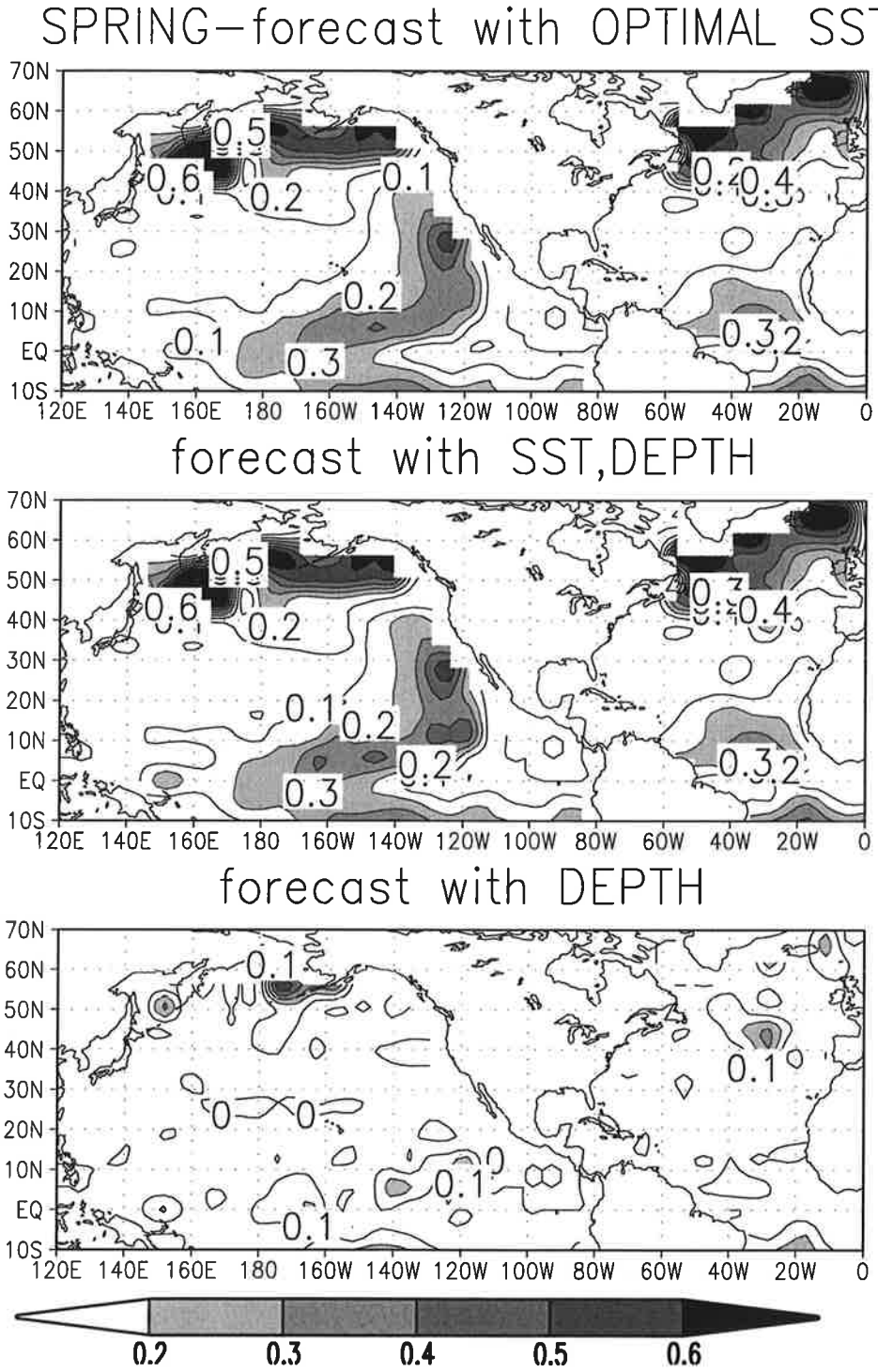

Figure 4.13: The skill Q_{skill} of the statistical forecast models F_{SST_2}, F_d and $F_{d,SST}$ predicting three month in forward starting at the month March. For details see text.

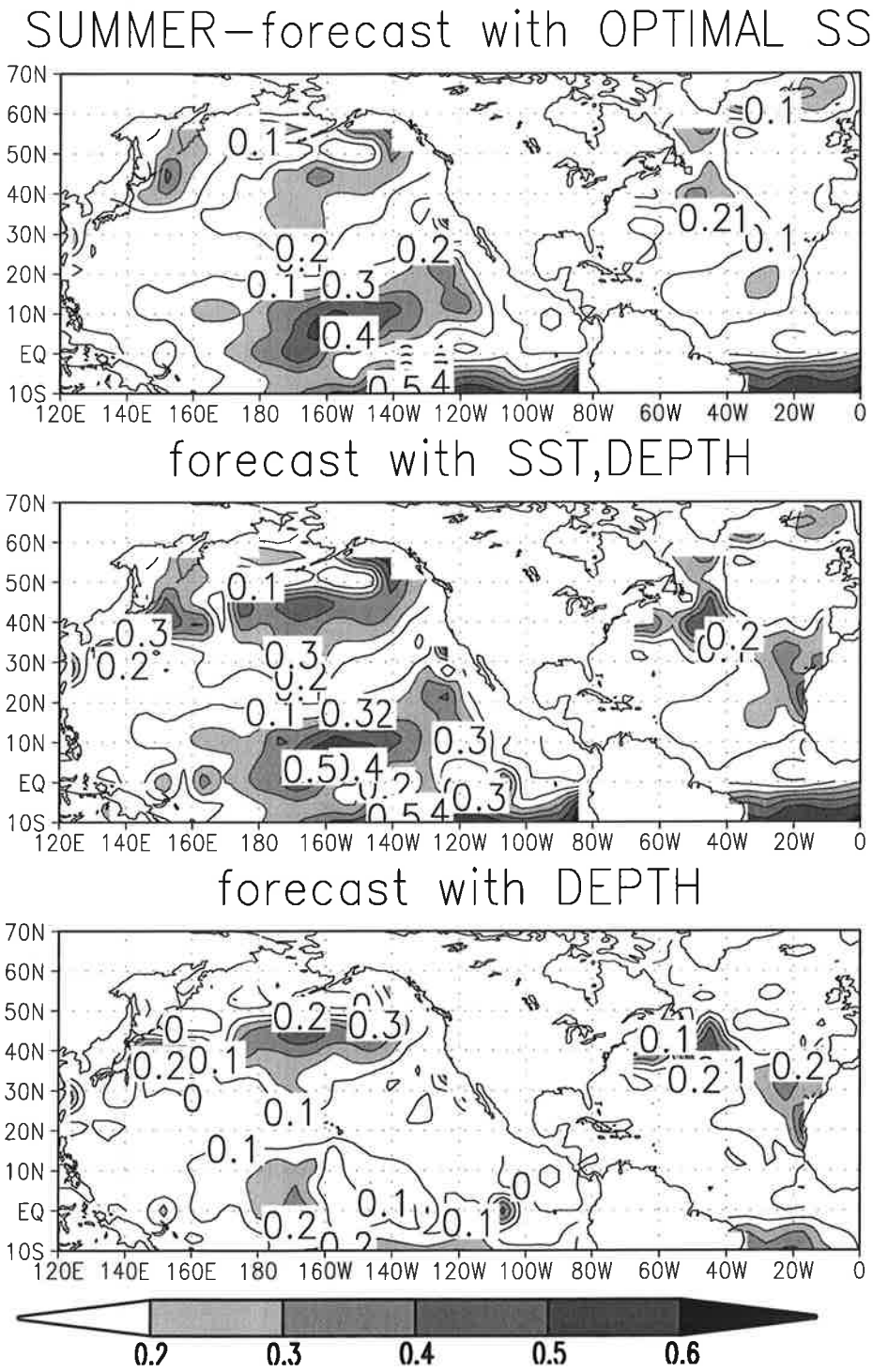

Figure 4.14: The skill Q_{skill} of the statistical forecast models F_{SST_2}, F_d and $F_{d,SST}$ predicting three month in forward starting at the month May. For details see text.

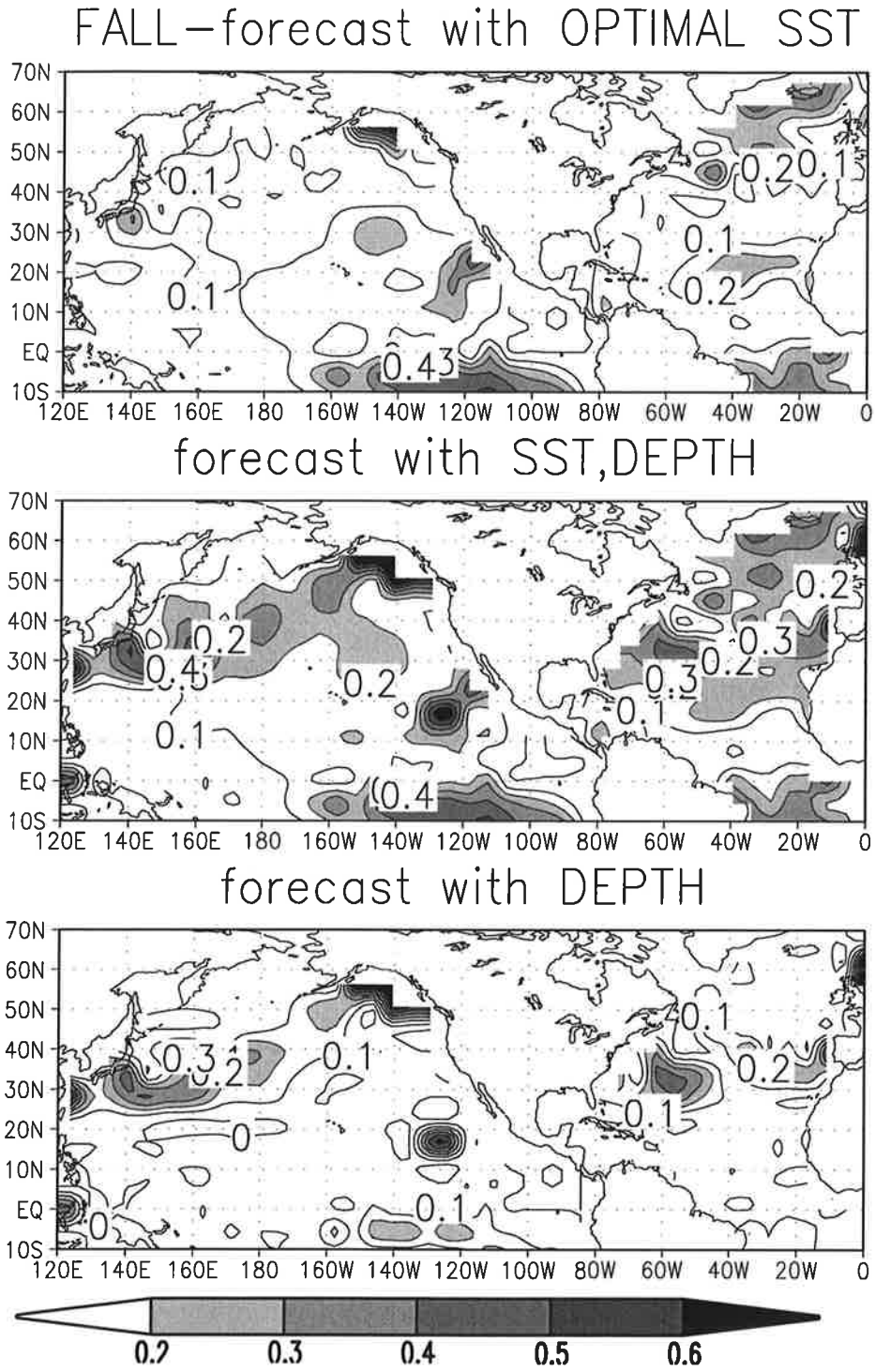

Figure 4.15: The skill Q_{skill} of the statistical forecast models F_{SST_2}, F_d and $F_{d,SST}$ predicting three month in forward starting at the month September. For details see text.

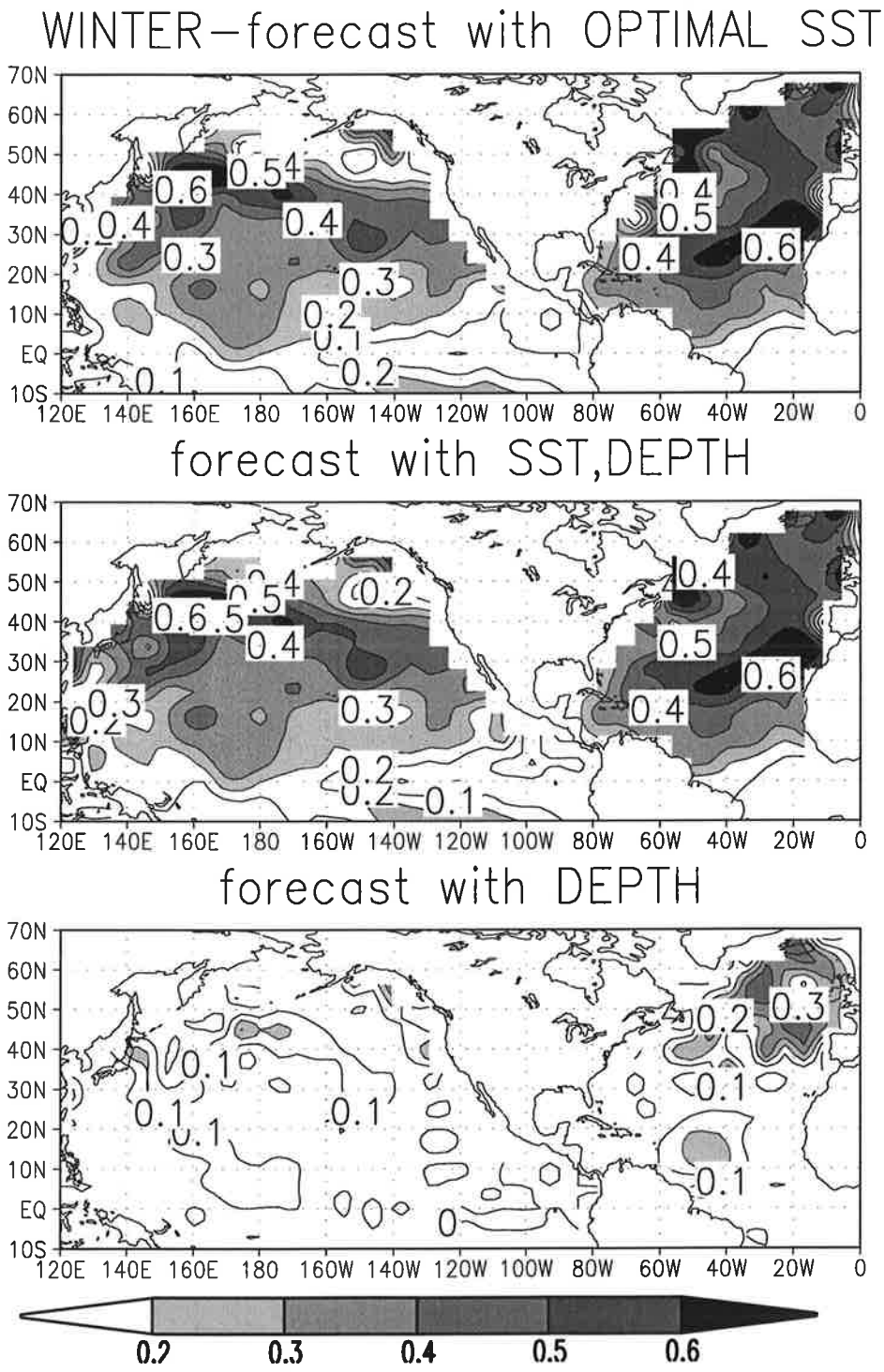

Figure 4.16: The skill Q_{skill} of the statistical forecast models F_{SST_2}, F_d and $F_{d,SST}$ predicting three month in forward starting at the month December. For details see text.

4.4 Summary and discussion

In this chapter, I have focused my analyses on a comparison of different model simulations with the observations in order to test whether the large-scale SST variability in the mid-latitudes of the Northern Hemisphere is consistent with the Null hypothesis, presented by Hasselmann's stochastic climate model (1976). From the comparison of the different model simulations with the observations, the conclusion has been reached that the SST variability in the midlatitudes is significantly different from Hasselmann's simplest stochastic climate model (AR-1 process) and that the processes in the ocean which are responsible for these differences can be identified.

The conclusions are based on two basic findings: First, the comparison of the different simulations with the observations shows that the simulations with the fully dynamical ocean models and the observations are significantly different in terms of the large-scale features of the SST variability compared to the simple MIX_{50} or MIX_{season} simulations. Second, the statistical test of the spectral distribution of the SST variability in the different models revealed that only the simple MIX_{50} or MIX_{season} simulations can be regarded as AR(1)-processes, while in all other simulations the spectral distributions of the SST variability are significantly different from the spectral distributions of the AR(1)-processes.

In addition to the unrealistically enhanced SST variability in the MIX_{50} simulation, the redness of the SST, which describes the increase of the SST variance with increasing periods, is also much larger in the MIX_{50} simulation than in the observations. Although the overall variance of the SST variability in the MIX_{50} simulation is larger than in the observations, the large redness of the SST variability in the MIX_{50} simulation leads to much weaker SST variability on monthly time-scales. In the realization of Hasselmann's stochastic climate model in the MIX_{50} simulation, the equation [3.1] for the integration of the atmospheric heat flux has only one free parameter, the mixed layer depth d_{mix}. Although a mixed layer depth of about 50 meters is a realistic assumption, one may argue that, for a stochastic climate model, a different mixed layer depth has to be chosen and the depth can be different at different ocean locations.

However, tuning by changing the mixed layer depth cannot modify the characteristics of the SST variability in the MIX_{50} simulation to be consistent with the observations. An increase of the mixed layer depth to decrease the standard deviation of the SST leads to further increase of the redness. A smaller mixed layer depth will increase the standard deviation of the SST, which is inconsistent with the observations.

I have also tested the spectral distribution of the SST variability against the hypothesis of an AR(1)-process. While it was found that the MIX_{50} and the MIX_{season} simulations are basically consistent with an AR(1)-process, the spectral distribution of the SST variability in the simulations with fully dynamical ocean models are significantly different. This is also true, although not to the same extent, for the $MIX_{dynamic}$ simulation. The difference

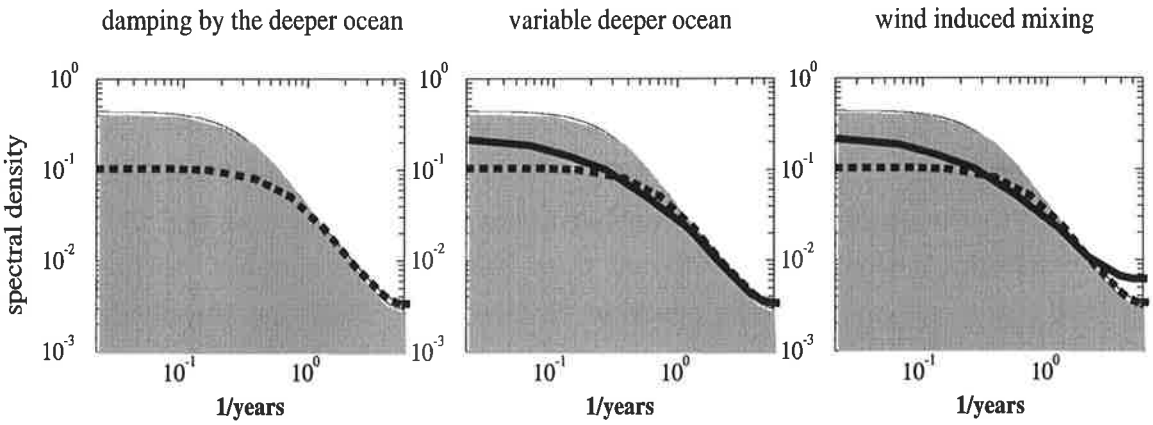

Figure 4.17: Sketch to illustrate the main characteristics of the spectral distribution of the midlatitudes SST variability in the $MIX_{dynamic}$ simulation . See text for details.

between the AR(1)-process and the SST spectra in the simulations with fully dynamical ocean models is characterized by a slower increase of the SST variance from the shorter time periods to the longer time periods, which leads to increased variance of the SST on the seasonal and the decadal time scale relative to the fitted AR(1)-process(see Figures 4.5). It is interesting to note that this deviation is similar to the deviation of the spectrum of the AR(1)-process relative to the spectrum of the monthly mean averaged AR(1)-process (see Figures 4.5 and 2.3).

The missing physical processes that are causing the differences between the observed SST variability and that simulated by the simple MIX_{50} model are better represented in the dynamical slab ocean model $MIX_{dynamic}$. In this model Hasselmann's stochastic climate model has been expanded by the introduction of a dynamical variation of the mixed layer depth. The following physical processes improved the spatial and temporal structures of the SST variability: wind induced entrainment of sub-mixed layer water into the mixed layer, the seasonal cycle of the mixed layer depth, and the heat exchange between the mixed layer and the sub-mixed layer ocean.

To summarize the characteristics of the large-scale SST variability in the midlatitudes, it is instructive to illustrate the differences in the spectral distribution of SST between the MIX_{50} simulation and the $MIX_{dynamic}$ simulation. This is shown in the idealized spectra of Figure 4.17. In all three plots the shaded area illustrates the spectral distribution of the MIX_{50} simulation, which is characterized by an AR-1 process. Compared to this AR-1 process the effect of the different processes in the $MIX_{dynamic}$ simulation can be illustrated.

The dashed spectra in the left plot illustrates the spectrum of the SST if a heat flux to the sub-mixed layer ocean is introduced. The spectrum of the SST is mainly decreased on the interannual to decadal time-scale, which leads to a more realistic standard deviation and also decreases the 'redness' of the SST spectra.

If we consider that the sub-mixed layer temperature has some interannual variability, then the heat flux to the sub-mixed layer ocean is an additional noise integrating process for the mixed layer, which is integrating the "red noise" of the sub-mixed layer ocean. In the middle plot the solid line illustrates the spectrum of the SST if the temperature variability of the sub-mixed layer ocean is considered for the heat exchange between the mixed layer and the sub-mixed layer ocean. The spectral distribution is now significantly different from an AR-1 Process with an increase to the SST variance from the interannual to the decadal time-scales.

The solid line in the right plot illustrates the effect of the wind induced mixing. The wind induced mixing entrains colder water of the sub-mixed layer ocean into the mixed layer, and is therefore leading to temperature changes in the SST. This leads to the increased SST variability on the seasonal time-scales and to the observed maximum of SST variability in the regions of the storm tracks.

In addition to the three processes illustrated in the Figure 4.17 the seasonal cycle of the mixed layer depth leads to a smaller persistence of the SST anomalies during the summer, when the mixed layer depth is small, and to a larger persistence of the SST variability in winter, when the mixed layer is very deep.

The analysis of the seasonal predictability of midlatitude SST anomalies in the $MIX_{dynamic}$ simulation has shown that the SST forecast skill varies significantly from season to season and that the skill of the forecast in the midlatitudes in summer and fall can be significantly increased by taking into account the mixed layer depth anomalies. The physical processes which are important for the change of the SST due to mixed layer depth anomalies are different in summer and fall.

In summer the mixed layer depth is mostly stable and shallow and the temperature profile underneath the mixed layer is very pronounced (see Figure 4.12). Therefore a mixed layer depth anomaly changes the effective heat capacity of the mixed layer, which changes the integration of the present heat flux. The normally strong positive heat flux during the summer period will in general warm the ocean. An anomalous deep mixed layer will lead to decreased warming, due to the larger heat capacity of the ocean and will therefore lead to negative SST anomalies and vice versa for anomalously shallow mixed layers. In winter the strong negative heat flux cannot influence the SST as strongly as in the summer, because the mixed layer in winter is much deeper and therefore the heat capacity is much larger. Additionally, the temperature gradient beneath the mixed layer is relatively small, which makes the heat capacity of the upper ocean almost independent of the mixed layer depth.

In fall the mixed layer depth is deepening, and associated with the deepening the mechanical energy input is dominating the change in SST during this season. An anomalously deep mixed layer will slow down the deepening of the mixed layer, because of the larger inertia of the increased mixed layer. Therefore, the entrainment of colder sub-mixed layer water will decrease, which will lead to anomalously warm SSTs and vice versa for anomalous

shallow mixed layers.

In winter and summer the model seems to be realistic because all important processes are simulated in the $MIX_{dynamic}$ simulation. However, in fall and spring the model is missing some important processes, which makes the interpretation of the results in those seasons difficult, if not useless.

In spring the detrainment of the mixed layer is artificially introduced at a fixed time step, while in the real world the detrainment of the mixed layer is caused by dynamical interactions between the atmosphere and the ocean. This can lead to variable time evolutions of the detrainment of the mixed layer during spring, which will lead to changes in the SST development during this period.

In fall the deepening of the mixed layer is entraining the colder water of the sub-mixed layer ocean. In the $MIX_{dynamic}$ simulation the temperature beneath of the mixed layer is only represented by an exponential decrease of the SST, which makes it impossible to simulate temperature anomalies in the sub-mixed layer ocean which are independent of the instantaneous SST. However, in the real world the sub-mixed layer ocean can have temperature anomalies which are independent of the instantaneous SST, which will be merged into the mixed layer during fall and will have an influence on the SST which is not simulated in the $MIX_{dynamic}$ simulation.

Finally, I would like to compare the characteristics of the seasonal to interannual SST variability in the midlatitudes with the SST variability of the tropical Pacific. In the tropical Pacific the SST variability is dominated by the El Niño Southern Oscillation (ENSO) phenomenon. The ENSO phenomenon leads to increased predictability in the tropical SST anomalies on the seasonal to interannual time-scale, which can only by simulated by fully dynamical coupled ocean-atmosphere models, whereby the horizontal advection and wave propagation of the ocean plays an important role. In my study I have shown that the SST variability in the midlatitudes is also influenced by dynamical processes in the ocean but, unlike in the tropical Pacific, the spatial and temporal structures of the SST variability in the midlatitudes can be simulated by the local air-sea interaction. It is also found that the SST variability is strongly influenced by the mixed layer depth variability. It can therefore be concluded that the seasonal and interannual predictability of the midlatitude SST anomalies can be significantly improved by the knowledge of the real mixed layer depth.

Chapter 5

Interannual to decadal variability in the Tropical Atlantic

Although the database of SST in the tropical Atlantic is as good or better than in the tropical Pacific, the variability of the SST in the tropical Atlantic is not as well understood as in the tropical Pacific. This might be due to the fact that in the tropical Atlantic the variability of the SST is weaker than in the Pacific. The latter is dominated by the El Nino / Southern Oscillation (ENSO) phenomenon. Although ENSO originates in the tropical Pacific, it affects the global climate. The physical mechanisms responsible for ENSO are well understood and ENSO forecast models have predictive skill up to approximately one year in advance.

The same physical mechanism which produces the ENSO mode in the Pacific can also produce an ENSO-like mode in the Atlantic, but due to the different basin geometry it is expected to be much weaker than in the Pacific (Zebiak 1993, Huang and Carton 1995, Latif et al. 1996).

Analyses of rainfall data over Northeast Brazil (Moura and Shukla 1981), a region that frequently experiences drought conditions, suggested that an interhemispheric dipole in the tropical Atlantic SST anomalies have a major impact on the rainfall in this region. The rainfall is strongly related to the position of the Intertropical Convergence Zone (ITCZ) in the early boreal spring, which in turn may be related to anomalous SST patterns.

Several EOF analyses of SST anomalies based on monthly or annual mean data found the interhemispheric dipole as one of the first two EOFs. Houghton and Tourre (1992) analysed a SST dataset of the tropical Atlantic for the period 1964-88 and found that the 2^{nd} EOF is associated with an interhemispheric dipole. However, a rotation of the first five EOFs reveals that the variability in the northern and southern hemispheres cannot be characterised by a dipole. The anomalies north and south of the ITCZ are not significantly correlated with each other in this time interval (Houghton and Tourre 1992).

This is confirmed by the analysis of Enfield and Mayer (1997), who analysed a record of SST of for the period 1950-92. They also analysed the correlation between the tropi-

cal Atlantic SST anomalies and ENSO indices and found that the Atlantic is significantly correlated with ENSO in the region 10°N -20°N with a time lag of about 4-5 month.

Mehta and Delworth (1995) analysed observed box averaged SST anomalies in the tropical Atlantic in both a 100 years data set and a 100 years simulation with a global general circulation model. They found two time scales of variability that significantly stand out above the background red noise. One type of variability with a time scale of approximately 8 to 11 years is characterised by independent variability to the north and south of the equator. The other type of variability has a time scale of approximately 12 to 20 years and consists of a dipole. However, Mehta (1998) found in a later study, by performing a reanalysis of the 100 years of SST observation of the tropical Atlantic, that there is no cross-equatorial dipole mode at any time scale in the tropical Atlantic.

Chang et al. (1997) studied the relationship between SST, wind stress, and net heat flux anomalies for this region. Additionally they used a coupled ocean-atmosphere model to examine the role of local air-sea interactions. They identified that the tropical SST dipole can be attributed to an unstable thermodynamic ocean-atmosphere interaction. They found a realistic parameter regime with a self sustained interdecadal oscillation of an interhemispheric dipole pattern. The oscillation can be described as follows: Suppose the northern tropical Atlantic exhibits a positive SST anomaly and that the southern tropical Atlantic a negative one. Then, the wind stress in the north will be weakened and that in the south strengthened. The resulting surface heat flux anomalies in both poles will reinforce the initial SST anomalies, which is a positive air-sea interaction feedback. The meridional advection of heat anomalies by the steady ocean currents will act as a negative feedback in both poles. Together the positive and negative feedbacks give rise to a self sustained interdecadal oscillation. Results from forecasts experiments with the same coupled ocean-atmosphere models show predictability skill for several years ahead (Chang et al. 1997).

In a recent study Penland and Matrosova (1998) analysed the predictability of tropical Atlantic SST anomalies by linear inverse modelling of observed SSTs. They found that the 6-month influence function in the north and south tropical Atlantic tend to be of the opposite sign and evolve into a clear dipole, when the analysis is confined to the tropical Atlantic only.

However, the existence of a distinct time scale or the existence of the dipole as a dominant mode of SST variability is still controversial. The observations of tropical Atlantic SST are limited in quality, and, in particular, in length. Therefore, it is questionable whether the existence of a decadal ocean-atmosphere interhemispheric dipole mode can be proven simply by analysing SST observations. For a better understanding of the processes which produce the observed SST anomalies, other quantities such as net heat flux, wind stress, and subsurface temperatures may be useful, but measurements of these quantities are rare in space and time, and are limited in quality.

Simulations with Coupled General Circulation Models (CGCMs) may provide additional

insights into the dynamics of the SST variability in the tropical Atlantic. Although the CGCMs do not model the climate system correctly in all respects, they have the advantage to provide all important quantities without spatial and temporal gaps and with equal quality. The study is mainly based on Empirical Orthogonal Functions (EOF) analyses of the observed SST anomalies and those simulated by four different CGCMs. It will be shown that the tropical Atlantic is dominated by SST variability, which is centred in the northern and southern trade wind zones. Furthermore, it will be shown that the centres in the northern and the southern trade wind zones are mainly independent of each other, and that, therefore, an interhemispheric dipole does not exist for time scales less than 25 years. A combined analysis of the SST, wind stress and the net heat flux anomalies indicates that the variability in the tropical Atlantic is induced by atmospheric forcing and that dynamic feedbacks of the ocean are less important.

Additionally experiments with an Atmospheric General Circulation Model (AGCM) forced by prescribed SST anomalies and coupled to a slab ocean model were performed. The results of these experiments support the results of the CGCM simulations and those obtained from the SST observations.

This chapter is organised as follows. The results of the analyses of the observed SSTs are presented in the following section. I describe the results of the CGCMs simulations in section 5.2. The role of the surface heat flux is discussed in section 5.3. I present the result of the AGCM-slab-ocean simulation in section 5.4. The forced experiments with the AGCM are described in section 5.5. Finally the dominant structures of the SST variability in the tropical Atlantic are compared to those of the tropical Pacific in section 5.6, while the paper is concluded with a discussion of the main findings in section 5.7. The work presented in this chapter will has been published in the Journal of Climate by the Dommenget and Latif (2000).

5.1 The GISST observations

The following analyses are based on the GISST-data set which provides monthly mean SSTs for the period 1903 -1994 (Parker et al. 1995). The data were interpolated onto a 2.8125^o x 2.8125^o grid. The analysis will be restricted to the tropical Atlantic from 30^{o}S - 30^{o}N. The monthly data were averaged to obtain annual mean data, and at each grid point the local linear trend was subtracted.

The statistically dominant SST-patterns in the tropical Atlantic can be determined by EOF analysis. Figure 5.1 shows the first two EOFs of the GISST observations explaining 33.8 % and 22.2 % variance of the SST variability respectively in the examined region. All in this paper presented EOF-patterns have been normalised, so that the PCs of the EOF-patterns have a standard deviation of 1.0.

EOF-1 is characterised by a uniform pattern with maximum values near the eastern

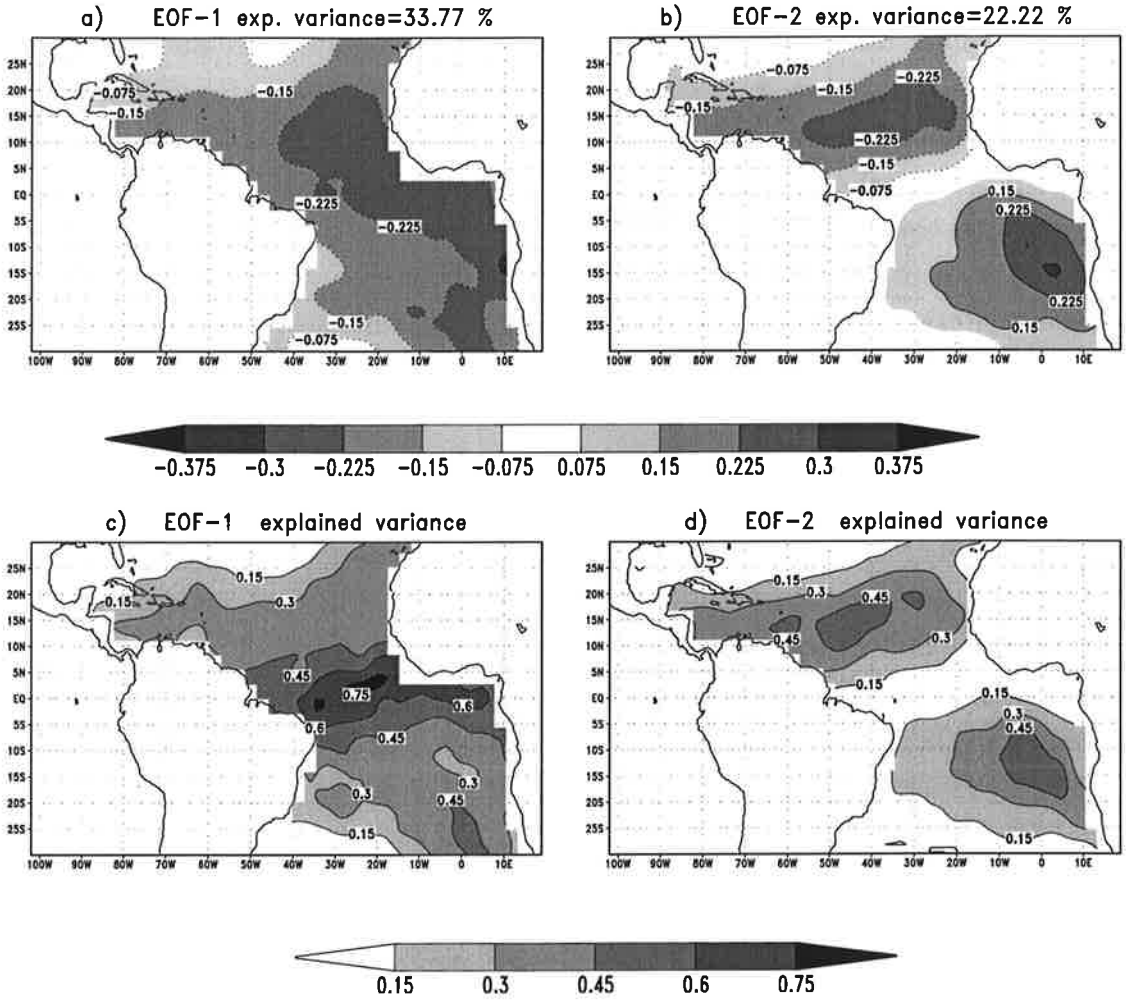

Figure 5.1: a) Leading EOFs of the GISST observations, explaining about 34 % of the variance. b) second most energetic EOF, explaining about 22 % of the variance. c) and d) spatial distribution of the explained variance for EOF-1 and EOF-2 ,respectively.

boundary. EOF-2 is characterised by a north-south dipole, with centres of action in the region of the trade wind zones. The 3rd and 4th EOFs (not shown) have maximum variability at the northern (30°N) and southern edges (30°S) of the examined region ; they explain only a few percent of the variability in the tropical Atlantic and are of minor interest. The variance explained by EOF-1 shows a maximum region close to the equator. The variance explained by EOF-2 is largest in the two centres of the dipole.

Figure 5.2 shows the spectra of the corresponding principle components PC-1 and PC-2. The spectra of the PCs are tested against the hypothesis that the spectra are produced by a first order auto-regressive process (red noise spectra), and a 95% confidence level for accepting the red noise hypothesis is also shown. This hypothesis was introduced by the stochastic climate model of Hasselmann (1976). The spectra are in good agreement with the red noise assumption, but have a slightly significant increase of variability for periods of 3 -

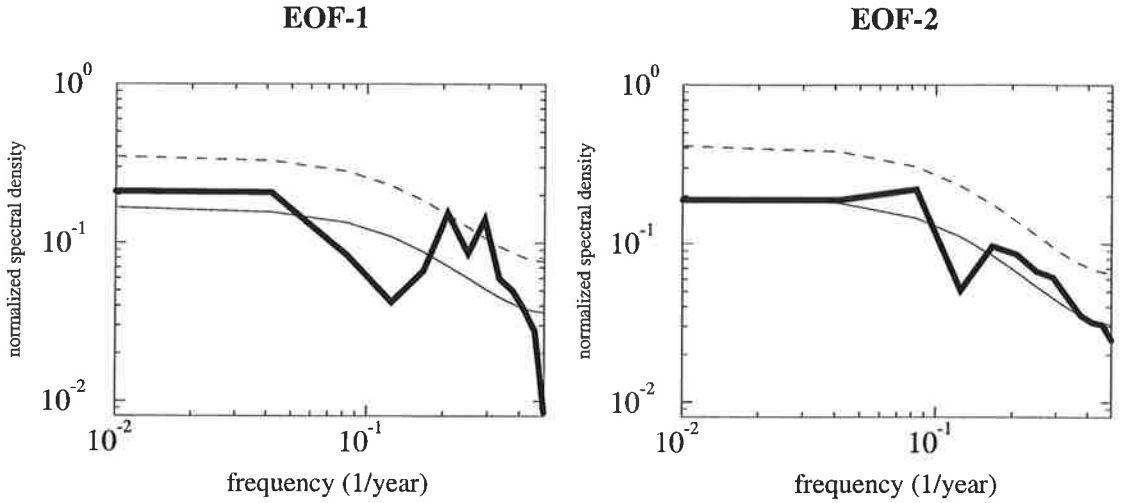

Figure 5.2: Spectra of PC-1 and PC-2 corresponding to EOF-1 and EOF-2 in Figure 5.1. The thin solid lines are the expected red noise spectra calculated as described in the text. The dashed lines are the 95 % confidence level for the null hypothesis of a red noise spectra.

5 years for the PC-1.

As it shall be shown in the following, the SST anomalies in the regions of the maximum trade winds cannot be explained by one single EOF pattern, but they have to be regarded as a linear combination of the two leading EOFs. The pattern of the EOF-2 alone could lead to the conclusion that variations north of the equator are anti-correlated with those south of the equator. This, however, is not the case.

The correlations of the near global SST anomalies with box averaged SST anomalies north and south of the equator are shown in Figure 5.3. The box north of the equator shows significant correlations with SSTs at higher latitudes of the Atlantic, but it has no significant correlation or anti-correlation with the south Atlantic. The box south of the equator also shows a relatively local correlation pattern in the southern hemisphere of the Atlantic. Both correlation maps lead to the conclusion that the SST anomalies in the northern and southern trade wind zones of the Atlantic are not significantly correlated with each other. Lag correlations of the two box averaged time series do not show either significant correlations for lags shorter than 10 years.

The two boxes in the tropical Atlantic are significantly correlated with the SST anomalies outside the Atlantic. The northern box is significantly correlated with the eastern Pacific and Indian Oceans. The southern box has generally smaller correlations with SST anomalies outside the Atlantic, but exhibits significant correlations in essentially the same regions as the northern box. Most of the teleconnections are probably due to the ENSO phenomenon. An exception is the correlation of the northern tropical box with the SST anomalies in the northern Atlantic, which indicates that the variability seen these two regions is related. This issue, however, will be discussed elsewhere.

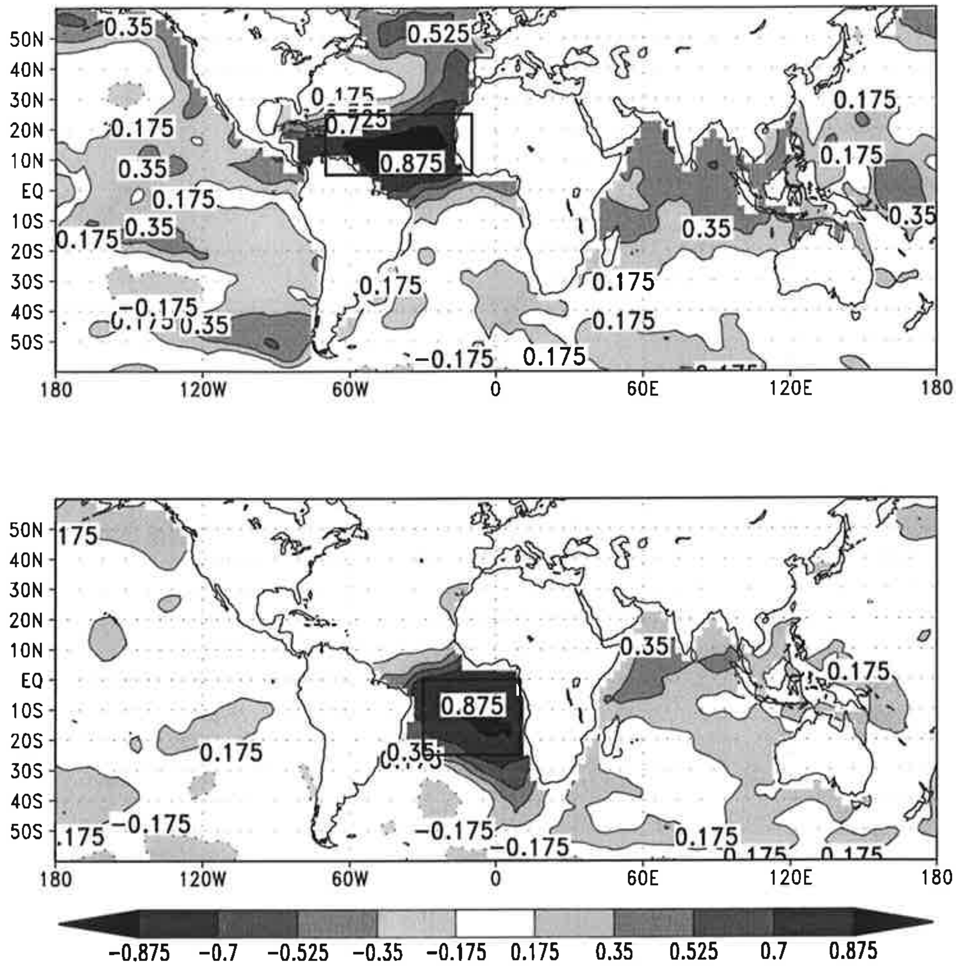

Figure 5.3: Correlation of box-averaged SST anomalies with near global SST anomalies. Shaded areas are significantly non zero correlations at the 95 % confidence level.

Although the EOF-2 of the tropical Atlantic SST anomalies is a dipole pattern, the SST anomalies in the two hemispheres of the tropical Atlantic are not anti-correlated with each other. As indicated by the correlation patterns in Figure 5.3, it is likely that the variability in the tropical Atlantic is dominated by two spatially separated patterns.

In addition to an ordinary EOF-analysis, a rotated EOF analysis can give a second set of orthogonal basis vectors. One useful criterion for this analyses is the VARIMAX criterion (Kaiser 1958, Kaiser 1959, and Richman 1986). The VARIMAX method for rotating EOFs leads to the orthogonal rotation with the highest possible localisation of the SST pattern. In other words, if an ordinary EOF-analysis distributes the variability of one region into different EOF patterns, as into EOF 1 and 2 of the analysis of the tropical Atlantic, the VARIMAX method finds the rotation in which the variability of that region is concentrated in one pattern as much as possible.

Applying the VARIMAX method 10 rotated EOFs have been computed. They were obtained by an orthogonal rotation of the 10 leading EOFs. The stability of the two dominant

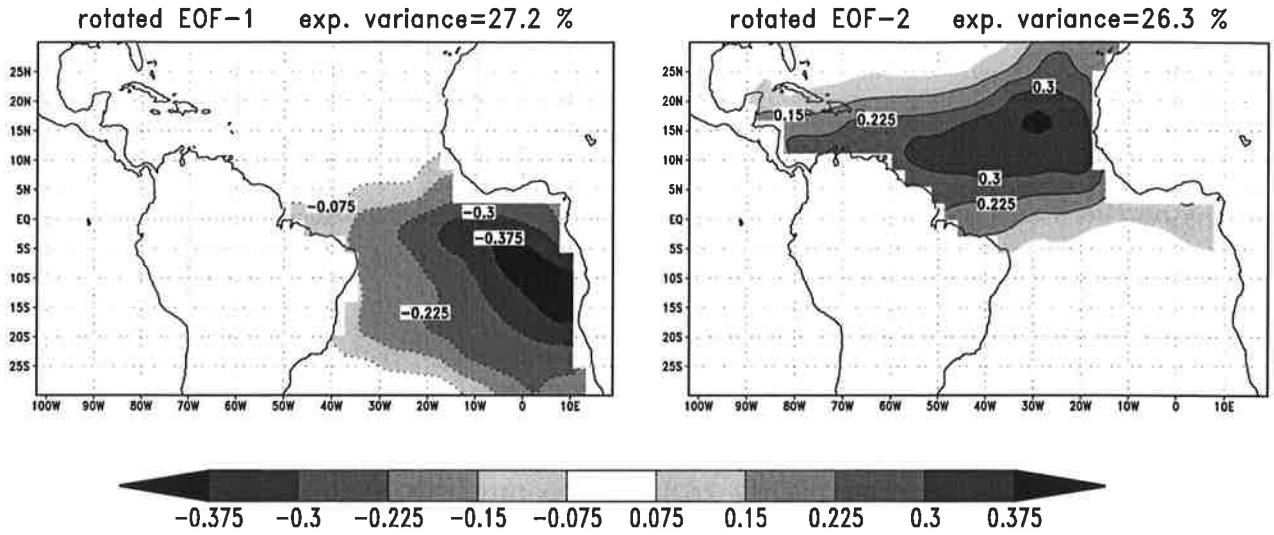

Figure 5.4: VARIMAX rotated EOF 1 and 2 of the SST of the GISST observations. Contours and shading as in Figure 5.1.

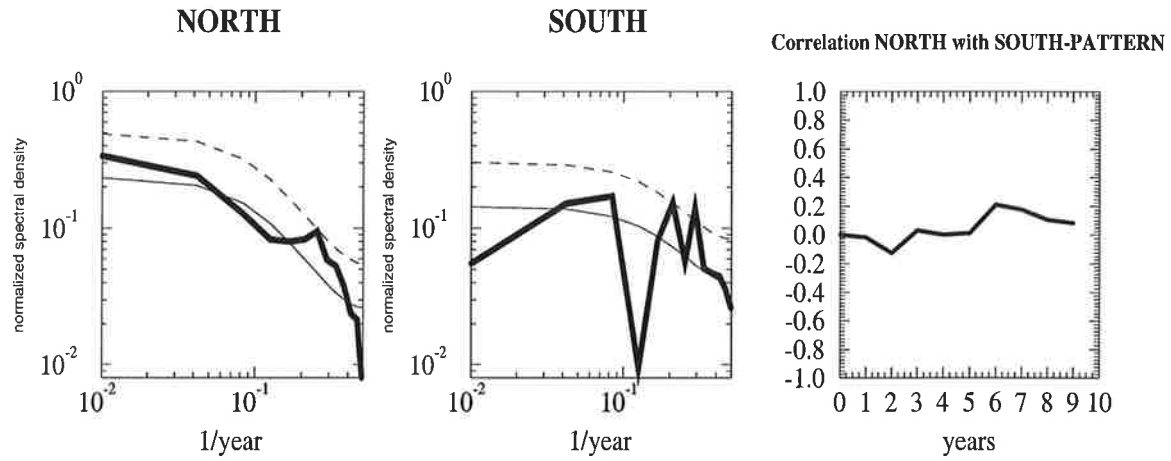

Figure 5.5: Spectra of the rotated EOF 1 and 2 shown in Figure 5.4.Thin lines and dash lines in the spectra plots as in Figure 5.2. The right plot shows the correlation between the rotated EOF 1 and 2 in subjection of the lag in time, while the northern patterns lags the southern.

pattern have not been found to be influenced by the number of EOFs chosen, even if only the first two EOFs were used for the rotation. The two leading rotated EOFs are shown in Figure 5.4. The patterns of the two leading rotated EOFs are spatially well separated and are almost equal to the two patterns obtained by the box correlation analyses shown in Figure 5.3. The time series of the northern box has a correlation of 0.99 with the PC of the leading rotated EOF and the southern box has a correlation of 0.98 with the PC of the second rotated EOF. Figure 5.5 shows the spectra of the PCs of the two leading rotated EOFs and the lag correlation between the two PCs. The spectra are consistent with a red

noise spectra, although both spectra show marginally significant increases in the variability at periods of 3 - 5 years. Furthermore, the two PCs are not significantly correlated for lags up to nine years.

The rotation of the 10 leading EOFs shows that a major part of the SST variability can be explained by two spatially separated and uncorrelated patterns. The patterns are centred in the northern and southern trade wind zones of the tropical Atlantic. A similar result has been obtained by Houghton and Tourre for a shorter SST-dataset (Houghton and Tourre 1992).

The question as to whether the two EOFs are degenerated statistically is not important for the SST variability in the tropical Atlantic. The fact that the two leading EOFs can be represented as two spatially well separated patterns with orthogonal time evolution is more important physically. Suppose that the EOF-1 is separated statistically from EOF-2, which, is almost the case in the GISST data set, then the two spatially separated patterns of the rotation are not a possible EOF system, but they are still a orthogonal base which can be used to describe the SST variability in the tropical Atlantic. Therefore, the dominance of the EOF-1 can be understood as a weak interaction between the two rotated patterns, which leads to the preferential EOF-system shown in Figure 5.1.

From a mathematical point of view the two representations of the SST variability are equivalent, but it has to be considered that, from a physical point of view, the different representations of the SST anomalies may lead to different explanations of the underlying physical mechanisms. For example, in the representation of the SST variability based on the two ordinary EOF-patterns, the SST anomalies are created by an equatorial mode and an orthogonal (independent) dipole mode, which explain comparable amounts of variability in the same regions. This may lead to the wrong conclusion that the tropical Atlantic SST variability is dominated by a dipole pattern. However, it has been shown that the two poles are not significantly anti-correlated with each other. Therefore, the patterns of the first two ordinary EOFs are not the best basis on which to explain the SST anomalies in the tropical Atlantic.

In the rotated representation the leading ordinary EOF, which has its maximum at the thermal equator, is a superposition of the two leading rotated EOFs. Therefore, there is no real dominant equatorial pattern in the tropical Atlantic comparable to the one found in the tropical Pacific, which is connected to the ENSO mode. In the following, the SST anomalies in the tropical Atlantic will be represented by rotated EOFs only.

5.2 The CGCM simulations

To examine interannual to decadal variability, a time series of 90 years may be too short as it has been seen above. It could not be shown rigorously that the SST variability in the northern and southern trade wind zones are independent of each other. Therefore, I additionally analysed the outputs of simulations with CGCMs.

Although the General Circulation Models do not model the climate system correctly in all features, they have the advantage to provide all important quantities without spatial and temporal gaps and with equal quality. It is possible, for instance, to analyse not only SST anomalies, but also the surface heat flux and surface wind stress anomalies which may produce them. The models are described in Chapter 3.

I analysed the outputs of four different CGCMs. For all four CGCMs the same analyses, as performed for the GISST-data, were conducted. Figure 5.6 shows the two leading VARIMAX rotated EOFs of each of the four different CGCMs. On the left hand side shown are the EOF with maximum in the northern trade wind zone are and on the right hand side the EOF (rotated pattern) with maximum in the southern trade wind zone.

For the ECHAM4-HOPE2, the ECHAM3-LSG and the ECHAM4-OPYC CGCM simulations, the differences between the two leading ordinary EOFs (not shown) and the two leading rotated EOFs are negligible. The two leading ordinary EOFs of the GFDL simulation are similar to the two leading ordinary EOFs of the GISST observations (see Figure 5.1). However a rotation of the ordinary EOFs with the VARIMAX criterion finds the spatially separated patterns (shown in Figure 5.6).

It is remarkable that all CGCMs show similar variability in the two leading rotated EOFs. Similar to the analysis of the GISST data the stability of the two dominant pattern of the CGCM simulations do not significantly depend on the number of EOFs chosen for the rotation. In all data sets the two leading rotated EOFs are also found by using only the first two EOFs for the VARIMAX rotation. The amplitudes are at comparable levels and the patterns are very similar in all CGCMs simulations. The spectra of the PCs of the two leading rotated EOFs of the four CGCMs are shown in Figure 5.7. None of the spectra of the northern and the southern patterns show any significant differences relative to the expected red noise spectra. I conclude from these analyses of the model simulations that the dominant SST variability in the tropical Atlantic is not linked to a specific time scale. In particular, there is no evidence for enhanced variability at decadal time scales, which was found by several authors (Mehta and Delworth 1995, Chang et al. 1997). Furthermore, I did not find much evidence for the existence of a tropical Atlantic dipole pattern in the CGCM simulations.

The Pacific SST variability is dominated by ENSO, which is an equatorial mode of variability. The dominant SST variability in the tropical Atlantic region is found in the trade wind zones, and there is no dominant equatorial mode. This does not mean that

there is no ENSO-like variability in the equatorial region of the Atlantic. Zebiak (1993) and Latif et al. (1996) have shown that an ENSO-like mode exists in the Atlantic. This mode, however, accounts for only a small fraction of the SST variability in the tropical Atlantic, which is reflected in the fact that the two leading rotated EOFs in all data sets are centred in the trade wind zones and not at the equator.

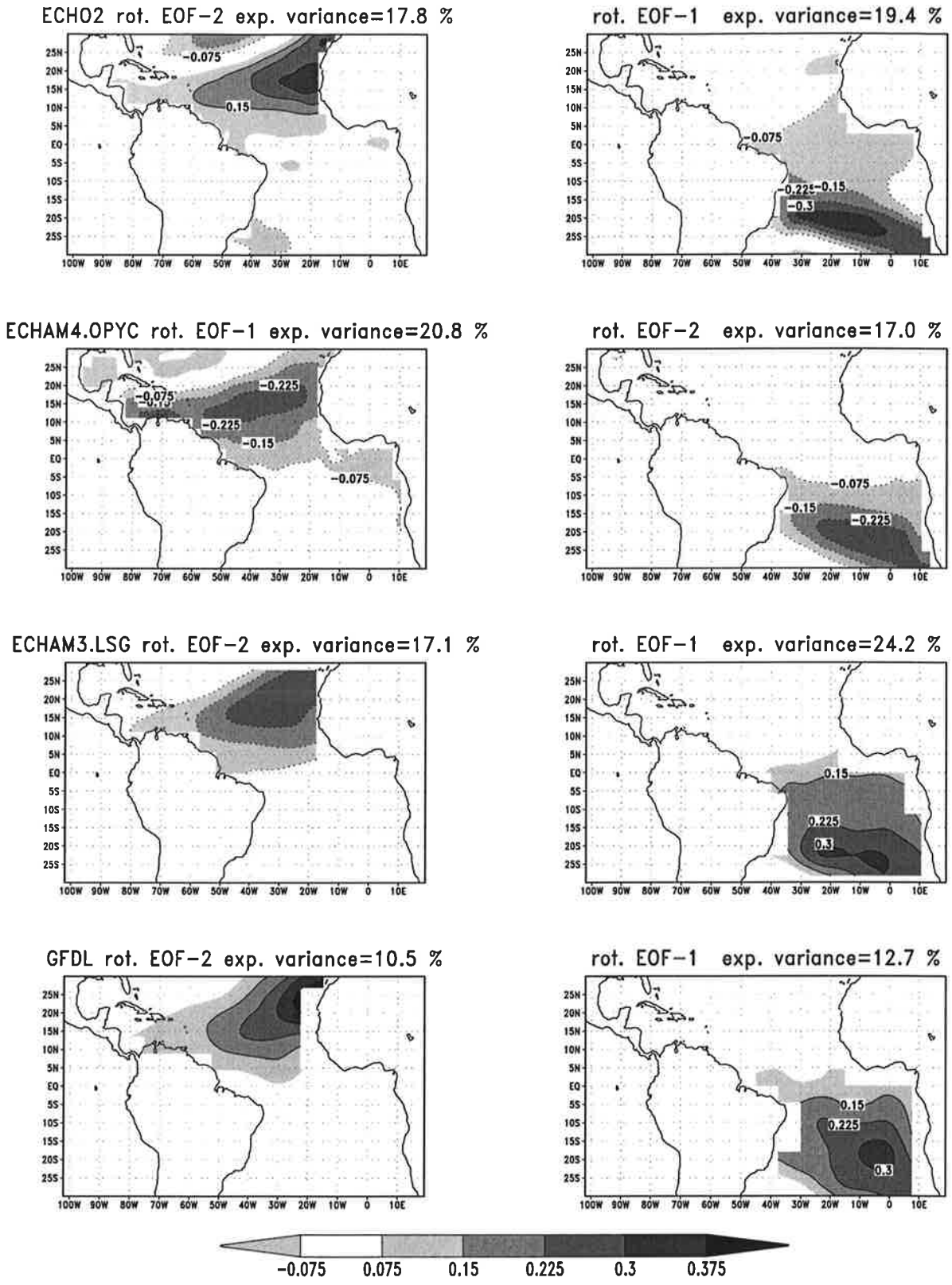

Figure 5.6: The two leading rotated EOF of four different GCM simulations. For details see inside the text. EOF patterns with the maximum in the northern hemisphere are on the left hand side and the patterns with maximum in the southern hemisphere are on the right hand side. Contours and shading as in Figure 5.1.

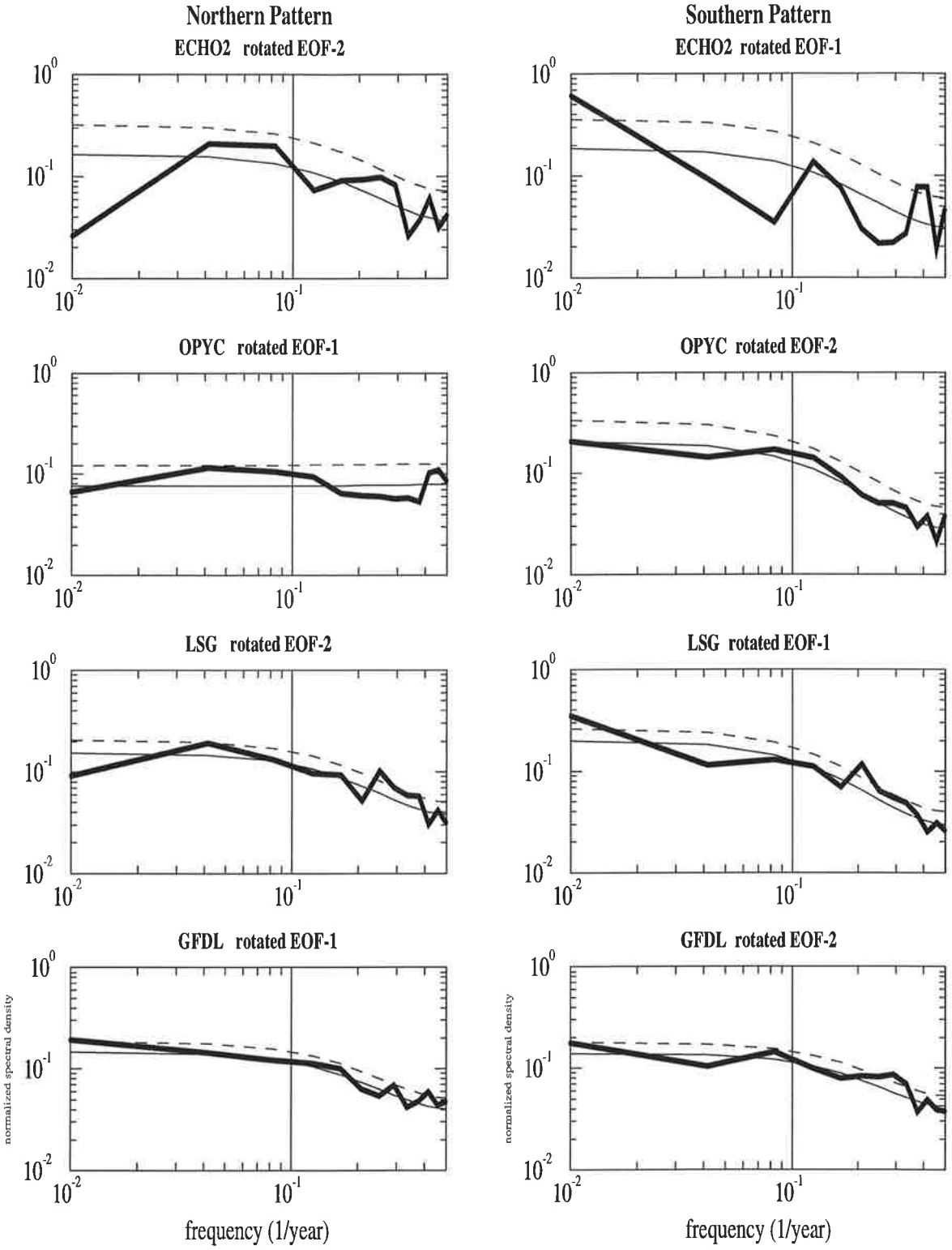

Figure 5.7: Spectra of the PCs of the two leading rotated EOFs derived from the coupled model simulations. The order of the spectra is equal to Figure 5.6 and the thin lines and dashed lines are defined as in Figure 5.2

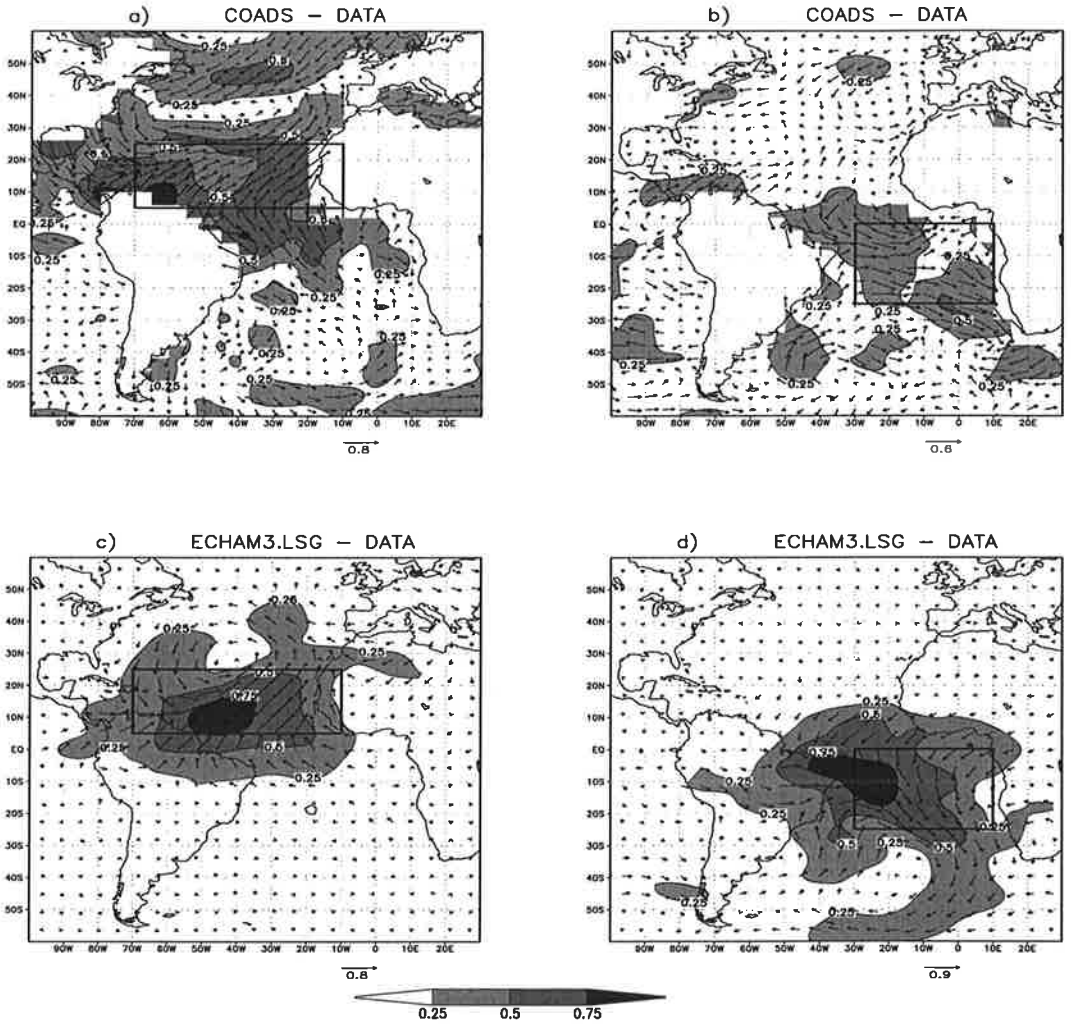

Figure 5.8: Upper plots: Correlations between GISST SST anomalies and COADS surface wind stress. a) Correlation of the SST anomalies in the northern box with the surface wind stress anomalies b) correlation of the SST anomalies in the southern box with the surface wind stress anomalies. Lower plots: Correlations between SST anomalies and surface wind stress from the ECHAM3/LSG CGCM simulation. c) Correlation of the SST anomalies in the northern box with the surface wind stress anomalies d) correlation of the SST anomalies in the southern box with the surface wind stress anomalies.

5.3 Relationship of the SST anomalies to the wind stress anomalies

The two leading rotated EOFs of the GISST observations are centred in the region of maximum trade winds. The same result was obtained from the CGCMs simulations. My hypothesis for the generation of the SST anomalies in the centres of action is the following: changes in the wind field lead to changes in the surface heat flux, which in turn drive the SST anomalies.

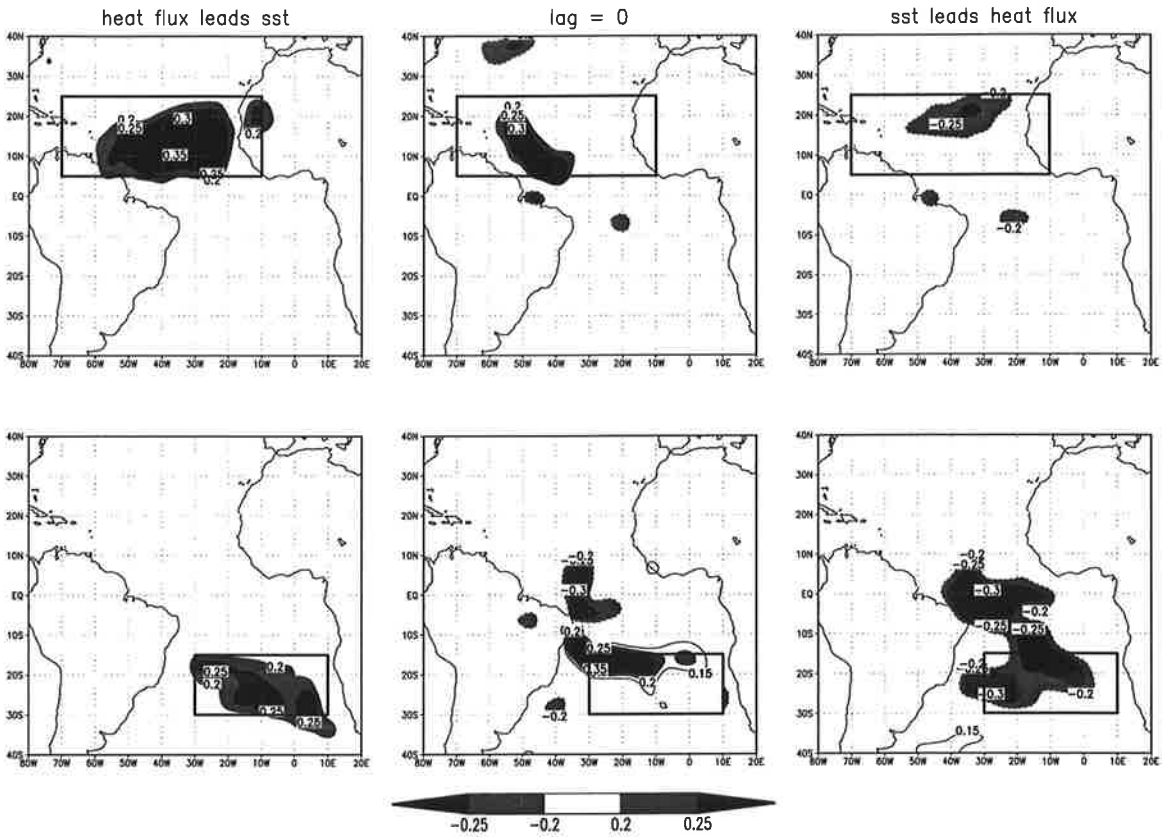

Figure 5.9: Lag correlation between net heat flux anomalies and the SST anomalies averaged over the drawn boxes, based on annual mean data from the ECHAM3-LSG simulation.

Figure 5.8 shows the correlations between the wind stress vector and the SST in the northern and southern trade wind zones (indicated by the boxes). The two upper plots show the correlations of observed (COADS) wind stress anomalies with the observed SST anomalies of the GISST dataset during the period 1945 - 1989. The lower plots show similar analyses for the ECHAM3-LSG CGCM. The wind stress anomalies are correlated with the SST anomalies in both trade wind zones. A positive SST anomaly is associated with weakened wind stress in both trade wind zones, or vice versa. This strong correlation between the wind stress and the SST anomalies may be the clue to the SST variability in the tropical Atlantic. If ocean dynamics, such as wave propagation, convection, and advection are of minor importance for the generation of the SST variability in the tropical Atlantic, atmospheric forcing has to be the dominant process for producing SST anomalies. The correlations between the wind stress and the SST anomalies in the tropical Atlantic are consistent with the picture that the ocean responds passively to changes in the atmosphere.

The lag correlations of the net heat flux and the SST anomalies are shown in Figure 5.9 as obtained from the ECHAM3-LSG CGCM simulation. When the net heat flux leads the SST anomalies, the correlations inside the trade wind zones is positive, which acts to

build up the SST anomalies. When the SST anomalies lead the net heat flux anomalies the correlation inside the trade wind zones is negative, which will act to restore the mean condition in the SST field. At lag = 0 the correlation of the net heat flux and the SST anomalies in the trade wind zones is still positive in some regions, namely in the western part of the northern trade wind zone and the northern part of the southern trade wind zone. This may be explained by the wind field itself, which will transport the air to these regions. The fact that the correlation is still positive and not zero indicates that there is a weak positive feedback between the ocean and the atmosphere inside the trade wind zones, which may be the reason why the trade wind zones are the regions of the strongest SST variability. There is no evidence for an interhemispheric connection between the net heat flux and the SST anomalies.

In summary it is likely that the changes in the wind stress field manifest themselves in variations in the surface heat flux, which will force the SST anomalies, as discussed in Chang et al. 1997.

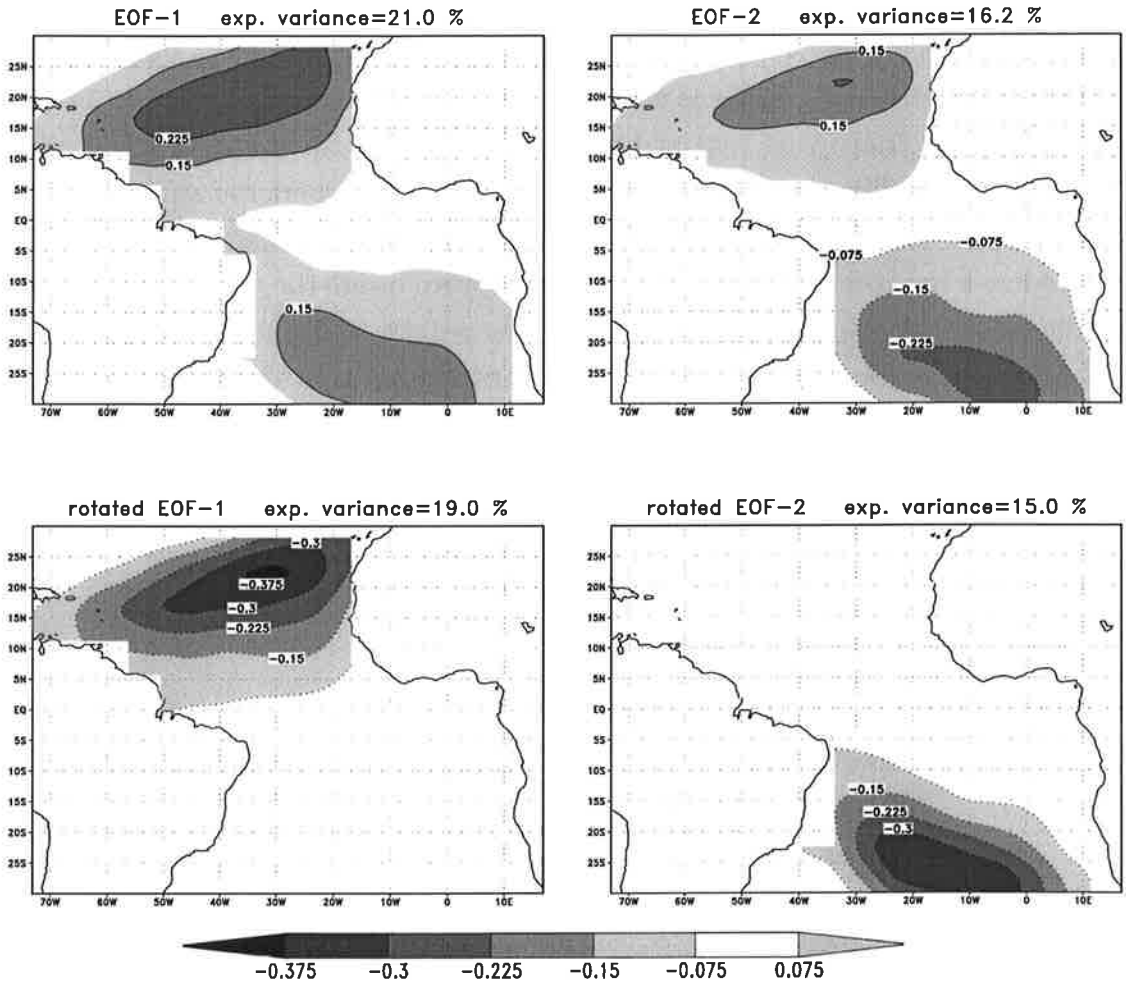

Figure 5.10: EOF 1 and 2 from the ECHAM3/mixed layer ocean simulation (upper plots). Lower plots show the VARIMAX rotated EOFs

5.4 An ocean mixed layer model

The results of the analyses of the observations and the CGCMs simulations lead to the conclusions that the SST variability in the tropical Atlantic can be explained by atmospheric forcing only, and ocean dynamics are of minor importance. In order to test this hypothesis, I coupled a mixed layer ocean model with the ECHAM3 atmosphere model. A more detailed description of this model is given in section 3.3, where the so called MIX_{50} simulation is described. The ocean mixed layer model does not carry (by construction) any ocean dynamics. In such a model only the variations of the atmospheric heat flux can produce SST anomalies. The mixed layer simulation can be compared directly to the ECHAM3-LSG simulation which employs the same atmosphere model. The years 21 to 220 of the MIX_{50} simulation were analysed in the same way the CGCM simulations and the GISST observations have been analysed.

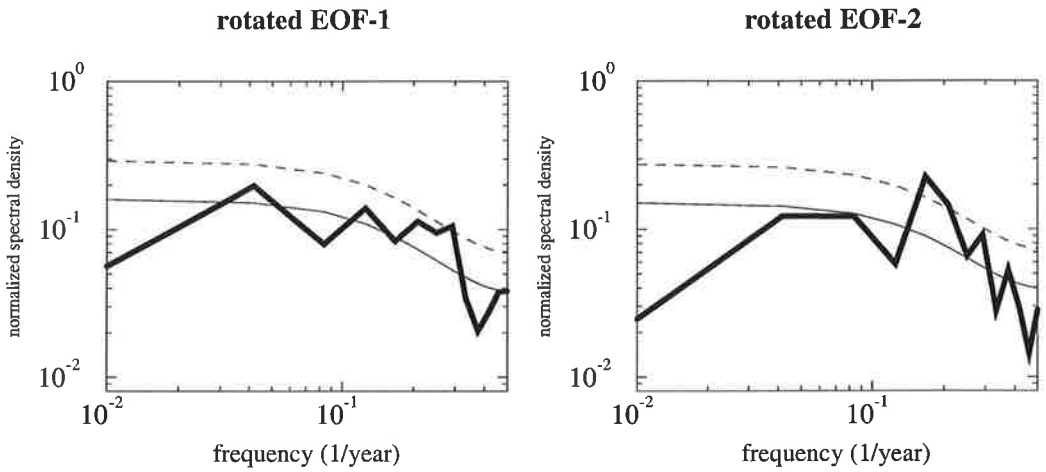

Figure 5.11: Spectra of the rotated EOF 1 and 2 from the ECHAM3/mixed layer ocean simulation.

The two leading EOFs of the SST variability of the mixed layer simulation are shown in Figure 5.10. The patterns of EOF-1 and EOF-2 are similar to that derived from the GISST observations. EOF-1 explains 21.0% and EOF-2 16.2% of the total variability in the examined region. Therefore, the two EOFs are separated significantly. Nevertheless the VARIMAX rotation of the 10 leading EOFs was applied. The two leading rotated EOFs are shown in the lower plots of Figure 5.10. The two leading rotated EOFs are very similar to those obtained from the GISST observations and the CGCM simulations. The spectra of the PCs of the two leading rotated EOFs are shown in Figure 5.11. The northern pattern exhibits increased variability for periods from 3 to 7 years, but overall the spectra of the PCs of the two rotated patterns are consistent with red noise processes.

It can be concluded from the results of the mixed layer simulation that the dominant SST variability in the tropical Atlantic is explained by atmospheric forcing only, and dynamic processes in the ocean, such as convection, advection and wave propagation, are not important in producing the basic spatial structure of the SST variability.

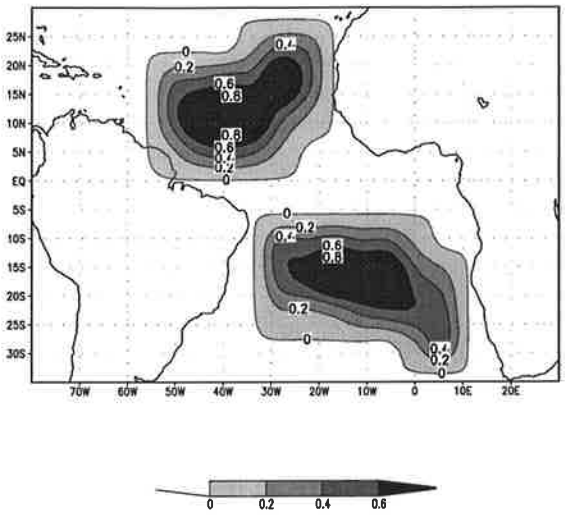

Figure 5.12: SST pattern for the atmosphere model simulations.

5.5 Atmospheric model forced by SST anomalies

To further investigate the connection between the SST anomalies and the atmospheric response, several simulations with the atmospheric circulation model ECHAM3 have been carried out. In these simulations the atmosphere model is forced by different SST anomalies. Five different simulations with different SST forcing have been conducted. A control simulation was integrated for 20 years. It is forced with climatological SSTs which were taken from the coupled ocean-atmosphere simulation with the ECHAM3-LSG CGCM. The other four simulations were integrated for 10 years, each with the same SST field plus different constant SST anomaly patterns added. The added SST anomaly patterns are shown in Figure 5.12. The SST anomalies are placed in the zones of maximum trade wind. The amplitudes are chosen to be about twice the standard deviation of the SST anomalies in these regions.

The purpose of the simulations is to analyse the effect that different SST anomalies in the trade wind zones have on the state of the atmosphere. Using the results of the simulations it is possible to study whether the response of the atmosphere is local or interhemispheric and whether the atmosphere has the tendency to amplify or damp the SST anomalies.

The results for the change in the wind stress and the net heat flux are shown in Figures 5.13 and 5.14 . The plots show the differences of the 10 years mean values of the response experiments and the 20 years mean values of the control run divided by the standard deviation of the annual mean values of the 20 years of the control run. The units are in standard deviations. Following a t-test, a change of 1.5σ in the mean state over a 10 year period represents a statistically significant change at the 95 % level.

In the upper left plot the simulation forced by the northern SST pattern is shown, the

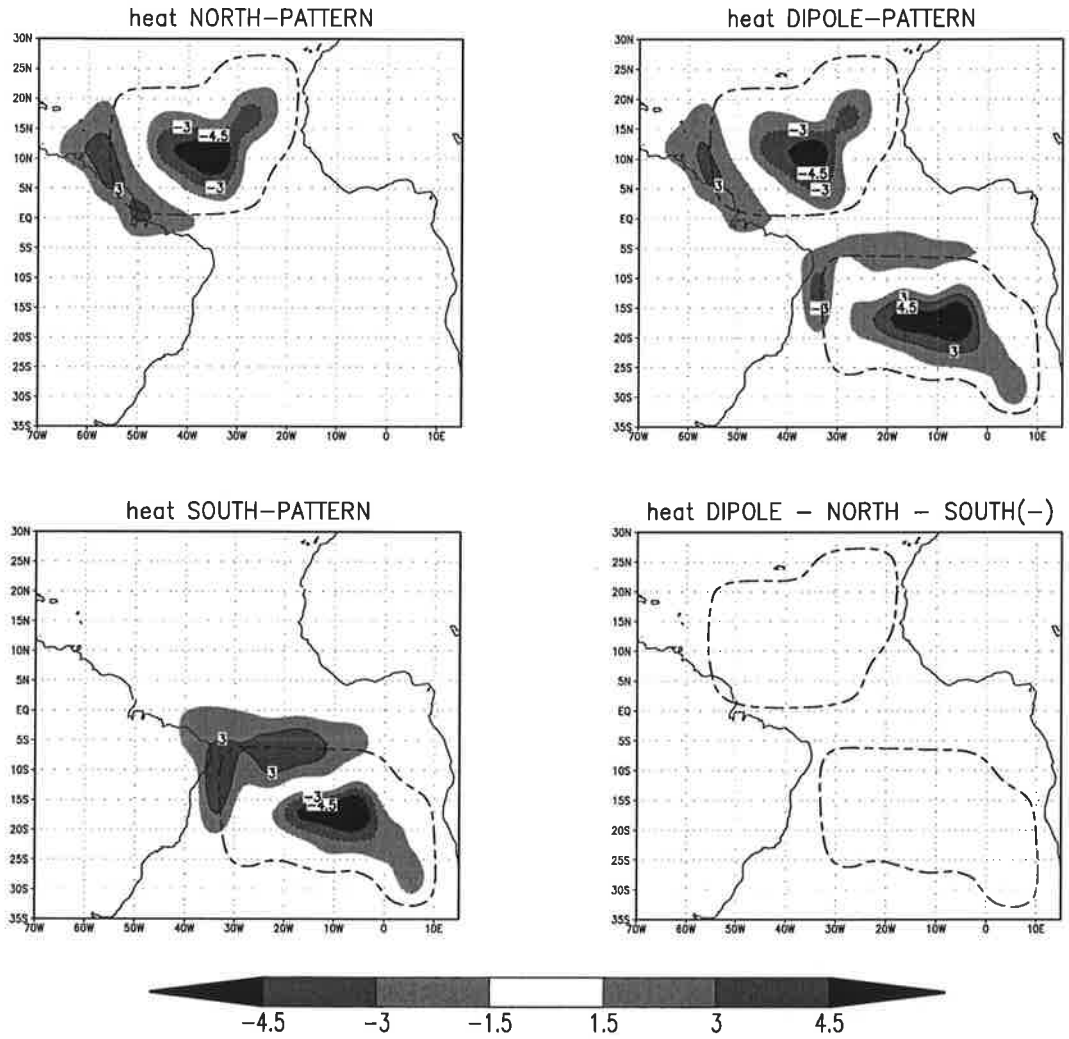

Figure 5.13: Results of the atmosphere model simulation, as described in the text. The plots show the difference between the 10 years mean of the net heat flux for each simulation and the 20 years mean of the net heat flux of the control run divided by the standard deviation of the annual mean values of the 20 years from the control run. The units are in standard deviation. The dashed line indicates the region with the changed SST for each simulation. The lower right plots shows the superposition of three simulation results.

lower left plot shows the simulation forced by the southern SST pattern, and in the upper right plot shows the simulation forced by the dipole (composed of the northern and the negative southern SST anomaly pattern). The difference between the dipole simulation and the sum of the simulations with the northern and the negative southern SST anomaly pattern are shown in the lower right plot. This last plot provides an indication of the linearity of the response. Although the atmospheric model is global, there is no significant change in the wind stress field or the net heat flux outside the tropical Atlantic.

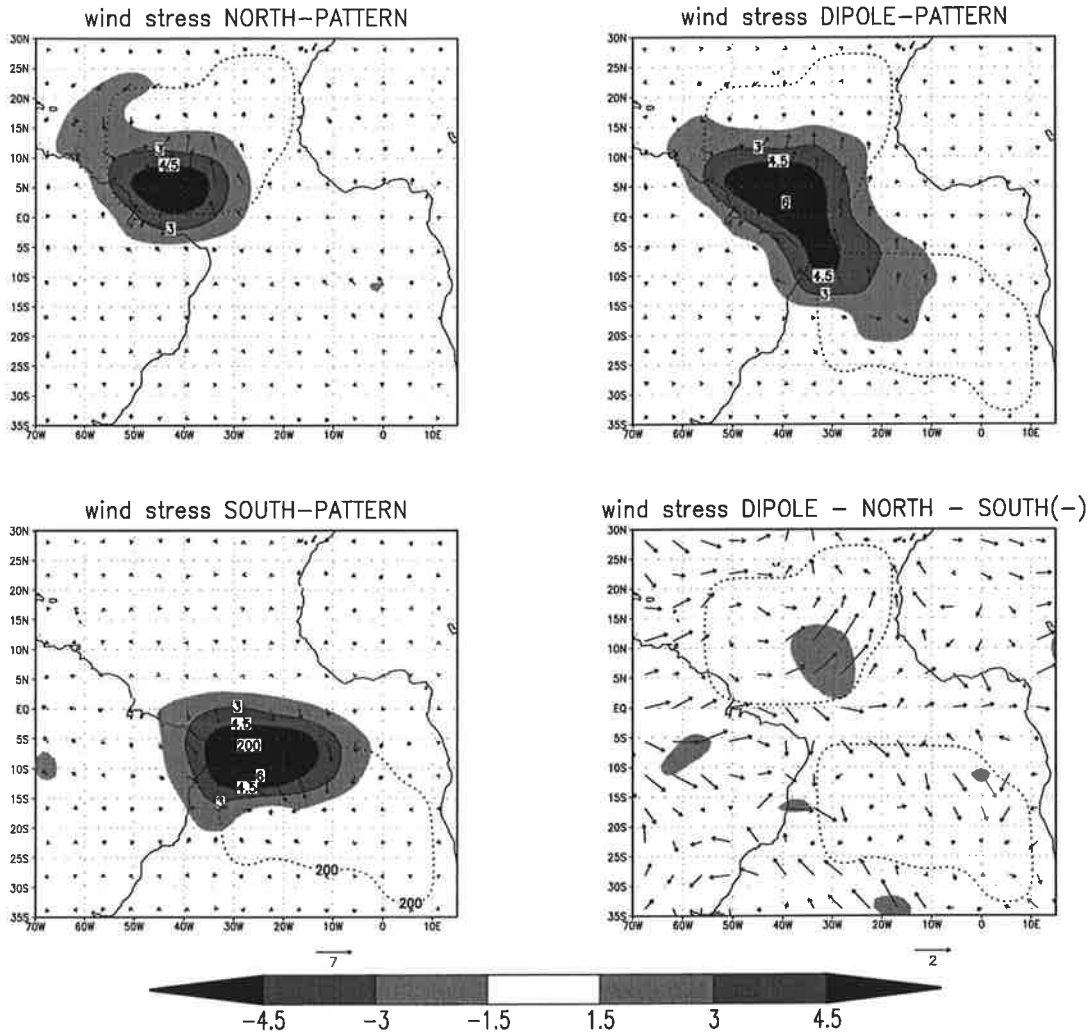

Figure 5.14: Results of the atmosphere model simulation, as described in the text. The plots show the vector difference between the 10 years mean of the wind stress for each simulation and the 20 years mean of the wind stress of the control run divided by the standard deviation of the annual mean values of the 20 years from the control run. The units are in standard deviation. The dashed line indicates the region with the changed SST anomaly for each simulation. The lower right plots shows the superposition of three simulation results.

A deviation from the climatological SST, results in a local negative feedback through the net heat flux in the centre of the SST anomaly (see Figure 5.13), while at the western edge of the SST anomaly pattern the net heat flux responses tend to create SST anomalies. In both experiments the response in the net heat flux and the in the wind field is limited to the region close to the SST anomalies and there is no significant interhemispheric response. It can therefore be concluded from the experiments with the northern and southern SST anomalies that the atmosphere responds locally to the SST anomalies and that SST anomalies in one

hemisphere of the tropical Atlantic do not effect the other hemisphere.

The response in the net heat flux is mainly caused by a change in the latent heat flux, while in the center of the SST anomalies the short wave radiative flux does also contribute to the change in the net heat flux (not shown). The response of the latent heat flux is basically due to the change in the strength of the trade winds which is caused by the warming over the SST anomalies. The mean winds in the two regions with the SST anomalies are easterly with a smaller component towards the equator. Thus, the response will lead to a weakening of the wind strength (see Figure 5.14).

From these experiments it can be concluded that the variability in the two centres of the trade winds is mainly driven by variations of the wind field, which will lead to a change in the latent heat loss of the ocean. These results have also been found in several other studies (e.g. Carton et. al. 1996, Wagner 1996)

The response of the atmosphere to an anomalous SST dipole (shown in the upper right side of Figure 5.13 and 5.14) can be understood as the superposition of the two single SST experiments with anomalies in the northern and southern trade wind zones. This is indicated by the difference between the dipole experiment and the sum of the experiments with the single northern and the single negative southern SST patterns shown in the lower right hand side of Figures 5.13 and 5.14. From these experiments it can be concluded that there is no specific atmospheric response to an interhemispheric SST anomaly dipole, which cannot be explained by a superposition of the local responses to the single SST anomalies in the northern or southern trade wind zones independently.

5.6 Comparison of the tropical Atlantic with the tropical Pacific

The presented analysis of the observed tropical Atlantic SST variability and of the CGCM simulations has clearly shown that the dominant SST variability is centred in the two trade wind zones, whereas the SST variability in the tropical Pacific is clearly dominated by the equatorial pattern of the El Nino phenomenon. It therefore seems that the SST variability in the tropical Atlantic and in the tropical Pacific are quite different, which may lead to the conclusion that the source of the SST variability is different in the two oceans.

However, a comparison of the two leading EOF patterns can illustrate that the tropical Atlantic and the tropical Pacific are still very similar. In Figure 5.15 the two leading SST EOF patterns of the tropical Atlantic and the tropical Pacific are shown. The comparison of the leading EOFs in the two oceans shows that in both oceans the first EOF is a monopole centred at the equator with its maximum close to the equator and larger amplitude at the eastern boundary of the ocean basin. The second EOF in both oceans is a dipole pattern with the amplitudes centred in the trade wind zones. The only characteristic difference in the two leading EOFs of the two oceans is that the EOF-1 of the tropical Pacific is significantly stronger than the EOF-2 and stronger than the EOF-1 in the Atlantic. It therefore can be concluded that the SST variability in the two tropical oceans is very similar and basically consists of three dominant patterns, an equatorial El Nino like pattern and the two patterns centred in the trade wind zones.

In the tropical Pacific the equatorial pattern is the dominant pattern and the two pattern centred in the trade wind zones are of minor importance. But in the tropical Atlantic the equatorial pattern is not as strong as in the Pacific and the two pattern centred in the trade wind zones are the most dominant patterns. In the orthogonal presentation of the dominant SST variability in the EOF or the VARIMAX analysis it does not become clear that the tropical Atlantic has three dominant pattern.

In order two illustrate that the tropical Atlantic has indeed an equatorial pattern, box correlations of the observed SST are shown in Figure 5.15. The box correlations show that the centres of the trade wind zones in the northern and the southern hemisphere are basically uncorrelated, whereas the equatorial region is significantly correlated with both trade wind regions. This indicates that an equatorial SST pattern exists which is influencing the two patterns centred in the trade wind regions. However, in such a situation, in which the dominant pattern are not independent of each other, an orthogonal presentation of the dominant SST variability can not give a good picture of the SST variability. In section 2.1.2 a Monte Carlo example of such a situation has been discussed. The discussion in this section shows that the SST variability in the tropical Atlantic may indeed be interpreted as an interaction between an equatorial pattern and the two patterns centred in the trade wind zones, whereas the pattern centred in the trade wind zones are mostly independent of each

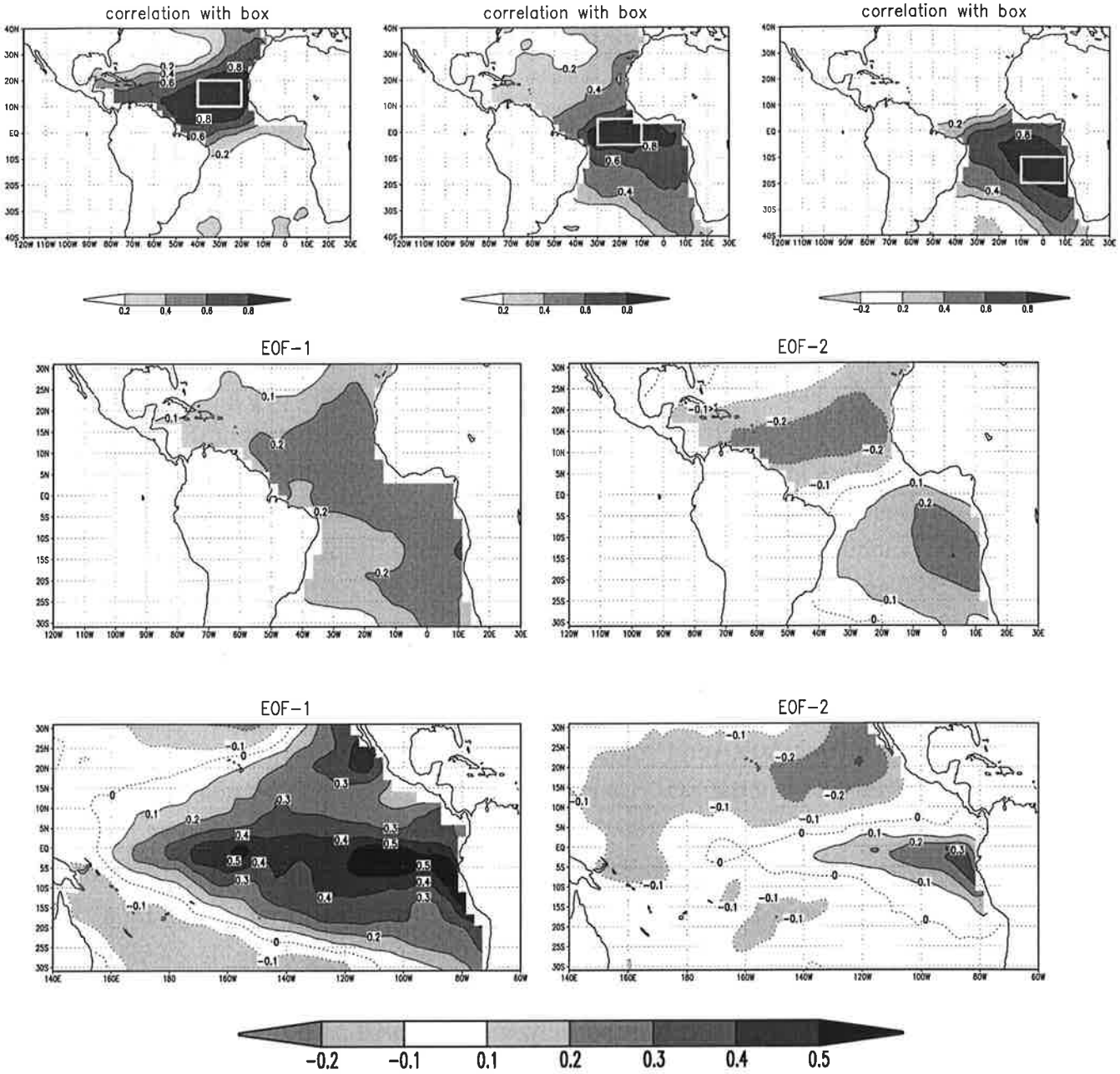

Figure 5.15: The upper three plots show the box correlation of the SST with the SST inside the boxes. In the middle plots the two leading EOFs of the tropical Atlantic and in the lower plots the two leading EOFs of the tropical Pacific are shown.

other.

5.7 Summary and discussion

EOF analyses of annual mean SST from the GISST observations during the period 1903 - 1994 and of four different CGCMs simulations show consistent results. The dominant SST variability is well represented by the two leading rotated EOFs for all data sets. The rotation has been calculated with the VARIMAX criterion. In all data sets the two leading rotated EOFs are centred in the two trade wind zones. The correlation between the SST fluctuations in the northern and in the southern trade wind zones is not significantly different from zero. An interhemispheric dipole or an anti-correlation of the SSTs in the northern and southern trade wind zones, which could be important for rainfall anomalies in e.g. north-east Brazil, does not exist. It can be concluded that the dipole pattern is an artifact of the EOF analyses technique used. This has been confirmed by coupled model experiments, by an ocean mixed layer experiment, and atmospheric response experiments. All of these experiments indicate that ocean dynamics are not important in the generation of tropical Atlantic SST anomalies, and that SST anomalies are forced by the atmosphere.

The ordinary EOF analysis of the GISST observations does not separate the two patterns centred in the trade wind zones. EOF-1 is an overall monopole and EOF-2 a dipole (see Figure 5.1). A rotation of the 10 leading EOFs with the VARIMAX criterion separates the SST variability in the trade wind zones into two patterns with orthogonal time evolution. The explained variances of the EOF-1 and EOF-2 of the GISST observations are comparable over large regions in the tropical Atlantic.

Although the two leading EOFs of the GISST dataset are separated by one standard deviation, the representation with two patterns centred in the trade wind zones is still physically useful. The question whether the two EOFs are statistically degenerated or not is of minor importance for the SST variability in the tropical Atlantic. The fact that EOF-1 and EOF-2 can be represented as two spatially well-separated patterns with orthogonal time evolution is physically more important. Consider EOF-1 as statistically separated from EOF-2, a fact that is almost statistically significant for the GISST observations and for the GFDL simulations, then the two spatially separated patterns from the rotation are not a possible EOF system, but they are still an orthogonal basis of the SST variability in the tropical Atlantic. Thus, the dominance of EOF-1 can be understood as a weak interaction between the two rotated patterns, which leads to the preferential EOF-system shown in Figure 5.1. This weak connection can have different origins. Due to the fact that in both the GISST observations and in the GFDL simulation EOF-1 has positive correlation coefficients on both hemispheres, a global non-linear trend can be responsible for the weak connection between the two hemispheres. The influence of the ENSO mode from the Pacific, which is expected to have equal signs in both hemispheres, may also be responsible for the weak connection. The two patterns centred in the trade wind zones are not completely spatially separated, but they overlap at the thermal equator and move with the seasonal cycle. Therefore, it is

very likely that this connection at the equator leads to a weak interaction between the two patterns.

The SST spectra in both trade wind zones are consistent with the assumption of red noise spectra of AR(1) processes.

There has been a discussion whether the SST exhibits increased variability at decadal time scales as found by Mehta and Delworth 1995 in the observations and in the GFDL CGCM data. In this analysis no evidence was found for significantly enhanced variability at decadal time scales. Although the spectra of the SST in the GFDL data and the observations do show slightly enhanced variance at decadal time scales relative to the estimated spectra of the AR(1)-processes , the spectra of the SST are still consistent with those derived from AR(1)-processes, which is in agreement with a later work of Delworth and Mehta 1998.

The general agreement of the spectral distribution of the SST variability in all analysed data sets with AR(1)-processes and the local structure of the two leading EOFs in all data sets leads us to the conclusion that the ocean is responding passively to the atmospheric forcing by simply integrating the atmospheric noise due to the large heat capacity of the ocean's mixed layer. This is the basic idea of the Hasselmann's stochastic climate model. Therefore, ocean dynamics, such as wave propagation, convection and advection are not important for producing SST variability in the tropical Atlantic. I would like to note, however, that this conclusion is restricted to the models analysed and that I cannot exclude that all models suffer from serious deficiencies. Furthermore, the SST observations available are rather short to study decadal variability, so that some uncertainty remains.

The relationship between SST, wind stress and net heat flux anomalies in the tropical Atlantic, as they have been found in analysing different simulations with an AGCM forced by different SST anomalies, is consistent with this picture. Furthermore a simple mixed layer ocean model coupled to an AGCM, which produces SST variability that is similar to that simulated by complex ocean-atmosphere general circulation models supports the idea that the SST variability is only a passive response to the atmospheric forcing and that ocean dynamics, which are not included in the simple mixed layer ocean model, are not important.

Carton et. al. (1996) conducted a series of experiments with an ocean GCM modifying surface forcing to investigate the nature of SST variability in the tropical Atlantic. They found that local wind-induced latent heat loss was the most important term in regulating interannual SST variability away from the equator, which is also consistent with my results. They also found that ocean dynamics were most important at the equator. Although, an equatorial pattern does not show up in my EOF analysis, the possibility that ocean dynamics are important at the equator cannot be excluded. My analysis, however, shows that this kind of ENSO-like variability does not account for a large fraction of the SST variability and does not significantly effect the structure of the dominant SST pattern.

No evidence was found for an interhemispheric coupled ocean-atmosphere mode that would imply increased predictability at decadal time scales as found by Chang et. al. (1997).

Unfortunately, this limits (if correct) the predictability of the tropical Atlantic SST variability and associated climate fluctuations to that derived from the persistence of the SST anomalies.

In the past, analyses of the Atlantic variability have either concentrated on the tropics or on the mid and higher latitudes. This differentiation was done because it was believed that different kinds of physical mechanisms are important in the different regions. The results of my analyses indicate that this is not the case.

It was found that the SST variability in the two hemispheres of the tropical Atlantic are mainly independent, but that the rotated EOFs that are centred in the northern tropical Atlantic are highly correlated to the first EOF of the SST anomalies in the midlatitudes of the North Atlantic (from 20°N to 60°N) for all data sets.

If I finally compare the tropical Atlantic Ocean with the tropical Pacific, it can be found that in the Pacific the equatorial variability dominates the SST variability of the tropical region, while in the Atlantic the equatorial region does not strongly influence the dominant SST patterns. Although the spectra of the EOF-1 does show some enhanced variance in the interannual time scale (see Figure 5.2) the rotation of the EOFs does separate the equatorial region into the two pattern centred in the trade wind zones. Thus the Atlantic and Pacific differ only in the strength of the equatorial SST variability, while the SST variability in the trade wind zones is similar in both oceans.

Chapter 6

Introducing an alternative technique for AMIP-type simulations

In the analysis of climate variability the question is often posed how the atmosphere responds to a given SST anomaly, whereby it is not important what the source of the SST anomaly itself is. In the past this question has often been analyzed by so called AMIP-type simulations, in which an atmospheric model is forced by a given SST anomaly added to an SST climatology and the response of the atmospheric model is then compared with a simulation forced by the SST climatology only. The difference between the two simulations is then assumed to be the response of the atmosphere to the given SST anomaly.

However, there are good reasons to believe that the response of the coupled ocean-atmosphere system can be very different. The main argument against the AMIP-type simulations is that they are uncoupled simulations using prescribed SST boundary conditions, which is an unrealistic assumption. It has to be considered that in a coupled simulation the variable SST and the different heat flux balance between the ocean and the atmosphere can lead to a completely different response in the atmosphere. In particular, the assumption that the SST variability can be prescribed and that the atmosphere is responding to the SST seems to be very critical, because on shorter time scales the SST is mainly forced by the atmosphere. A critical analysis of this problem can be found in Barsugli and Battisti (1998). They propose that seasonal forecasts should be done with ensembles of AGCMs coupled to a mixed layer ocean model instead of using AMIP-type experiments.

As a response to the criticism raised regarding AMIP-type simulations one can consider introducing the SST anomaly pattern or the historical SST time series into a coupled slab-ocean atmosphere model. In such a coupled simulation the SST can adjust and is mostly driven by the atmosphere. A simulation in which the SST anomaly pattern is introduced into the ocean mixed layer can still be a fully coupled simulation, and all of the problems mentioned for the AMIP-type simulations are no longer relevant for this type of simulation.

In the following section I shall present how an SST anomaly pattern or historical SST time series can be introduced in a coupled ocean mixed layer - atmosphere simulation and

how the new technique performs compared to the normal AMIP-type simulations. The following sections are mainly focused on the introduction of the new technique and not on the discussion of whether or not the SST response experiments are useful. The discussion in the following sections will indicate that the interpretation of the response to the forcing SST anomaly pattern can be very difficult.

6.1 The set-up of the experiments

In an atmosphere model coupled to a slab ocean model an SST anomaly can be introduced into the ocean mixed layer in different ways depending on the objective of the study. If the response to a local SST anomaly is to be studied one can simply replace the slab ocean, at the grid points at which the SST anomaly should be introduced, by a fixed SST which includes the SST anomaly of interest. However, this set-up has the same disadvantages, as the AMIP-type simulations, because at some grid points the SST is fixed again and the ocean and atmosphere are not coupled. It is therefore better to keep the slab ocean coupled to the atmosphere at all grid points and to introduce the SST anomaly in the ocean mixed layer itself. This can be done by introducing an additional heat flux $F_{pattern}$ to the equation 3.1, which leads us to the following equation:

$$\frac{d}{dT}SST = \frac{1}{(C_p \rho_{water} D_{mix})} * (F_{atmos} + F_{pattern}) + \Delta T_{clim} \tag{6.1}$$

The simplest approach for $F_{pattern}$ would be a constant value:

$$F_{pattern} = C_{flux} \tag{6.2}$$

However, this may not be the most practical solution. In most cases one would like to study the response of the atmosphere to a given SST anomaly pattern with a given amplitude. If $F_{pattern}$ is chosen as a constant heat flux, it is difficult to determine the right values for C_{flux} to get the desired SST anomaly pattern, and additionally C_{flux} has to be seasonally varying to get a realistic SST anomaly pattern in all seasons. On the other hand this approach has the advantage that the coupled system is not damped and that the heat flux $F_{pattern}$ is independent of the state of the coupled slab ocean - atmosphere system, which makes it look like a heat flux coming from the deeper ocean.

In most cases the following specification of $F_{pattern}$ may be the most practical to study the response of the atmosphere to a given SST anomaly pattern:

$$F_{pattern} = C_{damp} * (SST_{forc} - SST) \tag{6.3}$$

Here the $F_{pattern}$ is a damping heat flux, which forces the SST with the strength of the damping parameter C_{damp} to the desired SST_{forc}. The value of C_{damp} determines how close the SST is following the given SST_{forc}. In principle this approach is an intermediate solution

between keeping the SST fixed as in the AMIP-type simulations and leaving the coupled system unaffected as in a normal coupled simulation.

To introduce a historical SST time series one can modify equation 3.1 to obtain:

$$\frac{d}{dT}SST = \frac{1}{(C_p \rho_{water} D_{mix})} * F_{atmos} + \Delta T_{clim} + \Delta T_{ano} \tag{6.4}$$

Where ΔT_{ano} is the SST change in the historical time series at the given time step. The resulting SST in the mixed layer will not exactly match the historical SST time series but, depending on the strength of the heat flux F_{atmos} and depth D_{mix}, the ensemble mean of the SST in a set of integrations will be correlated to the historical SST time series on shorter time scales. In this set-up the coupled system of the slab ocean -atmosphere is almost unaffected and the added temperature change ΔT_{ano} will look like a tendency coming from the deeper ocean.

An important limitation of equation 6.4 is that only the change in the historical time series is given to the mixed layer model at each time step, whereas no information regarding the absolute SST anomaly of the historical time series is given to the mixed layer model. This can result in a "wash out" of the long-term SST anomalies of the historical time series due to the internal variability of the mixed layer, especially in those regions in which the atmospheric heat flux is relatively strong compared to the mixed layer depth. In order to account for the long-term evolution of the SST anomalies one can introduce a damping heat flux into equation 6.4:

$$\frac{d}{dT}SST = \frac{1}{(C_p \rho_{water} D_{mix})} * (F_{atmos} + F_{forcing}) + \Delta T_{clim} + \Delta T_{ano} \tag{6.5}$$

Here $F_{forcing}$ is defined in the same way as for SST anomaly patterns in equation 6.3 :

$$F_{forcing} = C_{damp} * (SST_{history} - SST) \tag{6.6}$$

Although the heat flux $F_{forcing}$ can force the SST to be close to the historical time series on all time scales, the damping effect of $F_{forcing}$ is strongly changing the characteristics of the coupled ocean-atmosphere system. The discussion in section 6.3 will show whether such a damping heat flux can be useful, and if so when.

In order to test the new technique five different SST response simulations have been carried out, with five different SST anomaly patterns, shown in Figure 6.1. Each of the five experiments have been integrated for 10 years with the usual AMIP-type atmospheric model and with the new set-up using the atmospheric model coupled to a slab ocean model. For the new set-up the $MIX_{seasonal}$ model has been changed by replacing the equation 3.1 by equation 6.1 and using equation 6.3 for $F_{pattern}$ with $C_{damp} = 100W/(m^2K)$. In order to get the same amplitude of the SST anomaly pattern in both simulation configurations (AMIP and coupled setup), the amplitude of the SST anomaly pattern has to be increased in the

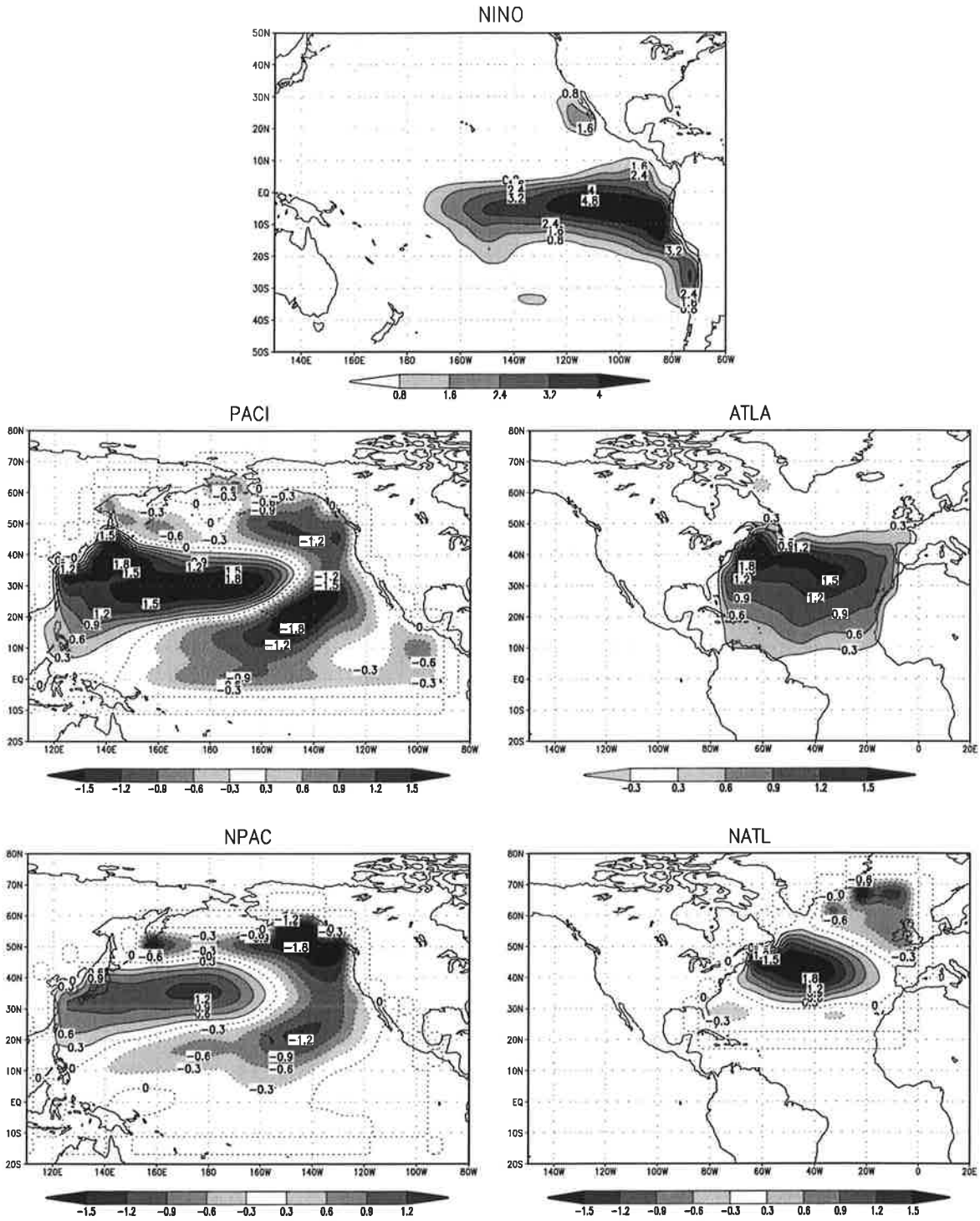

Figure 6.1: The SST anomaly patterns for the response experiments.

coupled configuration by a factor of about 1.2. The results of these experiment are discussed in the following section 6.2.

In order to test the new technique for historical time series four ensemble experiments have been conducted with the $MIX_{seasonal}$ model, in which equation 3.1 has been replaced by equation 6.4, and the simulation was named MIX_{GISST}. For the historical SST time series the years 1958-1994 from the GISST data set has been introduced globally. The results of this experiment are discussed in the section 6.3.

6.2 The general comparison of the atmospheric response to the different SST anomaly patterns

In the framework of this thesis there is not enough space to adequately discuss the individual experiments physically. Therefore, I shall only take a short look at the results of the experiments and leave a more comprehensive discussion to later studies. The analysis of the response to the SST anomaly pattern will be focused on the comparison of the different types of simulations.

In principle each of the five SST response experiments is connected to a different question. The NINO pattern (see Figure 6.1) was taken from the observed SST of December 1997, which was the largest El Niño event observed. Due to the fact that the teleconnection patterns in the atmosphere as well as the associated SST anomaly patterns, are well known for the El Niño phenomenon, the response of the simulations can be validated with observations. The two patterns PACI and ATLA are both the leading EOF of an ocean basin-wide EOF analysis based on 320 years of detrended annual mean 20-60 years band pass filtered SST from the CGCM simulation ECHAM-LSG.

The NINO, PACI and ATLA patterns do not reflect the internal variability of the MIX_{season} simulation. However it may be that the MIX_{season} model is more sensitive to patterns that resemble the internal variability patterns of this model. Therefore the patterns NPAC and NATL has been chosen additionally. Both have been derived from EOF-analysis of the monthly mean SST anomalies of the MIX_{season} simulation.

In Figures 6.2(SST), 6.3(net heat flux), 6.4(sea level pressure) and 6.5(300mb height) the responses to the different SST anomaly patterns are shown, and each Figure shows the response to all five SST anomaly pattern in a different quantity.

The response to the NINO SST anomaly pattern in the AMIP-type simulation and in the mixed layer simulation are very similar, and both are similar to the observed teleconnection patterns associated with El Niño. In particular the change in the sea level pressure over the Pacific resembles the typical response of the Southern Oscillation and the pressure decrease over the North Pacific is also simulated in both experiments. The response in the heat flux in the AMIP-type simulation and the response in the SST in the mixed-layer simulation are also in good agreement with the observed teleconnections in the SST. Overall, the responses to the NINO SST anomaly pattern basically show that both types of simulations are producing a realistic responses to the given tropical SST anomaly.

In a general comparison of the responses to all the different SST anomaly patterns, it can be said that the responses to the NINO, PACI and ATLA SST anomaly patterns are very similar in the AMIP-type simulation when compared to the mixed layer simulation, while the responses to the NPAC and NATL SST anomaly patterns are very different between the AMIP-type simulation and the mixed layer simulation. It has therefore to be concluded that the response of the atmosphere to a given SST anomaly pattern can indeed be very different

in a coupled simulation, and that the interpretation of the response to a SST anomaly pattern in AMIP type simulations may be very critical.

The comparison of the 300mb height responses shows that the response in the atmosphere-mixed-layer simulation is in general much larger if a SST anomaly pattern is introduced which does not resemble the internal variability of the MIX-season simulation (like NINO, PACI, ATLA). This indicates that the response of a coupled model to somehow artificial SST anomaly pattern is very different compared to the response to SST anomaly patterns of the internal variability. It therefore has to be taken into account that the response of the atmosphere-mixed-layer simulation to a SST anomaly pattern taken from other coupled systems or the observations can be purely artificial and may not give any information about how the other coupled system or the real world would respond.

One of the advantages of the mixed layer set-up is that the SST itself can respond to the introduced SST anomaly pattern, while in the AMIP-type set-up the response in the SST can only be estimated by the heat flux response. The response in the heat flux can in general only give the direction in which the SST will develop, but the amplitude to which the SST anomaly will change cannot be determined. A comparison of the responses to the NINO-pattern shows that the AMIP-type simulation has a large remote response in the heat flux, while the mixed-layer simulation has mostly no remote response in the heat flux. This is mainly due to the fact that the SST in the mixed-layer simulation is responding to changes in the atmosphere, which compensates the changes in the heat flux.

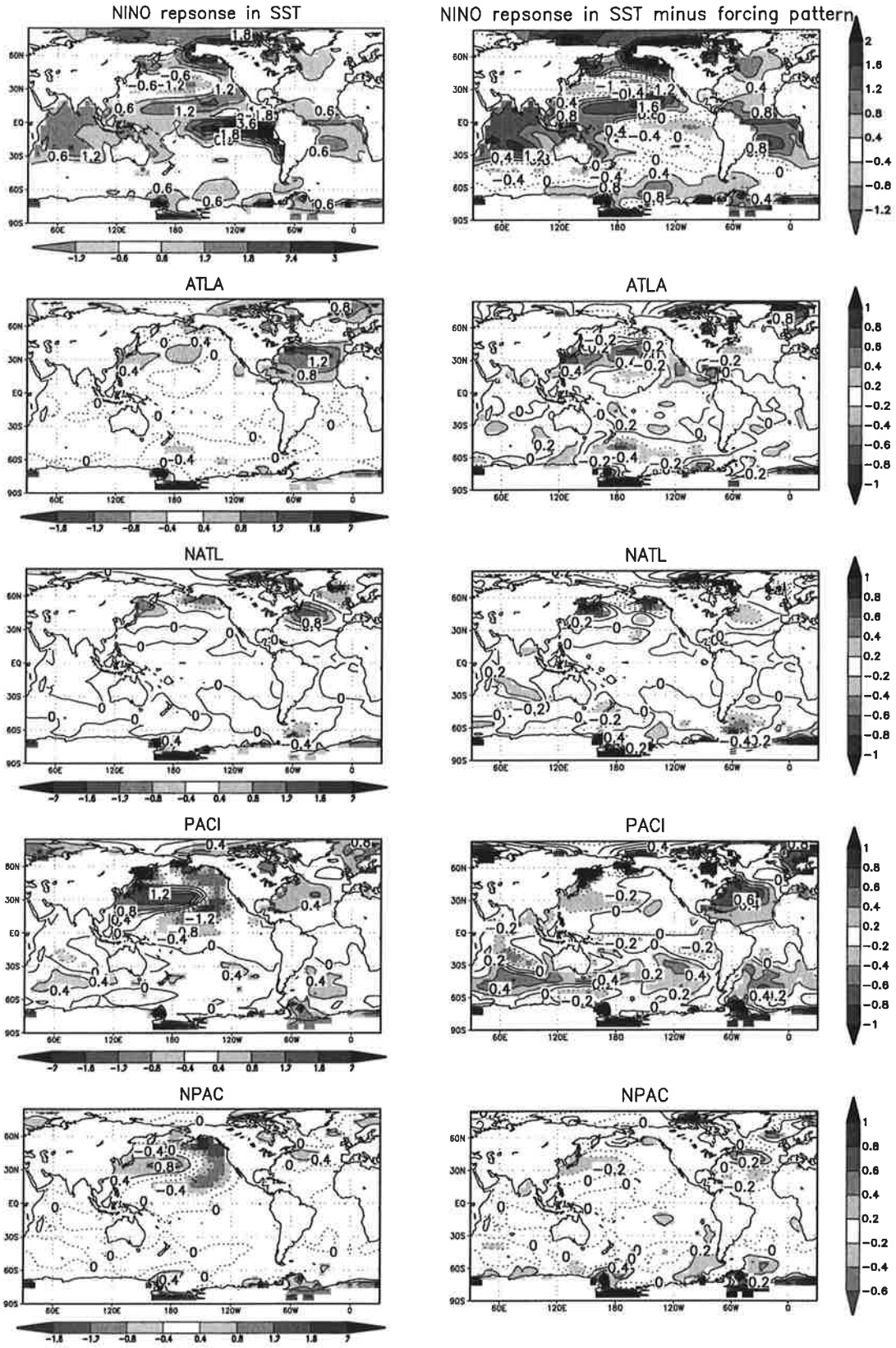

Figure 6.2: The response to the different SST anomaly patterns in the SST. The plots on the left side show the response in the mixed layer simulation and the plots on the right side show the response in the mixed layer simulation minus the SST anomaly pattern.

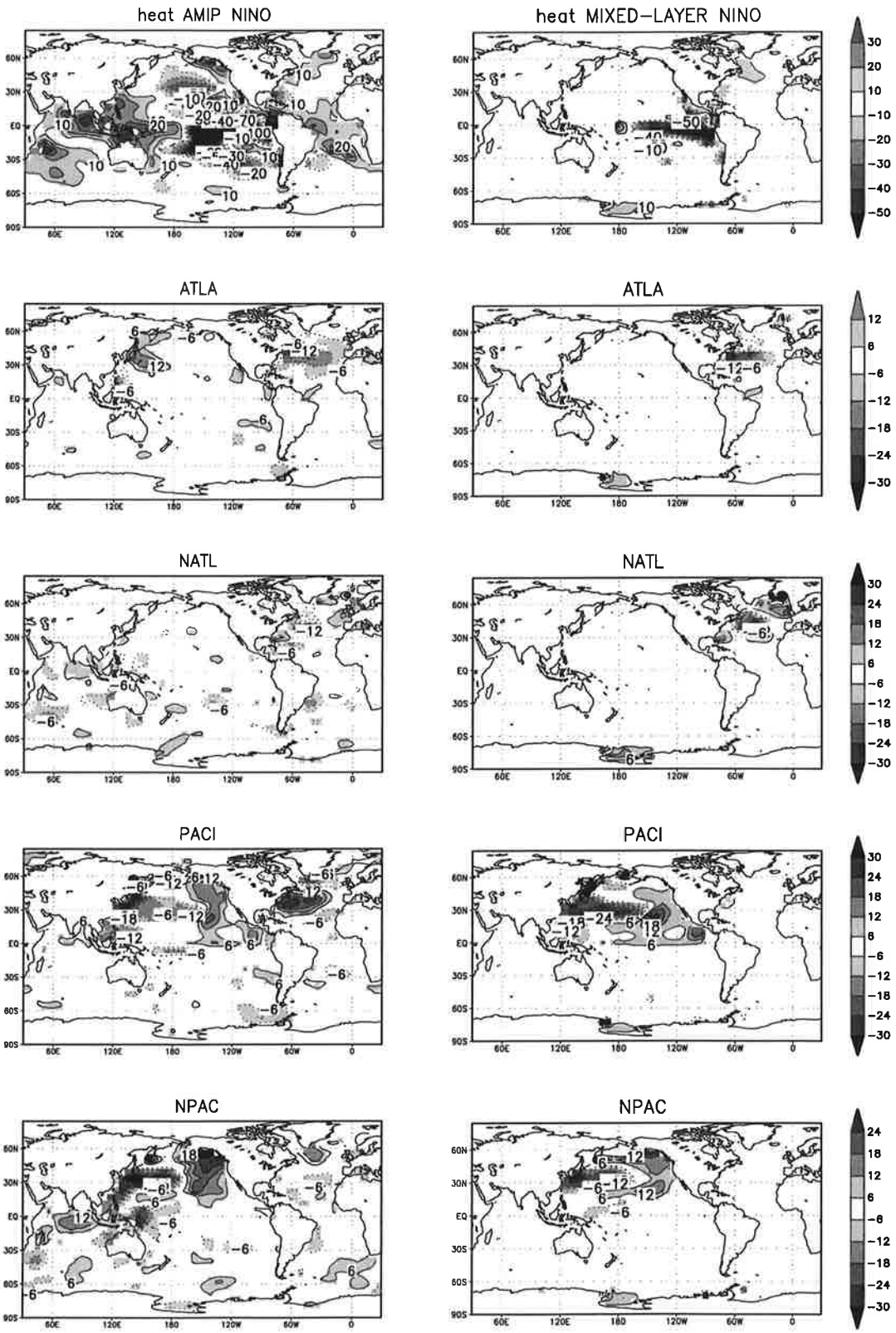

Figure 6.3: The response to the different SST anomaly patterns in the net heat flux. The plots on the left side show the response in the AMIP-type simulation and the plots on the right side show the response in the mixed layer simulation.

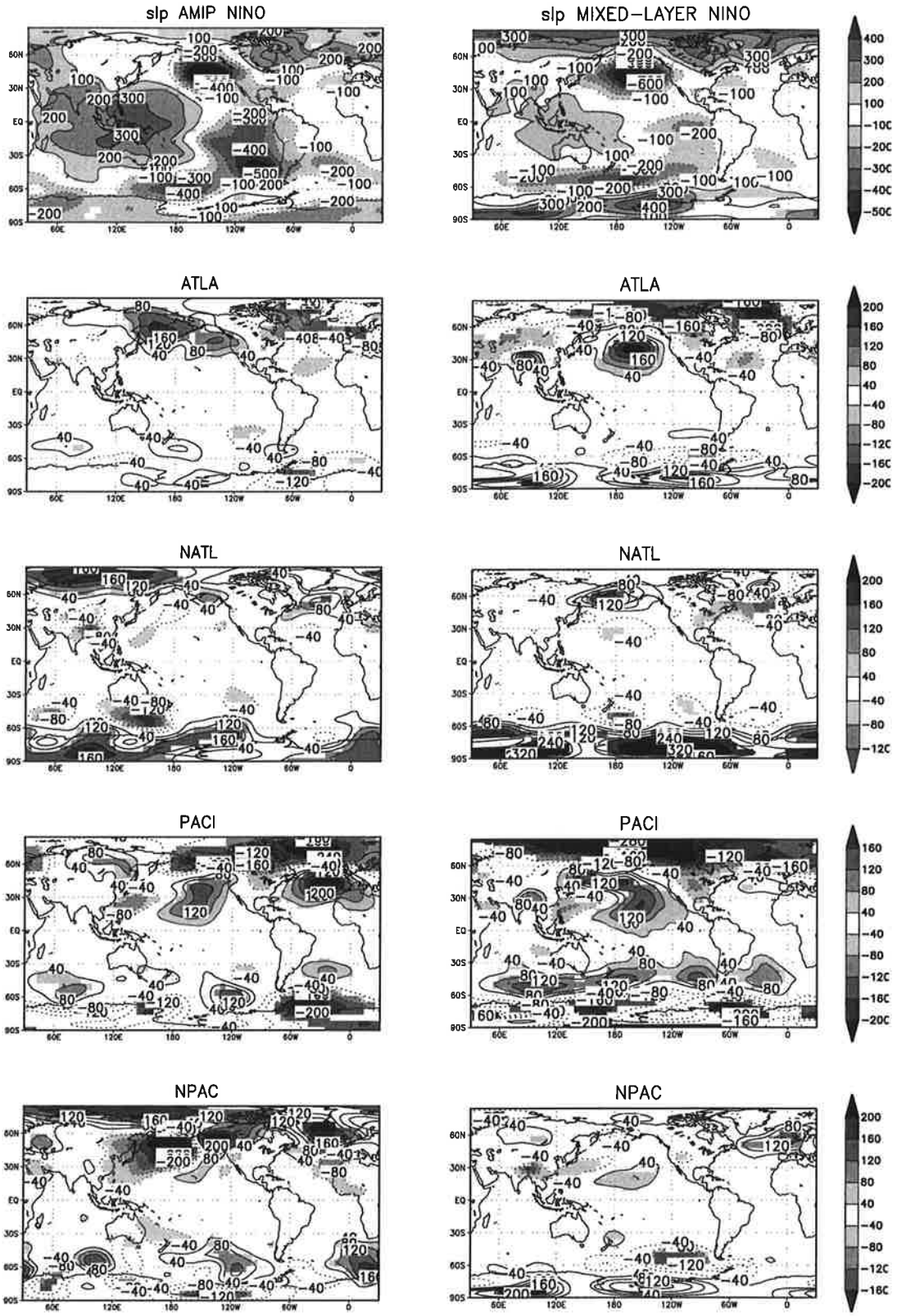

Figure 6.4: The response to the different SST anomaly patterns in sea level pressure. The plots on the left side show the response in the AMIP-type simulation and the plots on the right side show the response in the mixed layer simulation.

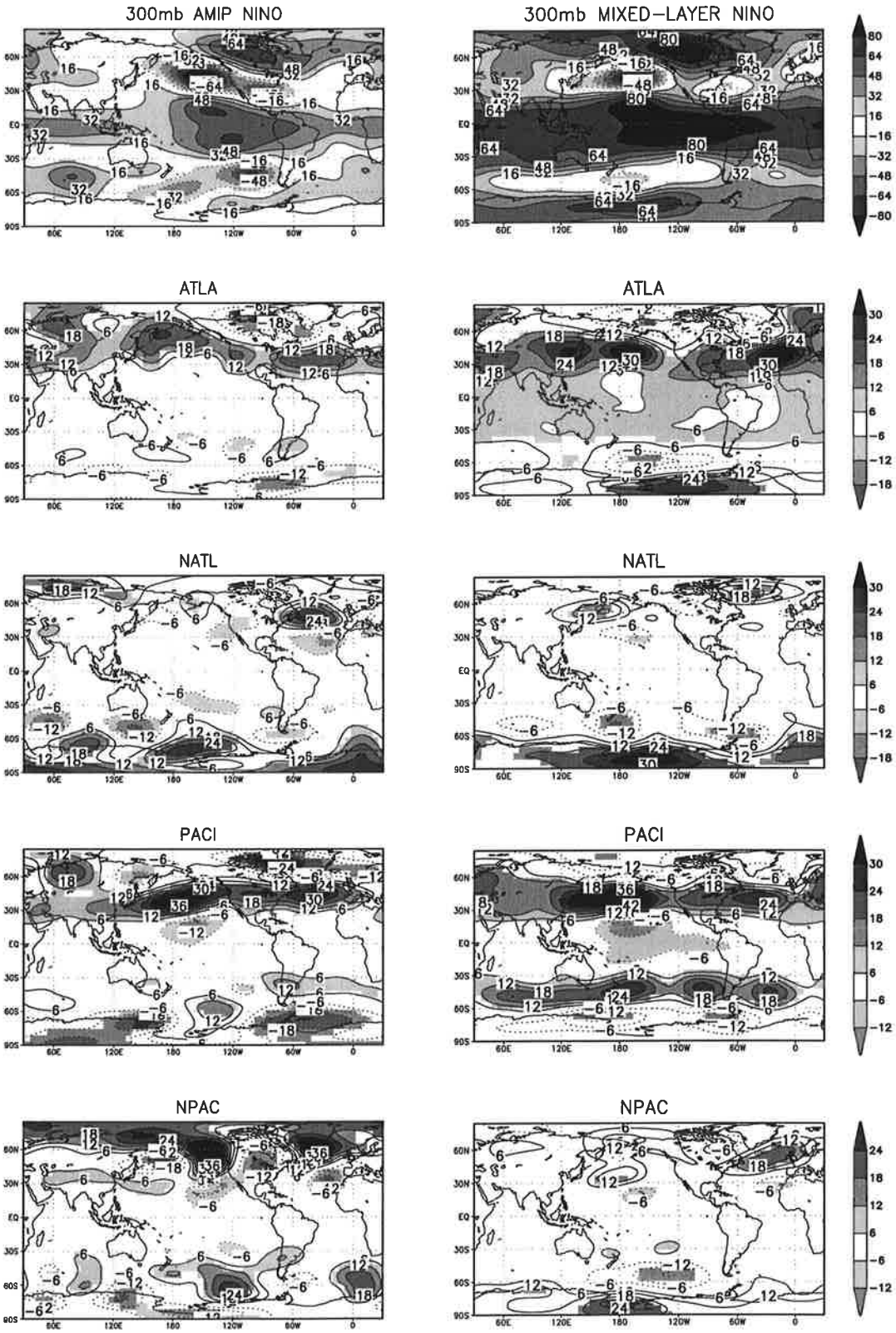

Figure 6.5: The response to the different SST anomaly patterns in 300 mb height. The plots on the left side show the response in the AMIP-type simulation and the plots on the right side show the response in the mixed layer simulation.

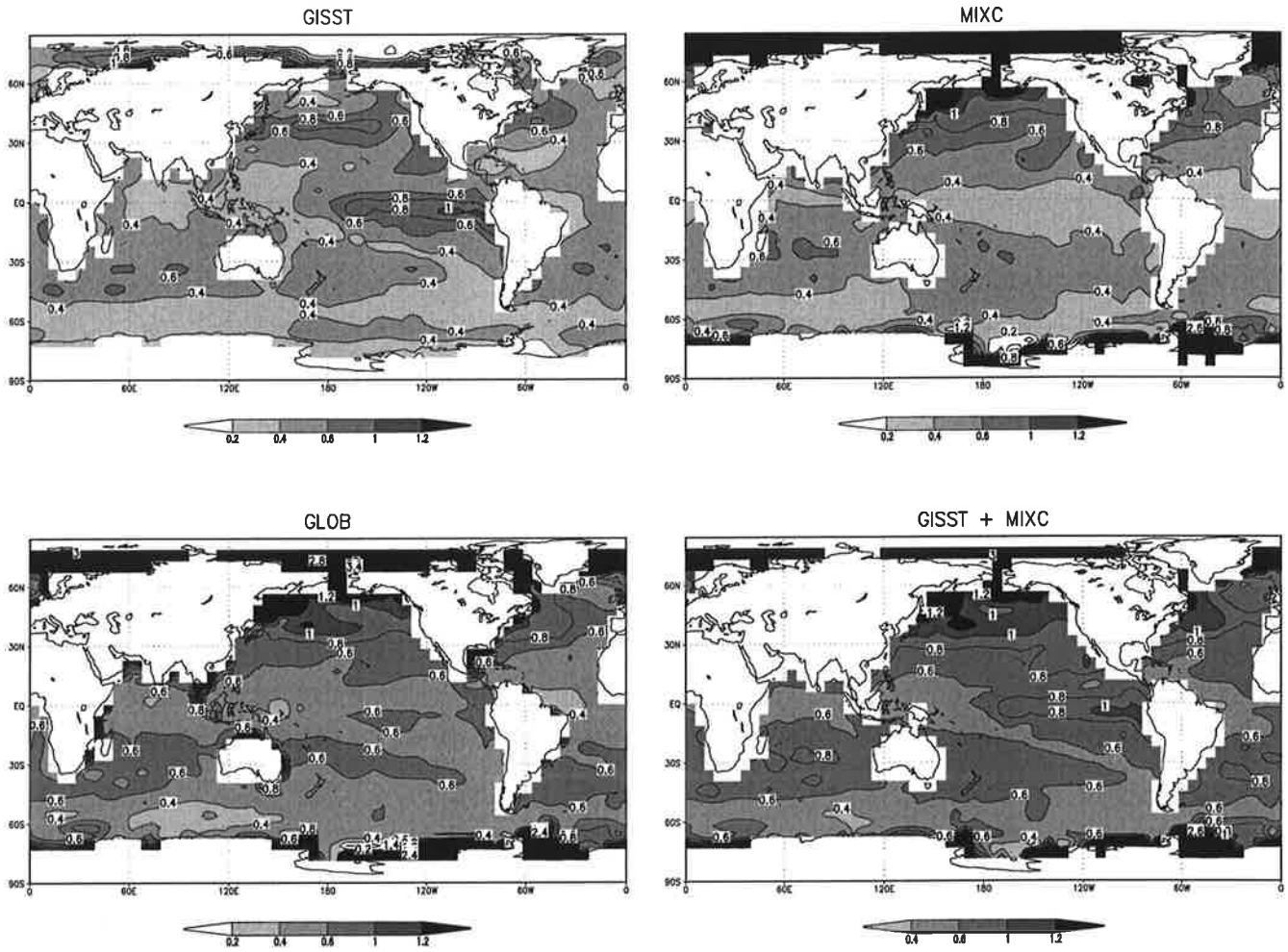

Figure 6.6: [The standard deviation of GISST, MIX_{season}, MIX_{GISST} and the added standard deviation of MIX_{season} and GISST SST.] The standard deviation of the GISST forcing SST, the MIX_{season} simulation, the MIX_{GISST} simulation and the added standard deviation of the MIX-season and the GISST forcing SST.

6.3 The MIX_{GISST} simulation response to a historical SST time series

In the MIX_{GISST} simulation the internal variability of the mixed layer together with the introduced SST forcing leads to a change in the standard deviation of the SST variability. If the two types of SST variability would simply be additive, the standard deviation of the SST in the MIX_{GISST} simulation should be:

$$\sigma[MIX_{GISST}] = \sqrt{\sigma^2[MIX_{season}] + \sigma^2[GISST]} \tag{6.7}$$

In Figure 6.6 the standard deviations of the SST in the MIX_{season} simulation (upper right plot), in the MIX_{GISST} simulation (upper left plot), in the GISST observations (lower left plot) and the linear superposition according to equation 6.7 (lower right plot) are shown.

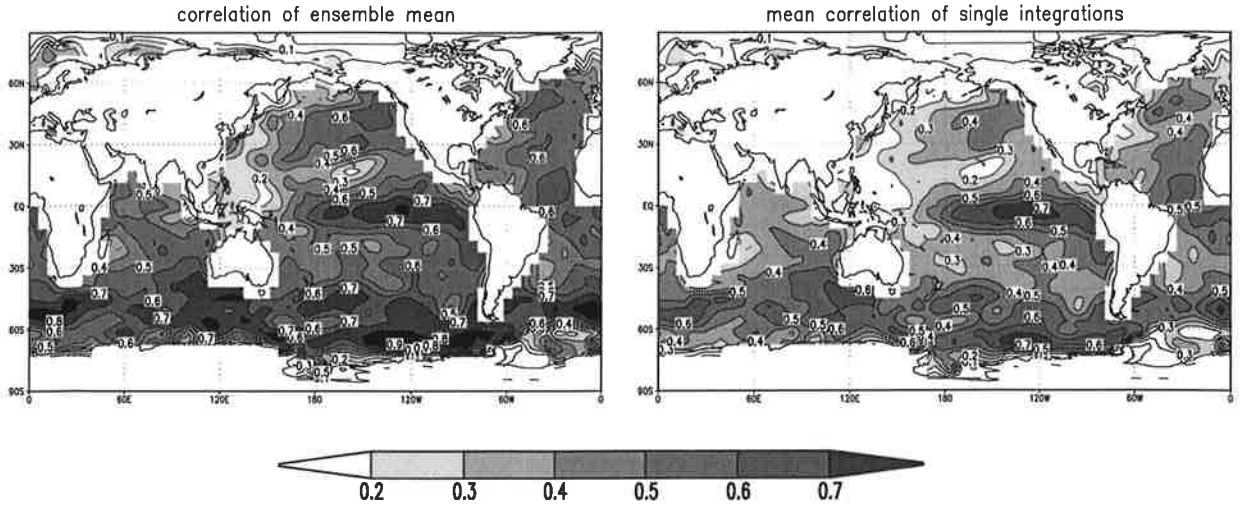

Figure 6.7: Correlation between the SST of the MIX_{GISST} simulation and the forcing SST.

The comparison of the linear superposition and the standard deviation of the SST in the MIX_{GISST} simulation clearly shows that the SST variability is not just the linear superposition, but it is strongly damped in those regions in which the standard deviation of the GISST forcing is much larger than the internal variability of the MIX_{season} simulation.

The introduction of the GISST SST anomalies into the mixed layer of the MIX_{season} simulation acts like an additional external forcing to the mixed layer. The sensitivity of the coupled system to additional forcing depends on the strength of the atmospheric heat flux and the depth of the mixed layer. In regions in which the atmospheric heat flux is relatively strong compared to the mixed layer depth, the coupled system will wash out the external forcing of the GISST SST, while in those regions in which the mixed layer depth is relatively deep and the atmospheric heat flux is relatively small, the external forcing of the GISST SST will be relatively dominant.

In Figure 6.7 the correlation between the SST of the MIX_{GISST} simulation and the GISST SST forcing is shown. It can be seen that the correlation has a pronounced spatial structure, which reflects the sensitivity of the coupled system to additional forcing.

In order to see how the SST of the MIX_{GISST} simulation is correlated to the forcing on different time scales, a cross spectral analysis between the simulated SST of one integration and the forcing SST of the central north Pacific ($Lat: 35^oN - 45^oN$, $Lon: 170^oE - 160^oW$) has been performed, which is shown in Figure 6.8.

The results using one single integration of the MIX_{GISST} simulation indicate that the SST of the MIX_{GISST} simulation gets less correlated with the forcing SST the longer the time scale. The SST of the MIX_{GISST} simulation is in phase with the SST of the forcing for shorter time scales, it gets out of phase for longer time scales. The same characteristics can be found for the mean of the four MIX_{GISST} simulations, but the coherence between the mean SST of the four simulations and the forcing SST is significantly higher on shorter time scales.

In equation 6.4 the forcing SST is only introduced by the temperature change per time

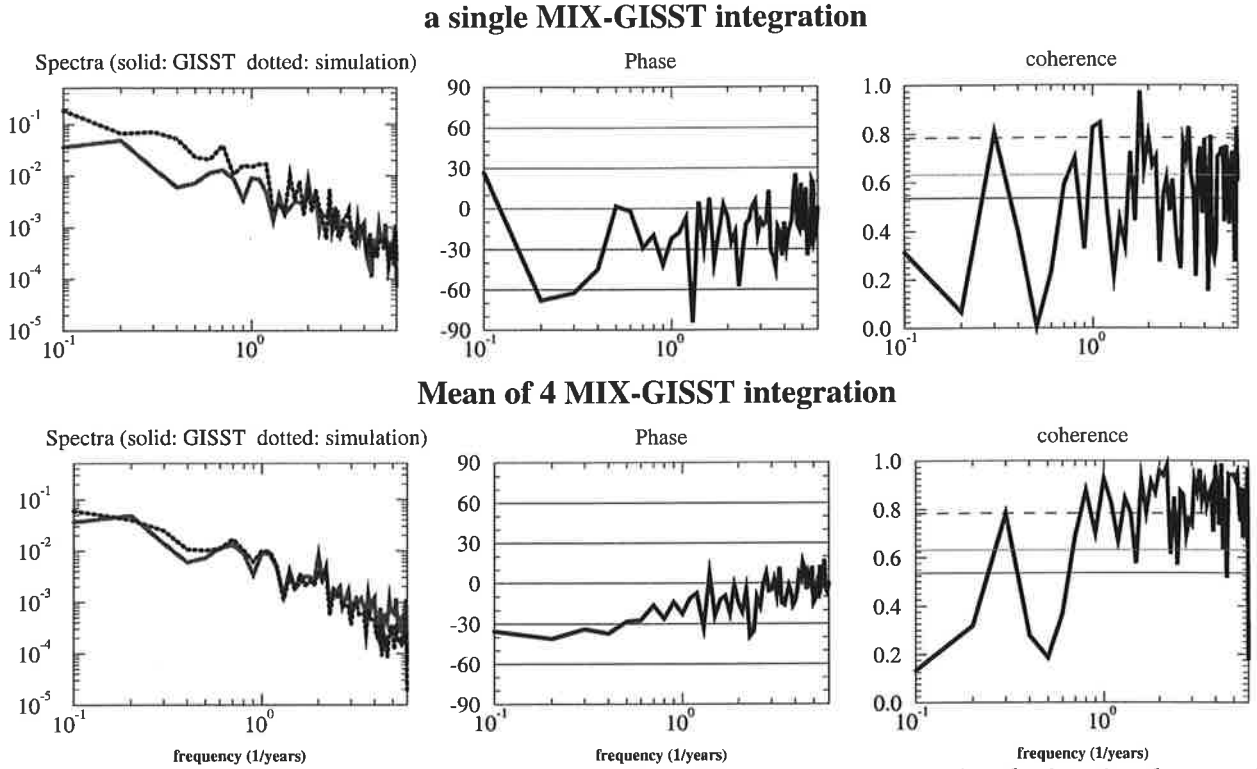

Figure 6.8: Cross spectral analysis of the SST of the MIX_{GISST} simulation in the north Pacific.

step, whereas no information about the absolute temperature of the forcing SST is given to the coupled model. Therefore, the internal variability of the mixed layer of the ocean is washing out the forcing SST on longer time scales.

In order to get a clear picture of how the forcing SST gets altered in the mixed layer simulation a simple Monte Carlo experiment can be instructive. The structure of the Monte Carlo experiments are similar to the one discussed in section 4.2.4, with the exception that now the equation 6.5 is used to study the SST integration of the historical SST time series.

In Figure 6.9 the cross spectra of three different Monte Carlo experiments are shown. The dashed lines present a Monte Carlo experiment with $F_{forcing} = 0$, which is comparable to the MIX_{GISST} simulation. This Monte Carlo experiment clearly shows that the simulated SST gets out of phase for longer time periods and the coherence between the simulated SST and the forcing SST gets smaller for longer time periods. The negative phase relation for longer time periods indicates that the simulated SST leads the forcing SST, which is due to the fact that the atmospheric forcing is always damping the forced SST anomalies, which leads to an earlier decrease of SST anomalies and therefore to an apparent phase lead with the simulated SST.

In order to correct for the long time scale mismatch of the simulated SST relative to the forcing one could introduce a damping heat flux $F_{forcing}$ which would force the SST on longer time scales to fit the forcing SST. The solid lines in Figure 6.9 present the cross spectra of a Monte Carlo experiment in which such a heat flux $F_{forcing}$ has been introduced

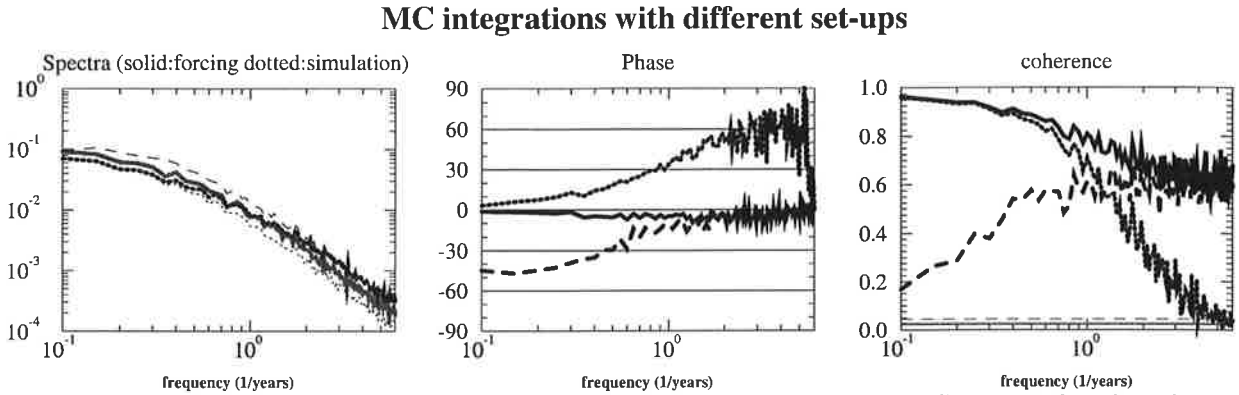

Figure 6.9: Cross spectral analysis of a Monte Carlo simulations. See text for details.

in equation 6.5. The Monte Carlo experiment clearly shows that the simulated SST is now mostly in phase with the forcing SST and that the coherence between the simulated SST and the forcing SST is increasing for longer time scales. Although the forcing SST is very well reproduced in this experiment the result has been achieved at a high price. The comparison between the spectral variance of the simulated SST with spectral variance of the forcing (shown in left plots) indicates that the SST variability in this simulation is strongly damped.

The dotted lines in Figure 6.9 represent the cross spectra of a Monte Carlo experiment in which only a heat flux $F_{forcing}$ was introduced in equation 6.5 and the temperature change ΔT_{ano} has not been introduced. In this Monte Carlo experiment the correlation of the simulated SST is high for longer time scales and very low on short time scales, whereas the simulated SST is in phase on longer time scales and out of phase for shorter time scales. The comparison of the spectral variance of the simulated SST with the spectral variance of the forcing SST indicates that, due to the smaller variance of the simulated SST on all time scales, the forcing SST is only simulated with a strongly damped amplitude.

From this Monte Carlo experiment study one has to conclude that the introduction of a heat flux $F_{forcing}$ is not significantly improving the simulation of the historical SST time series. However, the introduction of the damping heat flux $F_{forcing}$ may be useful for those regions in which the correlation between the simulated SST and the forcing SST is very low (see Figure 6.7). One could therefore consider the possibility of introducing a heat flux $F_{forcing}$ in equation 6.5 with a spatially variable damping constant C_{damp} to compensate for the low correlations in some regions.

In Figure 6.10 the cross spectral analysis of a single Monte Carlo integration and the mean SST of an ensemble with 10 members are compared. The comparison shows that the coherence of the mean simulated SST with the observations becomes higher on all time scales and that the spectral variance of the simulated SST becomes very close to the spectral variance of the forcing SST. However, the phase relation between the simulated and the forcing SST has not changed. It has therefore to be concluded that the drift in the phase

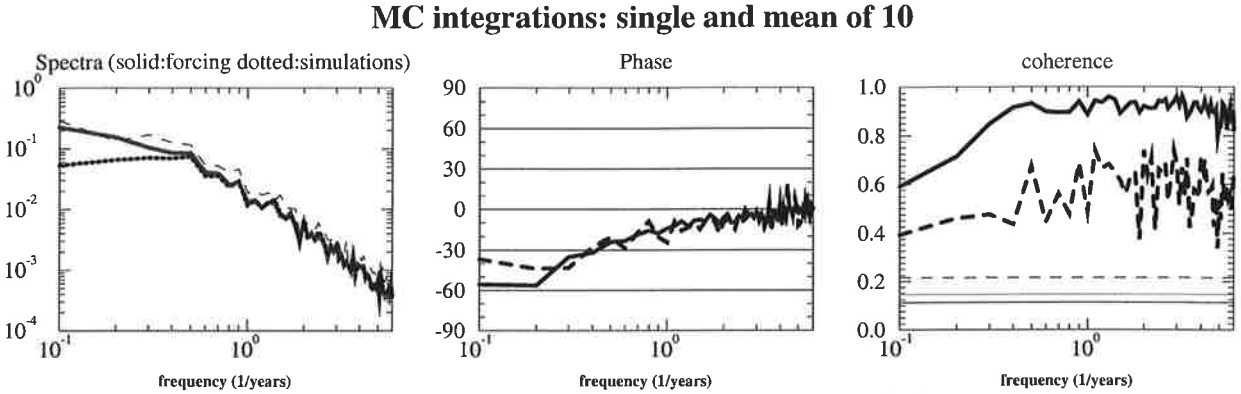

Figure 6.10: Monte Carlo comparison of the ensemble mean and the single integration. See text for details.

relation is a fundamental problem, which cannot be corrected by increasing the ensemble size.

The drift in the phase relation between the simulated SST and the forcing SST arises from the atmospheric feedback to the SST anomalies, which is in general damping all SST anomalies on longer timer scales. If one assumes that the atmospheric heat flux is in principle just damping, then the heat flux at the sea surface can be defined as:

$$F_{atmos} = -C_{damp} * (SST_{anomaly}) \tag{6.8}$$

If F_{atmos} in equation 6.4is replaced by equation 6.8 and one ignores the term ΔT_{clim}, then one can derive an equation for the effective change of the SST:

$$\frac{d}{dT}SST = -C_{atmos} * (SST_{anomaly}) + \Delta T_{ano} \tag{6.9}$$

Equation 6.9 shows that the effective change in the SST is not just ΔT_{ano}. In order to get the effective change in SST to be equal ΔT_{ano}, one has to build an effective forcing time series which leads to an effective change in SST $\Delta T_{ano-effect}$:

$$\Delta T_{ano-effect} = C_{atmos} * (T_{ano}) + \Delta T_{ano} \tag{6.10}$$

In principle the right hand side of equation 6.10 is not depending on the state of the system and can therefore be determined in advance as a correction to the original time series. The damping constant C_{atmos} can be derived from the lag correlation of the SST in the coupled MIX_{season} simulation. However, in practice the damping constant C_{atmos} cannot be determined exactly, but the following Monte Carlo simulation will show that the integration with the corrected time series can still improve the simulated SST if the damping constant C_{atmos} is only known within an error of 50%.

In the upper row of Figure 6.11 the cross spectral analysis of three different Monte Carlo integrations are shown. The thick solid lines in the phase- and coherence-plot represent a

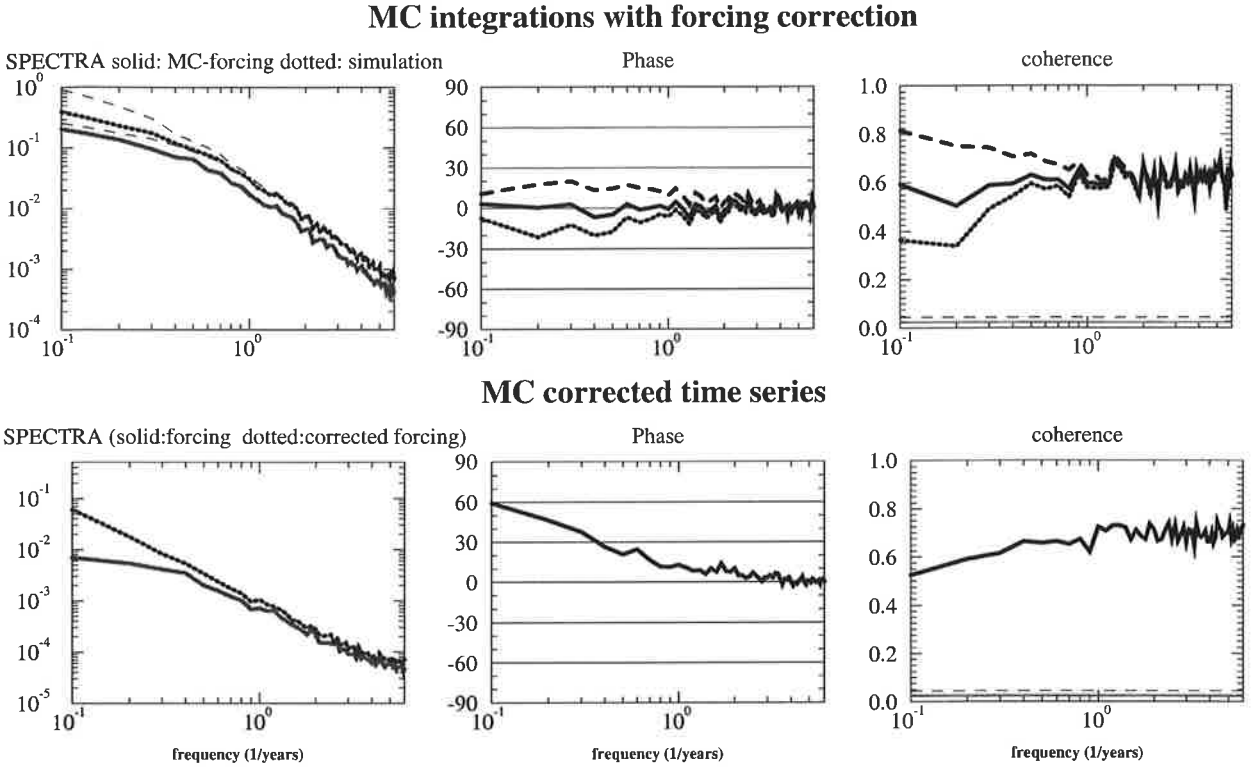

Figure 6.11: Monte Carlo cross spectra between the MC forcing and the corrected MC forcing. See text for details.

Monte Carlo simulation in which the damping constant C_{atmos} is perfectly known for the correction of the forcing SST time series, whereas the dotted and the dashed lines represent Monte Carlo simulations in which the damping constant C_{atmos} has been varied by $+/-50\%$. First of all, the case with the perfect determination of the damping constant C_{atmos} indicates that the correction of the forcing SST time series is correcting the phase and the coherence.

The two Monte Carlo simulations in which the damping constant C_{atmos} has been varied by 50% indicate that even if the damping constant C_{atmos} is not perfectly known, the phase and the coherence can be corrected by some amount, depending on the degree of accuracy to which the damping constant C_{atmos} has been determined. Thus, if the initial time series of our forcing SST is replaced with a corrected time series, the simulated SST will be better correlated to the forcing SST on all time scales and the phase will be close to zero on all time scales as well.

In the lower row of Figure 6.11 the cross spectral analysis between the MC forcing and the corrected MC forcing are shown. The comparison of the two spectra shows that the correction is basically increasing the long time scale variability in the forcing SST in order to correct for the damping of SST anomalies on longer time scales due to the atmospheric forcing.

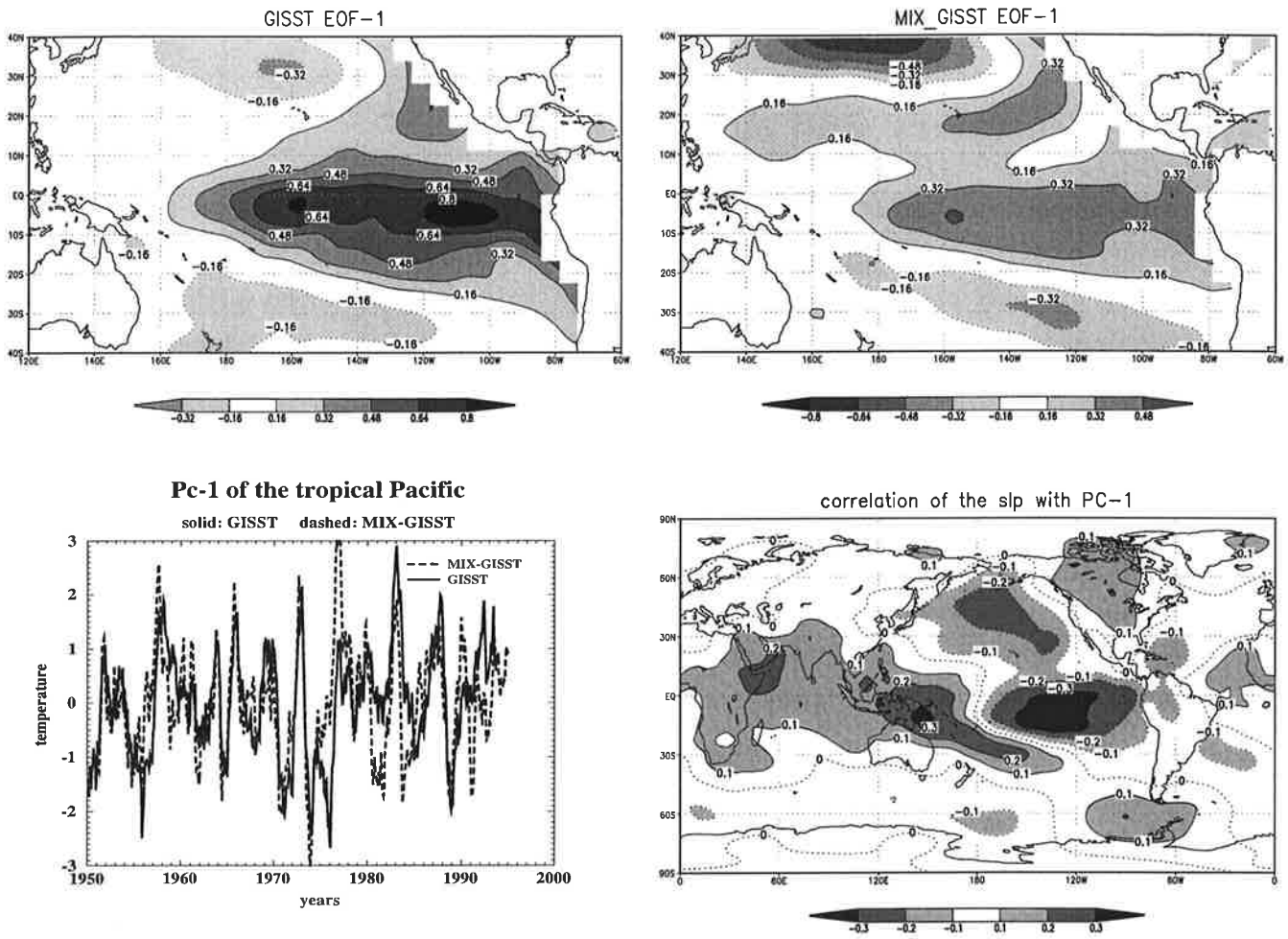

Figure 6.12: EOF-1 of the tropical Pacific SST in the GISST data set and in the MIX_{GISST} simulation.

6.3.1 El Niño in the MIX_{GISST} simulation

The SST variability associated with El Niño and its teleconnection patterns are the most dominant and best understood phenomenon controlling the observed SST variability. El Niño is therefore a good possibility to study the performance of the MIX_{GISST} simulation.

In Figure 6.12 the EOF-1 of the observed SST from the GISST data set and the EOF-1 of the MIX_{GISST} simulation are shown. The EOF-1 of the MIX_{GISST} simulation is significantly damped near the equator compared to the GISST EOF-1, which indicates that the introduced SST anomalies from the GISST data set are strongly damped in those region in which the internal variability of the MIX_{season} simulation is small. However, the comparison of the two PCs, shown in Figure 6.12, indicates that the time evolution of the SST in the MIX_{GISST} simulation is basically following that of the GISST data set.

The correlation of the sea level pressure with the PC-1 of the MIX_{GISST} simulation, shown in Figure 6.12, also indicates that the atmospheric response to the SST is consistent with the observed response. The Southern Oscillation and the intensification of the Aleutian

Low over the North Pacific are especially well reproduced.

6.4 Summary and discussion

In this chapter an alternative technique to simulate the atmospheric response to given SST anomaly patterns or historical SST time series has been introduced. In this new technique the SST anomaly pattern or historical SST time series are introduced in the mixed layer ocean model of the MIX_{season} simulation, and the response of the atmosphere is studied in the coupled simulation. In addition, to simply introduce a fixed SST anomaly pattern or a given historical SST time series, the mixed layer simulation offers many other possibilities.

The experiments have shown that the mixed layer simulations may produce a significantly different response compared to that of the AMIP-type simulation if the SST anomaly pattern resembles the SST anomaly pattern of the internal variability. On the other hand, the response is quite similar to that of an AMIP-type simulation if an SST anomaly pattern is introduced which differs significantly from the internal variability of the MIX_{season} simulation. However, the response of the mixed layer simulation to an SST anomaly pattern which differs significantly from the internal variability of the MIX_{season} simulation is significantly stronger than the response to an SST-pattern which resembles the internal variability of the MIX_{season} simulation. Thus, the response can be purely artificial and may not provide any information about how another coupled system or the real world would respond.

The analysis of the MIX_{GISST} run, in which the observed SST anomalies from 1950 to 1994 have been introduced into the mixed layer globally, has shown that the internal variability of the mixed layer is changing the SST, so that the simulated SST in some regions are only weakly correlated with the forcing SST on longer time scales. However, the analysis of the simulation has also shown that it is possible to simulate historical SST anomalies in the mixed layer model, if some corrections to the initial SST anomalies are introduced.

The additional SST forcing from the historical time series can be seen as an additional heat flux to the mixed layer. The sensitivity of the coupled system to this additional forcing depends on the strength of the atmospheric heat flux and the depth of the mixed layer. In regions in which the atmospheric heat flux is relatively strong compared to the mixed layer depth the coupled system will wash out the external forcing of the GISST SST, while in those regions in which the mixed layer depth is relatively deep and the atmospheric heat flux is relatively small, the external forcing of the GISST SST will be relatively dominant. It therefore has to be considered that in those regions, in which the atmospheric heat flux is relatively strong, the forcing SST should be introduced by an additional heat flux $F_{forcing}$ as defined in equation 6.5, which will force the simulated SST towards the forcing SST.

Due to the atmospheric damping of SST anomalies, the simulated SST is out of phase with the forcing SST on longer time scales and the coherence is also decreasing at longer time scales. However, this effect can be corrected if the initial SST forcing is replaced with

a SST forcing in which the long-term SST variability is amplified compared to the original SST forcing.

Compared to the AMIP-type simulations the mixed layer simulations offers many more possibilities to introduce particular SST anomalies. By introducing a fixed SST anomaly pattern in the mixed layer the damping constant C_{damp} has to be chosen. The strength of C_{damp} determines how strongly the SST is forced to the SST anomaly pattern. If the damping constant C_{damp} is relatively small, the SST anomaly pattern will only be fixed on longer time scales, while the short time scale SST variability is mainly unaffected. Instead of introducing a constant SST anomaly pattern one can also consider introducing a constant or seasonal heat flux pattern into the mixed layer.

One way to understand the atmospheric response to historical SST anomalies is that the atmosphere is forced by the long time variability of the SST, while the short time SST variability is mainly due to the atmospheric forcing. In the mixed layer simulations it is possible to introduce a low -pass filtered SST time series into the mixed layer, which will force the SST only on longer time scales, while the short-term SST variability is forced by the atmosphere.

Chapter 7

Outlook and Summary

7.1 Outlook

7.1.1 A dynamical mixed layer ocean model

In the study of the midlatitude SST variability the approach with the dynamical mixed layer ocean model $MIX_{dynamic}$ has been very successful in simulating seasonal to interannual SST variability. However, the $MIX_{dynamic}$ model is only a slab ocean model which has some variability in the mixed layer depth without looking at the characteristics of the variability in too much detail. Now since the model has been proven to be a good model for the SST variability in the midlatitudes, it seems worth to work out the model dynamics using a more realistic ocean mixed layer model.

The main problem of the $MIX_{dynamic}$ model is the idealized density profile for the dynamical mixed layer equation, which is only temperature dependent. A correct determination of the density profile with both salinity and temperatures also allows the SST to be colder than the sub-mixed layer temperatures, which is not possible in the $MIX_{dynamic}$ model. For further studies one could consider introducing salinity as a dynamical model quantity, which may be important for higher latitudes and for some regions in the tropics (see section 4.2.4).

The second main problem of the dynamical mixed layer model is the inability of the Kraus and Turner approach to simulate the fast detrainment of the mixed layer during the spring period. It would be a very important improvement of the $MIX_{dynamic}$ model and perhaps for ocean models in general if a mixed layer model can be developed, which is able to simulate a fast detrainment of the mixed layer during the spring period as observed.

Another problem of the dynamical mixed layer model is the simulation of the temperature profile of the sub-mixed layer ocean, which is important for the analysis of decadal SST variability and for the study of the seasonal predictability of midlatitudes SST anomalies in fall and winter. In the $MIX_{dynamic}$ model the temperature profile of the sub-mixed layer ocean is described by an exponential decrease of the SST to a fixed deep ocean temperature. This limits the temperature anomalies of the sub-mixed layer ocean to be proportional to

the SST, which is not realistic. Due to the fixed temperature profile, the heat flux between the mixed layer and the sub-mixed layer ocean has been introduced as a pure damping in the SST equation.

In a more realistic simulation the sub-mixed layer ocean should be capable of representing temperature anomalies that are independent of the present SST anomalies, which can be realised by introducing an intermediate layer between the mixed layer and the fixed deep ocean temperature.

7.1.2 Seasonal predictability of midlatitudes SST anomalies

The analysis of the seasonal predictability of midlatitude SST anomalies in the $MIX_{dynamic}$ simulation has shown that knowledge of the mixed layer depth anomalies is important for the development of SST anomalies in summer and fall, while the $MIX_{dynamic}$ simulation has some limitations in the dynamical development of the mixed layer depth in spring and fall. It would therefore be interesting to study the seasonal predictability of midlatitude SST anomalies in an improved version of the $MIX_{dynamic}$ model, in which the problems of the detrainment in spring and the re-emergence of temperature anomalies in fall have been solved.

Until now all the results of the predictability study are based on a model. It would be interesting to do a similar analysis with observed mixed layer depth and SST anomalies, in order to test whether the importance of the mixed layer depth anomalies is merely a model artefact or whether it is real.

However, it will be difficult to perform this analysis with observations, because the mixed layer depth is not well observed for the real ocean, and in order to define a mixed layer depth one needs the measurements of the temperature and salinity of the upper 400 meters of the ocean, which are only available for some regions. Additionally, the measurements should be taken over a time interval of at least 10 years in order to analyse the relation between SST and mixed layer depth.

7.1.3 Decadal SST variability in midlatitudes

The discussion regarding decadal SST variability in the midlatitudes of the Northern Hemisphere is still very controversial. Many competing theories or models exist which describe mechanisms for decadal variability in the Northern Hemisphere. Most of the theories which propose coupled ocean-atmosphere modes are based on studies with only one CGCM.

The analysis of the midlatitude SST variability presented in this thesis has been based on the detection of differences to an AR-1 process and the determination the physical processes relevant to these differences. By comparing a hierarchy of different ocean model simulations with the observations the relevant ocean processes for decadal SST variability can be determined. Similar to the case with the analysis of the slab ocean models in Chapter 4

an improved mixed layer ocean model can be developed, which includes salinity variability and captures the interaction between the mixed layer and the sub-mixed layer ocean more realistically than the $MIX_{dynamic}$ simulation.

7.1.4 Atmospheric response to midlatitude SST anomalies

In Chapter 6 a new technique for AMIP-type simulations has been introduced. Although there are some indications that the SST anomalies in the midlatitudes are important for the atmospheric circulation (Blade (1997), Barsugli and Battisti (1998)), this has not been quantified in detail. The new technique with a seasonal mixed layer model may be a good tool to analyse the atmospheric response to midlatitude SST anomalies within a coupled framework.

7.2 Summary

In this these the SST variability of the northern midlatitudes and the tropical Atlantic have been analysed. The analysis has been based on the comparison of the observations with a hierarchy of different coupled simulations.

The analysis of the midlatitude SST variability has shown that the large-scale features of the SST variability cannot be simulated by a fixed depth mixed layer ocean model and that the spectral distribution of the SST is significantly different for an AR-1 process on time scales from seasons to decades. The processes that are important for these differences are the seasonal variability of the mixed layer depth, the wind induced mixing, which entrains water from the sub-mixed layer ocean, and the heat exchange between the mixed layer and the sub-mixed layer ocean. The observed increase in the SST variance from the interannual to the decadal time scale is due to the heat exchange between the sub-mixed layer ocean and the mixed layer and not, as in the MIX_{50} simulation, merely an effect of the integration of atmospheric noise. All these processes can be simulated by the local air-sea interactions in the dynamical ocean mixed layer $MIX_{dynamic}$. The analysis of the seasonal predictability of the SST in the $MIX_{dynamic}$ simulation indicates that the knowledge of the actual mixed layer depth is important to predict the SST development in summer and fall.

In the analysis of the tropical Atlantic SST variability, it was found that the two dominant SST patterns of the observed SST and in all analysed CGCMs are centred in the northern and in the southern trade wind zones, whereas the correlation between the two patterns is not significantly different from zero. An interhemispheric dipole, or stated differently, an anti-correlation of the SSTs in the northern and southern trade wind zones, which could be important for rainfall anomalies in e.g. north-east Brazil, does therefore not exist. I conclude that the often cited dipole pattern is an artifact of the EOF analysis technique used. The fact that the simple slab ocean model produces the same pattern, indicates that the SST anomalies are forced by the atmosphere consistent with the Null hypothesis of SST variability.

In the final chapter of this work I have introduced a new technique to study the response of the atmosphere to a given SST pattern in a coupled simulation. In this new technique the SST anomaly patterns or historical SST time series is introduced by an additional heat flux into the seasonal mixed layer ocean model. The comparison of the atmospheric response in the coupled simulation with the usual AMIP-type simulation has shown that the response in the midlatitudes can be significantly different and that the response of the atmosphere is very sensible to the structure of the given SST anomaly pattern. In general the new technique seems to be a good tool to study the atmospheric response to SST anomaly pattern in the midlatitudes and instead of introducing a fixed SST pattern or a given historical SST time series, the mixed layer simulation offers many other possibilities.

Danksagung (Acknowledgements)

Zuerst einmal möchte ich mich bei Mojib Latif bedanken, für die gute Betreuung meiner Arbeit und für die Leitung einer sehr netten wissenschaftlichen Gruppe, in der es viel Spaß gemacht hat zu arbeiten. Ein doppelter Dank geht auch an Prof. Dr. Klaus Hasselmann für die Begutachtung meiner Doktorarbeit und für die Ermöglichung dieser Arbeit im Bereich der Abteilung Klima des MPI-Meteorologie.

Desweiteren möchte ich mich bei Dr. Detlef Müller für die äußerst hilfreichen Diskussionen zur Entwicklung des $MIX_{dynamic}$ Modells und bei Ulirch Schlese für die unbezahlbare Hilfe in der technischen Umsetzung des $MIX_{dynamic}$ Modells im ECHAM Atmosphären Modell. Für die Durchsicht meiner Doktorarbeit möchte ich mich bei Dr. Keith Rodgers und Dr. Stephan Venzke bedanken.

Zu guter Letzt möchte ich mich bei meinen Eltern bedanken die mein Studium immer voll unterstützt haben und sich über meinen Doktortitel mindestens genau so doll freuen wie ich.

References

Alexander, M.A., C. Penland, 1996: Variability in a mixed layer ocean model driven by Stochastic atmospheric forcing.*J. Climate*, **9**, 2424-2442.

Bacher, A Oberhuber, JM Roeckner, E , 1998: ENSO dynamics and seasonal cycle in the tropical Pacific as simulated by the ECHAM4/OPYC3 coupled general circulation model . *Clim. Dyn.*,**14**, 431-450.

Bladé, I. 1997: The Influence of Midlatitude Ocean-Atmosphere Coupling on the Low-Frequency Variability of a GCM. Part I: No Tropical SST Forcing. *J. Climate*, **10**, 2087-2106.

Barsugli, JJ Battisti, DS , 1998: The basic effects of atmosphere-ocean thermal coupling on midlatitude variability . *J. Atmos. Sci.*,**55**, 477-493.

Carton, J. A., X. Cao, S. G. Benjamin and A. M. Da Silva, 1996: Decadal and interannual SST variability in the tropical Atlantic. *J. phys. Oceanogr.*, **26**, 1165-1175.

Chang, P., L. Ji and H. Li, 1997: A decadal climate variation in the tropical Atlantic Ocean from thermodynamic air-sea interactions. *Nature*,**385:(6616)**,516-518

Delworth, T. and V. M. Mehta, 1998: Simulated interannual to decadal variability in the tropical and sub-tropical North Atlantic. *J. Geophys. Res. Lett.*, **25**, 2825-2828.

Dommenget, D. and M. Latif, 2000: Interannual to decadal variability in the tropical Atlantic . *J. Clim.*,**13**, 777-792.

Enfield, D. B. and D. A. Mayer, 1997: Tropical Atlantic sea surface temperature variability and its relation to El Nino-Southern oscillation. *J. Geophys. Res.*, **102**, 929-945.

Frankignoul, C., and K. Hasselmann, 1977: Stochastic climate models, II, Application to sea-surface temperature variability and thermocline variability, *Tellus*,**29**,284-305.

Frankignoul, C., 1985: Sea Surface Temperature Anomalies, Planetary Waves, and Air-Sea Feedback in the Middle Latitudes. *Rev. of Geophys.*, **23**, 357-390.

Frey, H., M. Latif and T. Stockdale, 1997: The coupled GCM ECHO-2. part I: The tropical Pacific. *Mon. Wea. Rev.*, **125**, 703-719.

Hall, A. and S. Manabe, 1997: Can local linear stochastic theory explain sea surface temperature and salinity variability ? *Clim. Dyna.*, **13**, 167-180.

Hasselmann, K.,1976: Stochastic climate models. Part I: Theory, *Tellus*, **28**, 473-485.

Houghton, R. W. and Y.M. Tourre, 1992: characteristics of low-frequency sea surface temperature fluctuations in the tropical Atlantic. *J. Climate*, **5**, 765-771.

Huang, B., J. A. Carton, and J. Shukla, 1995: A Numerical Simulation of the Variability in the Tropical Atlantic Ocean, 1980-1988. *J. Phys. Oceanogr.*, **25**, 835-854.

Kaiser, H. F., 1958: The VARIMAX criterion for analytic rotations in factor analysis. *Psychometrika*, **23**, 187.

Kaiser, H. F., 1959: Computer program for the VARIMAX rotation in factor analysis. *Educ. Psych. Meas.*, **19**, 413.

Karaca, M. and D. Müller, 1991: Mixed-layer dynamics and buoyancy transports. *Tellus*, **43A**, 350-365.

Kraus, E. B. and J. Turner 1967: A one-dimensional model of the seasonal thermocline. *Tellus*, **19**, 98-105.

Latif, M. and T.P. Barnett, 1994: Causes of decadal climate variability over the North Pacific and North America. *Science*, **266**, 634-637.

Latif, M., A. Grötzner and H. Frey, 1996: El Hermanito: El Nino's overlooked little brother in the Atlantic. *MPI Report No.196*, Available from: Max-Planck-Institut für Meteorologie, Bundesstr.55, 20146 Hamburg, Germany.

Latif, M. , 1998: Dynamics of interdecadal variability in coupled ocean-atmosphere models. *J. Climate*, **11**, 602-624.

Lemke, P. and T. Manley 1984: The seasonal variation of the mixed-layer and the pycnocline under polar sea ice. *J. Geo. Res.*, **89**, 6494-6504.

Levitus, S., 1982: Climatological Atlas of the World Ocean, National Oceanic and Atmospheric Administration, 173 pp. and 17 microfiche.

Maier-Reimer, E., U. Mikolajewicz, K. Hasselmann, 1993: Mean Circulation of the Hamburg LSG model and its sensitivity to the thermohaline surface forcing. *J. Phys. Oceanogr.*, **23**, 731-757.

Manabe, S., R.J. Stouffer, M.J. Spelman, and K. Bryan, 1991: Transient response of a coupled ocean-atmosphere model to gradual changes of atmospheric CO2. Part I: Annual mean response. *J. of Climate*, 4, 785-818.

Manabe, S., and R.J. Stouffer, 1996: Low-Frequency Variability of Surface Air Temperature in a 1000-Year Integration of a Coupled Atmosphere-Ocean-Land Surface Model. *J. of Climate*, **9**, 376-393.

Mehta,V. M. , 1998: Variability of the tropical ocean surface temperature at decadal-multidecadal time scales, part I: Atlantic ocean. *J. Climate*, **11**, 2351-2375.

Mehta, V. M. and T. Delworth, 1995: Decadal variability of the tropical Atlantic ocean surface temperature in shipboard measurements and in a global ocean-atmosphere model. *J. Climate*, **8**, 172-191.

Moura, A. D. and J. Shukla, 1981: On the dynamics in northeast Brazil: Observations, theory and numerical experiments with a general circulation model. *J. Atmos. Sci.*, **38**, 2653-2674.

Namias, J. and R. M. Born, 1970: Temporal coherence in North Pacific sea surface temperatures.*J. Geophys. Res.*, **75**,5952-5955.

Namias, J. and R. M. Born, 1974: further studies of temporal coherence in North Pacific sea surface temperatures.*J. Geophys. Res.*, **79**,797-798.

North, G. R., T. L. Bell, R. F. Cahalan and F. J. Moeng, 1982: Sampling errors in the estimation of empirical orthogonal functions. *Mon. Wea. Rev.*, **110**,699-706.

Penland, C. and L. Matrosova, 1998: Prediction of Tropical Atlantic Sea Surface Tempera-

tures Using Linear Inverse Modeling. *J. Climate*, **11**, 483-496.

Parker, D. E., C. K. Folland, A. Bevan, M. N. Ward, M. Jackson and F. Maskell, 1995: Marine surface data for analysis of climate fluctuations on interannual to century time-scales. In: *"Natural Climate Variability on Decadal to Century Time scales" edited by D. G. Martinson et al. National Academy Press.*, 241-250.

Reynolds, R. W., 1978:Sea surface temperature in the North Pacific Ocean, *Tellus*,**30**,97-103.

Richman, M. B.,1986: Review article: Rotation of principal components. *J. Climatology*, **6**, 293-335.

Roeckner, E., K.Arpe, L. Bengtsson, S. Brinkop, L. Dümenil, M. Esch, E. Kirk, F. Lunkeit, M. Ponater, B. Rockel, R. Sausen, U. Schlese, S. Schubert, M. Windelband,1992: Simulation of the present-day climate with the ECHAM model: Impact of model physics and resolution, Report no.93, October 1992, 171 pp. Available from: Max-Planck-Institut für Meteorologie, Bundesstr.55, 20146 Hamburg, Germany.

Roeckner, E., J. M. Oberhuber, A. Bacher, M. Christoph and I. Kirchner, 1996: ENSO variability and atmospheric response in a global coupled atmosphere-ocean GCM. *Climate Dynamics*, **12**, 737-754.

Schlittgen, Streitberg (4.Edition 1991): Zeitreihenanalyse, *R. Oldenbourg Verlag München*, section 5.3.2, 236-24.

Sutton, R.T., M.R. Allen 1997: Decadal predictability of North Atlantic sea surface temperature and climate.*Nature*, **388**,563-567.

Voss, R., R. Sausen, U. Cubasch, 1998: Periodically synchronously coupled integrations with the atmosphere-ocean general circulation model ECHAM3/LSG. *Climate Dyn.* **14** (4),249-266.

Wagner, R. G., 1996: Mechanisms controlling variability of the interhemispheric sea surface temperature gradient in the tropical Atlantic. *J. Climate*, **9**, 2010-2019.

Weng, WJ Neelin, JD , 1999: Analytical prototypes for ocean-atmosphere interaction at midlatitudes. Part II: Mechanisms for coupled gyre modes . *J. Clim.*,**12**, 2757-2774.

Zebiak, S.E., 1993: Air-sea interaction in the equatorial Atlantic region. *J. Climate*, **6**,

1567-1586.